

# Strike-slip faults in the Cambro-Silurian rocks of the Oslo Rift - Caledonian compression or Permian transtension?

Sofie Hildegard Ryen



Master Thesis in Geosciences  
Structural Geology and Tectonics  
60 credits

Department of Geosciences  
The Faculty of Mathematics and Natural Sciences

UNIVERSITY OF OSLO

November 2020



# Strike-slip faults in the Cambro-Silurian rocks of the Oslo Rift - Caledonian compression or Permian transtension?



Sofie Hildegard Ryen

© Sofie Hildegard Ryen, 2020

Strike-slip faults in the Cambro-Silurian rocks of the Oslo Rift - Caledonian compression or Permian transtension?

Supervisors: Anders Mattias Lundmark (UiO) and Lars Eivind Augland (CEED, UiO)

This work is published digitally through DUO – Digitale Utgivelser ved UiO

<http://www.duo.uio.no/>

Trykk: Representeren, Universitetet i Oslo

*Title page: Photograph of an imbricate structure at Hukodden, southern Bygdøy, Oslo. The structure involves the Tøyen, Huk, and Elnes formations of the Lower Palaeozoic, and is described in detail in this thesis. The photograph is taken facing NE, by Sofie Hildegard Ryen.*

## Abstract

The Oslo Region provides the opportunity to study both the development of the late Silurian Caledonian fold-and-thrust belt and the formation of the Permo-Carboniferous continental Oslo Rift. The complex structural evolution of the region is reflected in the Lower Palaeozoic sediments that have been downfaulted and preserved in the Oslo Rift. This study investigates, through detailed mapping and the construction of balanced cross-sections, the characteristics and origin of sub-vertical strike-slip faults found within the Oslo Region. Previous investigations of the tectonic evolution of the region have regarded such faults as representative of several Permo-Carboniferous strike-slip regimes related to the formation of the Oslo Rift. On a larger scale, it has been proposed that the Oslo Rift is connected to the Variscan orogenic front and the Sorgenfrei-Tornquist Zone through the Permo-Carboniferous Skagerrak and Horn grabens, and the strike-slip faults have been proposed to reflect Variscan compressional tectonics and related transpression and dextral strike-slip on the Sorgenfrei-Tornquist Zone.

Approximately 3 months of detailed mapping at Huk and Slemmestad in the Oslo Region, deemed representative of the regional geology, revealed small scale tear faults terminating in overlying and underlying Caledonian thrust faults. On a larger scale, adjacent domains of differing compressional structures were observed, where the lateral break in geology can only be explained by Caledonian tear faults. These observations demonstrate that some steep strike-slip faults were formed as part of Caledonian thrusting, rather than post-dating it. The prevalence and impact on the surrounding geology make the Caledonian tear faults an integral part of the Caledonian structural style. This study therefore suggests that sub-vertical strike-slip faults in the Oslo Region should be individually mapped and checked against a set of criteria proposed in this thesis to distinguish between Caledonian tear faults and strike-slip faults of a Permo-Carboniferous age.

This study further suggests that Caledonian tear faults likely have been misinterpreted in previous studies, and included in the analyses of some of the tectonic phases relating to the Oslo Rift. Furthermore, investigation of the sills in the study areas suggests, in contrast to some earlier studies, that a late Carboniferous compressional phase is not required to explain sill emplacement. Consequently, the Variscan orogeny probably had less of an impact on the initiation of rifting than previously assumed. Since early compression and strike-slip regimes have been used as arguments for passive rifting in the Oslo Rift, this weakens the argument from field observations for the passive rifting model.

## Acknowledgements

First, I would like to thank my fantastic supervisors, Associate Professor Anders Mattias Lundmark and Researcher Lars Eivind Augland, for the opportunity to write this thesis, and for always taking the time to engage in scientific discussions and for challenging my hypotheses. I am grateful for the generous and invaluable support, guidance, and feedback you have provided during both the fieldwork and the writing process. Your knowledge and enthusiasm for the field and your encouragement whenever things went awry have inspired me and kept me striving to always do better. Our memorable canoe field trip adds to it all!

Beyond my supervisors, I also contacted other specialists. I am very grateful to Professor Hans Arne Nakrem and Professor Øyvind Hammer at NHM for discussions on the Lower Palaeozoic stratigraphy of the Oslo Region, and who with great enthusiasm accompanied me in the field to help me differentiate between certain lithostratigraphic formations.

Special thanks to Professor Arild Andresen for guidance on, and for compelling discussions regarding, balancing geological cross-sections. I would also like to thank Senior Engineer Luc Girod for providing and operating the drone used in this study; the photos are incredible!

I am grateful to Researcher Øystein Nordgulen at NGU for an interesting discussion on my fieldwork and for providing me with geological maps by J.F. Bockelie and T.G. Bockelie of the Oslo Region. I would also like to thank Researcher Odleiv Olesen at NGU for providing me with an interesting report regarding the depth to basement in the Oslo Region.

I am very thankful to the student administration at the Department of Geosciences, and to Adviser Karl Johan Ullavik Bakken in particular, for their help, their advice, and their hard work during the covid-19 pandemic of 2020.

Finally, a huge thank you goes to my loving and supportive family for always having faith in me. You are my rock (pun intended). Thank you to my father for inspiring my passion for geology. Our numerous discussions throughout the years have been invaluable to me. I am also grateful that we can form an alliance against the non-geologists in the household. Thank you to my mother for providing guidance in the world of tribal academia and for being an amazing role model. And lastly, my brother, thank you for the encouragements and for the music recommendations to keep me going, and for all the free toothpaste (he's a dentist).

# Table of content

Abstract.....	v
Acknowledgements.....	vi
<b>1. Introduction</b>	<b>1</b>
1.1 Purpose of study.....	2
<b>2. Method</b>	<b>3</b>
2.1 Introduction.....	3
2.2 Traditional mapping equipment.....	3
2.3 Digital mapping equipment.....	4
2.4 Previous work.....	6
2.5 Fieldwork.....	6
2.6 Maps and cross-sections.....	7
2.7 Other figures.....	11
<b>3. Theory</b>	<b>12</b>
<b>4. Regional Geology</b>	<b>17</b>
4.1 Introduction.....	17
4.2 Lower Palaeozoic Depositional Environment.....	21
4.3 Stratigraphy of the Lower Palaeozoic Successions.....	22
4.4 Lithostratigraphy of the Study Areas.....	24
4.5 The Caledonian Orogeny and the Plate Tectonic Framework .....	25
4.6 Caledonian Structures in South Eastern Norway and the Oslo Region.....	27
4.6.1 Structural style of folds and thrust faults.....	29
4.7 Late Carboniferous to Permian extension and rifting.....	30
4.7.1 Theory of passive rifting.....	32

4.7.2	Theory of active rifting.....	33
4.7.3	The six stages of the Oslo Rift.....	33
4.7.4	Palaeostress reconstructions from kinematic indicators.....	35
<b>5.</b>	<b>Results</b>	<b>38</b>
5.1	Introduction.....	38
5.1.1	On choosing the study areas.....	38
5.2	Southern Bygdøy – Huk.....	39
5.2.1	Cross-sections at Huk.....	42
5.2.1.1	Depth to Basement.....	42
5.2.1.2	Balanced cross-sections.....	45
5.2.2	Sub-area 1: Hukodden, the headland west of the bay.....	46
5.2.3	Sub-area 2: The restaurant at Hukskjærgrunnen and northwards approaching Maurtubukta.....	49
5.2.4	Sub-area 3: Maurtubukta.....	52
5.2.5	Sub-area 4: Eastern side of the Huk naturist beach headland.....	54
5.2.6	Sub-area 5: Western side of the Huk naturist beach.....	57
5.2.7	Sub-area 6: Hukodden, the headland east of the bay.....	61
5.2.8	Sub-area 7: Hukodden bay.....	79
5.2.8.1	The identified tear fault between Sub-areas 1 and 6.....	81
5.2.9	Sub-area 8: Bekkebukta bay.....	82
5.2.10	Permo-Carboniferous intrusive rocks at Huk.....	83
5.2.11	Summary of Huk.....	85
5.3	Slemmestad.....	85
5.4	Tear faults identification.....	88



<b>6. Discussion</b>	<b>94</b>
6.1 Introduction.....	94
6.2 Causes for tear faulting at Hukodden.....	94
6.3 Caledonian tear faults in the Oslo Region.....	94
6.4 Caledonian tear faults vs. Permo-Carboniferous strike-slip faults.....	96
6.4.1 Strike-slip faults and the Permian transfer zone.....	96
6.5 Late Carboniferous compressional stress regime and palaeostress reconstructions.....	97
6.6 Late Carboniferous to Early Permian strike-slip and palaeostress reconstructions.....	99
6.7 Late-Permian to post-Permian strike-slip and palaeostress reconstruction.....	106
6.8 Implications for hypothesis of passive rifting in the Oslo Region.....	106
6.8.1 Late-Variscan far-field stresses.....	106
<b>7. Conclusion</b>	<b>108</b>
7.1 Recommended further research.....	110
<b>8. References</b>	<b>111</b>
<b>Appendix 1: Comprehensive descriptions of lithostratigraphic units</b>	
<b>Appendix 2: Suggestion for order of tectonic events at Hukodden</b>	
<b>Appendix 3: Geological maps, legend, balanced cross-sections, cross- sections, figures         accompanying balanced cross-sections, and drone photo</b>	

# 1. Introduction

The Palaeozoic structural evolution of the Oslo Region (*sensu* Bruton et al., 2010) includes both the development of the foreland of the late Silurian/Early Devonian Caledonian fold-and-thrust belt and the formation of the continental Permo-Carboniferous Oslo Rift. The Permo-Carboniferous Skagerrak and Horn grabens may represent a connection of the Oslo Rift to the front of the Variscan orogeny further south, including the Sorgenfrei-Tornquist Zone (Wilson et al., 2004; Larsen et al., 2008).

The Palaeozoic rocks that reflect these developments have been downfaulted and preserved in the Oslo Rift, which formed within the Precambrian basement of Southern Norway. This makes the Oslo Region an easily accessible field laboratory in which to study two major tectonic settings (thrust belts and rifts), and the possible effects of a strike-slip regime proposed to precede the main Permo-Carboniferous rift phase (Sundvoll and Larsen, 1993; Heeremans et al., 1996; Larsen et al., 2008). The region holds keys to understanding important parts of the geological evolution of Baltica, including the Fennoscandian Border Zone along which the the Sorgenfrei-Tornquist Zone was reactivated (Olaussen et al., 1994).

The aim of this thesis is to investigate the nature and origin of the sub-vertical strike-slip faults that have formed within the Oslo Region in this tectonic framework. Previous, published work in the Oslo Region has explored different aspects of the structural evolution of the region, but has mainly ignored the possibility of Caledonian tear faults as the origin of these faults. Instead, studies have focused on the Permo-Carboniferous rifting and proposed numerous tectonic phases relating to the rift in order to explain field observations of differently oriented, sub-vertical strike-slip faults. The emphasis of this thesis in relation to these faults, however, will be on investigating the potential existence and role of tear faults belonging to the Caledonian compressional regime.

Detailed fieldwork is carried out to attempt to better understand the involvement of sub-vertical faults in the Caledonian compressional deformation in the region. New findings and new understanding are used to re-examine the role and significance of these faults in the structural/tectonic evolution of this region.

## 1.1 Purpose of study

The objective of this study is to investigate Caledonian compressional tear faults in the Oslo Region, and to explore the implications their potential existence may have on the Caledonian structural style and on the published interpretations of post-Caledonian stress regimes. The main goals of the study are to:

- Determine the presence and extent of Caledonian tear faults in selected field areas through detailed field mapping.
- Characterise the field appearance and geometry of the tear faults (if present) through detailed field mapping.
- Construct balanced cross-sections from field data to illustrate the effect of the tear faults (if present) on adjacent Caledonian structural geology.
- Use the new data to investigate the possibility that some proposed Permo-Carboniferous tectonic phases may reflect Caledonian tear faults.
- Investigate the proposed relationship between the late Carboniferous compressional stress regime and sill emplacement against field observations and theory.
- Identify the regional implications of changes (if any) to the Permo-Carboniferous tectonic phases.

## 2. Method

### 2.1 Introduction

This chapter will present the different methods, materials, and softwares used to collect and process data for this thesis. The two study areas, Bygdøy and Slemmestad were mapped using traditional and digital mapping tools. Three geological maps and seven cross-sections were constructed using the collected data.

The geological map of Slemmestad (Fig. 5.3.1) was made using traditional mapping equipment and was mapped at a 1:4300 scale. The map of southern Bygdøy (Fig. 5.2.1) was made digitally. This meant that the mapping scale was altered by zooming in and out on the iPad. It was possible to map at a 1:40 scale if desired. However, most of the mapping was done at a scale of approximately 1:2000, with the exception of the structure at the headland east of the bay at Hukodden (Fig. 5.2.7.1). This detailed mapping was done at a scale of approximately 1:100.

Three of the cross-sections were balanced using the principles laid out by Woodward, Boyer, and Suppe (1989). The remaining four cross-sections closely follow the principles of Woodward, Boyer, and Suppe (1989), but calculations and the construction of concept sketches were not performed to ensure no volume change of the lithologies. There might therefore be some added or lost volume between the detachment zone and surface.

In addition to the detailed mapping at southern Bygdøy, a drone was used to take aerial photographs.

No samples were collected as both study areas are protected.

### 2.2 Traditional mapping equipment

A Silva Expedition S compass was used to measure the orientation of planar and linear features. The compass was adjusted for a declination of 3° (determined before fieldwork using <http://misvisning.kartverket.no/js-misv.html> (Kartverket, n.d.a)). The right hand rule was applied when collecting data on planar structures. A folding ruler was used to measure fault offset and the width of intrusions and beds. A 30x21mm hand lens was used to identify mineral grains in intrusions, and to view fossils and sedimentary structures difficult to see

with the naked eye. A3 print-outs of a topographical map of the area were used during traditional mapping of Slemmestad.

## 2.3 Digital mapping equipment

At Bygdøy, mapping was done with the help of an iPad and the application (app) FieldMove (version 1.3.0.59999 by MidlandValley, now Petroleum Experts). FieldMove includes a clinometer compass feature and can measure the orientation of planar and linear structures. The app also lets the user take pictures and make text notes that are listed along with the recorded measurements, all in chronological order. The program was adjusted for a declination of 3°.

A geo-referenced topographical basemap in GeoTIFF format was created in ArcMAP from the same WMS-address as was used for the print-out maps of Slemmestad. The WMS-address was provided by NGU (<https://www.ngu.no/emne/api-og-wms-tjenester> (NGU, 2019)). The map was imported into FieldMove, which saved all measurements, pictures, and text notes at their exact field location and displayed them on the map. The precision and accuracy of the FieldMove app measurements depend on the sensors on the tablet (Petroleum Experts, n.d.a, n.d.b). The tablet used during fieldwork was an iPad, model A1709, with iOS version 11.3.1 (15E302). The decision to use FieldMove on an Apple device rather than on an Android device was made based on two recent studies of FieldMove as a mapping tool (Allmendinger et al., 2017; Novakova & Pavlis, 2017). The two articles tested the accuracy of data collection by different mobile devices.

They advice extreme care when using a digital geological compass on an Android device. In regard to Apple devices, Allmendinger et al. (2017) conclude that iOS devices produce measurements with a high degree of accuracy and can therefore work as reliable substitutes for traditional clinometer compasses. They stress that it is important to periodically check the accuracy of the digital clinometer compass in the field. Therefore, comparisons of digital and traditional measurements were done during the fieldwork (Figure 2.3.1).

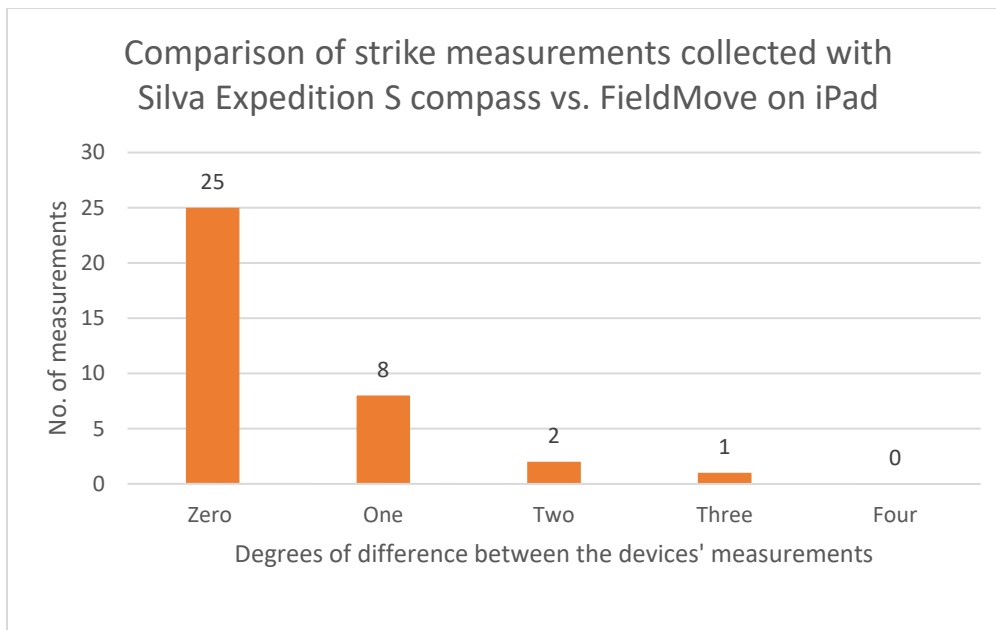


Figure 2.3.1: Comparison of strike measurements collected by the iPad and the Silva Expedition S compass. 36 measurements done digitally with FieldMove was double-checked using traditional means during fieldwork at Bygdøy. No comparison of dip measurements as the traditional and digital equipment consistently measured the same dip.

Based on the results (Fig. 2.3.1) it was concluded that the accuracy of FieldMove was perfectly adequate for the field mapping.

One of the biggest benefits of digital mapping is that it allows for a great number of measurements to be collected in a short span of time. In this regard, it is more effective than collecting data with an analogue compass and a physical map. Additionally, the GPS of the iPad paired with the imported basemaps make it easy to know where one is located in the terrain at all times. This is much quicker than having to establish precise positions by triangulation.

There were a few negative aspects of using the FieldMove app for iPad. The most prominent one was that sometimes the GPS would randomly be disabled in the app without any alert to the user. All data subsequently collected, such as measurements, notes, and photos, would be saved at the same exact location where the GPS turned itself off. The GPS was easily turned on again, but the faulty data had to be re-entered at the right coordinates.

Another downside to digital mapping was that it was close to impossible to interact with the iPad's touch screen when it got wet. This meant that it was difficult to collect data digitally on

rainy days. One can argue that pen and paper does not hold up well in rain either, but from experience, modern field notebooks are very resistant to water.

FieldMove also promises the option to create polygons in order to mark the different geological units in the area (Petroleum Experts, *FieldMove User Guide*), but a technological hiccup caused the app to exclusively allow pink polygons with 100% opacity during the entire summer of 2019. Due to this, the polygon feature was not utilised for this project, and a geological map created in FieldMove has not been included in this thesis.

## 2.4 Previous work

In preparation for the fieldwork, existing maps of the area were studied (Henningsmoen, 1955; Bockelie & Bockelie, 1970-1976a, 1970-1976b, 1970-1976c, 1970-1976d; Nordgulen et al., 1998; Graversen, 2015; Graversen et al., 2017; Lutro et al., 2017). The modern nomenclature and stratigraphical scheme for the Ordovician successions of the Oslo Region presented by Owen et al. (1990) were used during field mapping. Field identification of the different lithostratigraphic units was done based on works by Henningsmoen (1955), Bjørlykke (1973, 1974), and Owen et al. (1990), in addition to personal communication with Øyvind Hammer and Hans Arne Nakrem from the Museum of Natural History, Oslo.

## 2.5 Fieldwork

Fieldwork was carried out during July-August 2018, June-September 2019, and in October 2019. Additionally, some days were spent in the field during April, May, October, and November 2019 and May-July 2020 when the tide was particularly low. The abnormally low tide these days revealed outcrops that are normally submerged and difficult to map. The information on predicted tide and water level was gathered from the «Se Havnivå» feature at Kartverket's website (Kartverkets vannstands- og tidevannsinformasjon). Local water level is not entirely dependent on the lunar cycle, but is also influenced by precipitation and atmospheric pressure. Due to this, the autumn and early winter of 2019 provided rather few days of low tide, and almost no days of extremely low tide. The Huk skerries were reached by old fashioned swimming as well as by canoe.

It was not possible to perform geological mapping of the naturalist beach at Huk during the months of late May- late September, since the beach-goers did not accept the presence of a clothed geologist. The data from this sub-area were therefore collected during the low tide days of October and November 2019, as well as early May of 2020.

Large parts of both study areas are covered in vegetation, roads, and buildings, so most of the data were collected along the shoreline, in addition to some road cuts inland. Some parts of the shoreline at Bygdøy have been artificially covered by sand for the enjoyment of the summer guests. This means that outcrops of the local geology is only visible here during extremely low tide.

## 2.6 Maps and cross-sections

The maps and cross-sections were constructed by hand and digitised in Adobe Illustrator CC 2017 on an Asus Ultrabook with Windows 8.1.

Seven cross-sections, two at Slemmestad and five at southern Bygdøy, were constructed without vertical exaggeration. The cross-sections were located on either side of identified tear faults in the study areas to illustrate how the tear faults affect the lateral continuity of Cambro-Silurian strata and Caledonian contractional tectonics. Three of the cross-sections were balanced, and two of them are supported by accompanying figures that illustrate the progressive deformation of the beds.

The goals of the balanced cross-sections are to illustrate and constrain shortening at three sub-areas at Huk as accurately as possible. To achieve this, the placement of the line of section is very important. Woodward et al. (1989) states that the line of the cross-section should not deviate more than  $5^\circ$  from the true tectonic transport direction of the region. A deviation greater than this will lead to major errors when one tries to balance the profile. For example, beds that were originally next to one another will appear to overlap, and they will be impossible to restore to their original position.

In some cases, the strike of planar features in the map were not perpendicular to the bearing of the cross-section. In these instances, the apparent dip was used to construct accurate profiles. This was calculated using Equation 2.6.1.

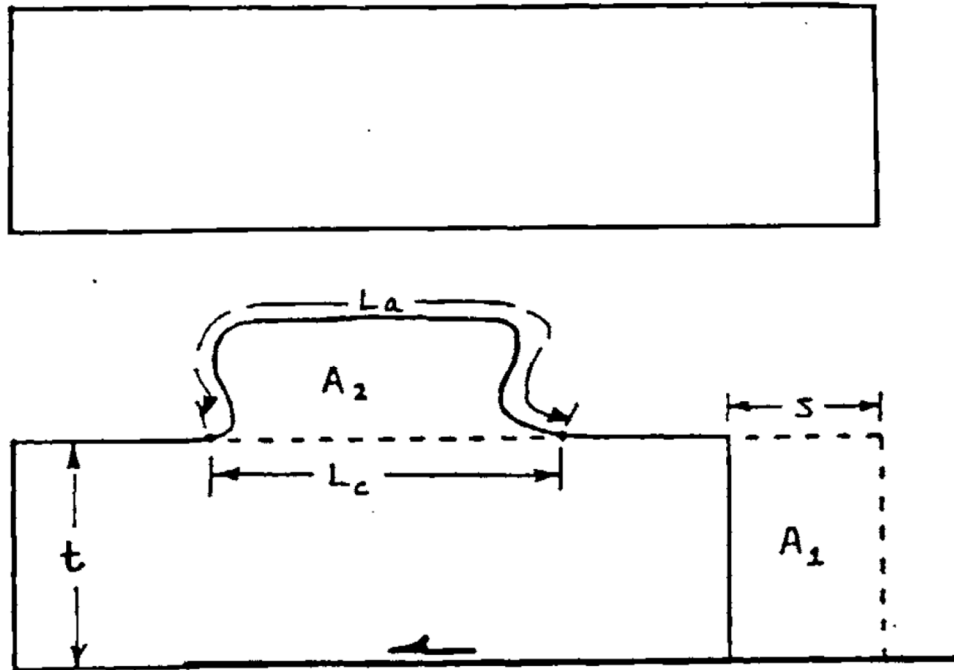


$$\tan\delta' = \tan\delta \times \cos\alpha$$

Equation 2.6.1: Equation used to calculate apparent dip of planar features when constructing a cross-section, from Groshong (2006). The components of the equation are as follows:  $\delta'$  – apparent dip,  $\delta$  – true dip, and  $\alpha$  – the strike of the cross-section minus true dip direction (strike of the beds/thrust plus 90°).

Determining the depth to basement, or depth to detachment, is vital when attempting to balance a geological cross-section. The cross-section should include deformed strata overlying undeformed, autochthonous structural basement. This structural basement is not necessarily the crystalline basement, although that is most often the case (Woodward et al., 1989). For the cross-sections in this thesis, the decision has been made to balance the geology above a local detachment zone in one of the dark shale lithologies. This was done as limited data made it difficult to predict the lithologies and geological structures found below 220 metres depth (Pascal et al., 2010).

In order to find the depth of this local detachment zone, the depth-to-detachment method presented by Woodward et al. (1989) was utilised (Fig. 2.6.1). This method also allows for projection of folds and faults to depth. The method for calculating compressional shortening presented by Woodward et al (1989) was also used in this thesis.



$t$  = Thickness of Deformed Section

Plane Strain:  $A_1 = A_2$

Shortening:  $s = L_a - L_c$

$A_2 = A_1 = t \cdot s = t(L_a - L_c)$

$$t = \frac{A_2}{L_a - L_c}$$

Figure 2.6.1: Depth-to-detachment method and accompanying equations, one of which is used to calculate compressional shortening. Figure and equations from Woodward et al. (1989).

Some assumptions about the deformation at Huk had to be made in order for the depth-to-detachment method to work. For balancing, plane strain deformation was assumed. Plane strain means no movement into or out of the section plane. In order to restore the beds to their original horizontal position, the line-length and bedding thickness of the formations have to be preserved. This implies no volume loss or compaction during deformation. If these assumptions are valid, the area of shortening will be equal to the area of uplift in the case of thrust tectonics. This is demonstrated in Figure 2.6.1 (Woodward et al. 1989).

To illustrate how two of the Huk cross-sections were balanced, two accompanying figures were prepared. They show the order in which faults and folds form and displace lithological

formations. When viewed in reverse, they show the restoration of the section to a flat layer-cake stratigraphy.

The figures were constructed along the same lines of section as the cross-sections from Huk, accurately reflecting the topography, thickness of the lithologies, and the angles of planes measured in the field. The construction of the figures was in itself a part of the balancing process. Drawing the deformation progress step-by-step on tracing paper ensured no change in volume between the start of the deformation (horizontal strata) and the end-result (the structure as it is visible in the field today). Since the drawings were done on tracing paper, the movement of the hanging-wall of thrusts could be mimicked by moving one layer of tracing paper over another. This made it possible to construct a figure where both the imbricates and the fault-truncated folds in the section can be restored with accuracy. It can be difficult to estimate volume by eyesight alone, so the use of tracing paper ensured that none of the thrust or folded lithologies experienced a sudden change in volume between deformation steps.

The type of structures and how they relate to each other in the cross-sections were determined from field data. The structural features that can be observed in the field are the most important tool for determining the structural style of a cross-section (Woodward et al., 1989). However, it is also vital that the cross-sections' portrayal of structural geometry at depth and inferred above today's erosional line is achievable in nature. Woodward et al. (1989, p. 4) put it well when they said "*The key is "what can reasonably be inferred to exist," for our whole purpose in balancing sections is to limit the unknown to that which we consider to be geologically reasonable*" (Woodward et al., 1989, p 4). This also applies to the progressive deformation of the structures, from birth to termination. The structures have to develop and interact with each other in a way that matches the wider structural style observed in the field and the physical properties of the lithologies. To ensure the quality of the cross-sections and figures, multiple articles on thrust tectonics and contractional structures were consulted (Morley 1986a, 1987, 1994; Woodward et al., 1989; McClay, 1992; Bruton et al., 2010, Cawood & Bond, 2020).

A number of these articles specifically discuss the thrust tectonics and structural style of the Oslo Region (Morley 1986a, 1987, 1994; Bruton et al., 2010). The literature on the theory of compressional structures, their geometry, and life cycle was very valuable when interpreting field data, and the articles on the investigated areas were immensely useful, as they discuss qualities of specific geological formations and the structural style of the area.

## 2.7 Other figures

Other figures produced for the thesis include stereonet, conceptual sketches, and photos from the field.

All stereonet presented were created in Stereonet, version 11.1.3 (Allmendinger, 2020).

Colouring of different measurements in the stereonet was done in Adobe Illustrator CC 2017.

Photos accompanying the text were taken using the iPad and a Nikon D7500 digital single-lens reflex (DSLR) camera, and a Mavic Pro (first generation) drone was used to take aerial shots of Huk. Photos were edited in Adobe Illustrator CC 2017 to highlight and point out relevant features.

### 3. Theory

Tear faults are sub-vertical strike-slip faults that accommodate lateral differences in amount of displacement/translation between segments in systems under tectonic compression (shortening) or tension (extension; Twiss & Moores, 1992). In this thesis, the focus will lie on tear faults in contractional regimes.

According to Twiss and Moores (1992), in compressional systems, tear faults may accommodate the following cases of lateral variations in geometries and deformation:

- differences in the translation between adjacent segments of a thrust sheet, (caused e.g. by the formation of ramp geometries, duplexes and imbricates)
- differences in the propagation and deformation of different parts of folds, typically in recumbent folds
- differences in the translation and deformation geometry in systems of *en echelon* folds
- differences in the translation, deformation and structural style in systems of *en echelon* and /or alternating thrusts and folds.

When sub-horizontal thrusts exist at two different stratigraphic levels, steep reverse faults are often found running through the more competent layers in between to connect the top and bottom thrusts. The resulting structure is called a duplex structure. The sub-horizontal thrusts are referred to as roof- and floor thrusts, and the steeper reverse faults are known as ramps. The block of rock in between the ramps in a duplex are bounded by faults on all sides, and are known as horses. Imbricate fans are similar to duplex structures, but lack a roof thrust (Ramsey & Huber, 1987; McClay, 1992; Fossen, 2014). Imbricate fans consist of a trail of overlapping fault-propagation faults where the thrusts that splay off the floor thrust, or detachment zone, are referred to as blind thrusts. As the blind thrusts are not linked with any overlying roof thrust, the displacement along the thrust must be transferred by different means beyond the tip line. This is accomplished by folding or development of cleavage at higher structural levels (McClay, 1992). The block of rock between thrust faults in an imbricate fan can be referred to as imbricate units (Ramsay & Huber, 1987). When viewing an imbricate system in the field, it can be difficult to determine whether the structure is an imbricate fan or

a duplex structure if the erosional level lies below a possible roof thrust (Ramsay & Huber, 1987; McClay, 1992; Fossen, 2014). McClay (1992) categorises duplexes that have the roof thrust removed by erosion as an imbricate system, alongside imbricate fans.

Thrust systems such as duplex structures and imbricate fans consist of a series of linked thrusts. The main fault is the sub-horizontal detachment zone, which is also sometimes referred to as a floor thrust or sole thrust. The main fault can be a local detachment zone or the décollement zone of a foreland basin system (basal detachment zone). The steeper faults usually originate in the main fault, and are called secondary faults, or splay faults (Ramsay & Huber, 1987; McClay, 1992). In some instances, new splay faults branch off second order faults, creating third order faults. Ramsay and Huber (1987) refer to these third order faults as diverging splays.

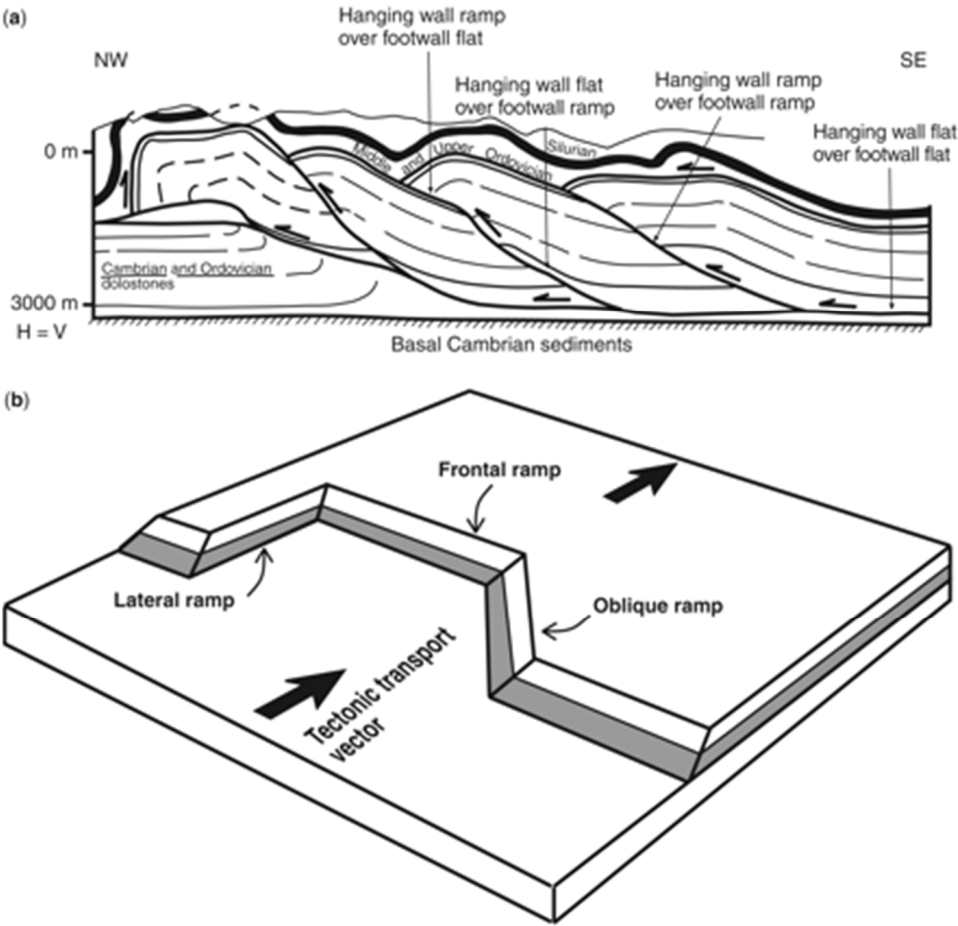


Figure 3.1: “(a) Geological section across the Nittany anticlinorium, Central Appalachians (section originally from Perry (1978) and simplified by (Geiser 1988)) showing a staircase geometry of the thrust surfaces and different hanging-wall and footwall ramp and flat situations. (b) 3D sketch showing the geometry of a thrust surface including frontal, oblique and lateral ramps.” from Poblet and Lisle (2011).

When two sub-horizontal thrusts are linked by a steep reverse fault, it creates a structural ramp between two stratigraphic levels. There are three kinds of ramps that form in contractional regimes: frontal ramps, oblique ramps and lateral ramps (Fig. 3.1). Frontal ramps form perpendicular to the transport direction, and display dip-slip movement parallel to dip direction. These ramps can form anywhere within the active thrust sheet, and are not limited to the thrust front (Ramsay & Huber, 1987). Oblique ramps are neither perpendicular, nor parallel to transport direction, and show oblique-slip. Lateral ramps form parallel to transport direction, and are usually steep. They display strike-slip movement, and connect one frontal or oblique ramp segment to another (Fossen, 2014).

When a thrust sheet encounters a ramp of any sort, the change in thrust surface geometry will lead to the formation of fault-bend folds or fault-propagation folds (McClay, 1992; Poblet & Lisle, 2011).

Lateral ramps, or tear faults, are sometimes also referred to as transfer faults, as they transfer slip between ramps (Fossen, 2014), and within duplex structures and imbricate zones (Twiss & Moores, 1992). Most articles that discuss tear faults refer to the definition coined by Twiss and Moores in their book *Structural geology* (1992; see beginning of chapter). Older literature, for example Ramsay and Huber's (1987) *The Techniques of Modern Structural Geology Volume 2: Folds and Fractures* do not differentiate between smaller scale strike-slip faults, and refer to tear-, wrench-, transcurrent-, and lateral faults simply as strike-slip faults. Tectonic plate boundaries with strike-slip displacement are referred to as transform faults by both Ramsay and Huber (1987) and Twiss and Moores (1992). According to Twiss and Moores (2006), a transfer fault is larger in scale than a tear fault, and it may transfer more slip. However, they do not state how large the fault must be to be categorised as a transfer fault rather than a tear fault. Mueller and Talling (1997) refer to "*large tear faults*" in their paper on Wheeler Ridge, California, but do not give further information on the size of these faults (Mueller & Talling, 1997, pp.409). In this thesis, I will not differentiate between tear faults and transfer faults sensu Twiss and Moores (2006), but use the term tear fault regardless of scale.

Tear faults form in the hanging-wall blocks of thrust faults (Twiss & Moores, 1992). They form when something causes one part of the thrust sheet to lag behind, whilst the adjacent part keeps moving forwards. To accommodate the difference in displacement, a fault with strike-

slip movement forms between the two parts. When a thrust sheet is divided into multiple parts by tear faults, each part can be referred to as a tear block (Poblet & Lisle, 2011).

Tear faults can also form if the development of a thrust sheet is controlled by different contractional structures in different places. One part of the thrust sheet can be dominated by thrusting and the other part by folding. The structures can accommodate the shortening of the area in different ways, which leads to more shortening in one part. Thus, the two parts will move forwards at different speeds (Twiss & Moores, 2006; Poblet & Lisle, 2011).

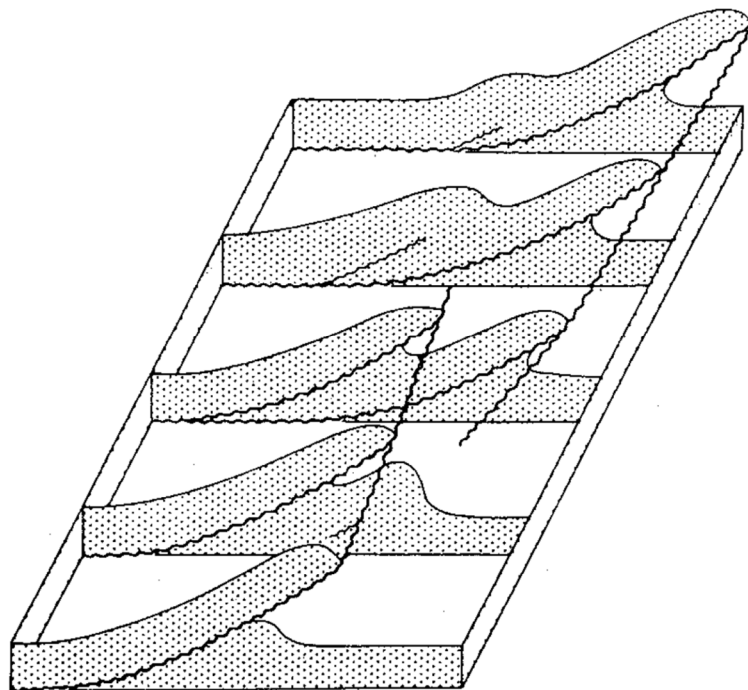


Figure 3.2: “A simple transfer zone where one thrust fault dies out and the displacement is transferred through the transfer zone to an *en echelon* thrust fault” from Twiss and Moores, 1992.

A thrust fault does not necessarily terminate against a tear fault; a thrust fault that is dying out can have its displacement transferred to an overlapping thrust by a transfer zone (Fig. 3.2). This happens when a thrust fault dies out along the strike direction and terminates in a tip line. As the displacement of the dying thrust decreases, the excess shortening of the area will cause a fold in the footwall. Subsequently, a thrust fault will branch from the detachment zone and cut the fold. The original fault will eventually be reduced to a fold in the hanging-wall of the new thrust fault (Fig. 3.2).



The Wheeler Ridge, California is an example of a fault-bend fold in the hanging-wall of a system of blind thrusts (Mueller & Talling, 1997). Here, tear faults accommodate lateral propagation of the fault-bend fold. Both the active thrust and the fault-bend fold terminate abruptly at the youngest tear faults. The tear faults have formed due to along-strike uplift of the fold related to fault displacement. They do not show horizontal strike-slip movement, only vertical. Mueller and Talling present a few different mechanisms and conditions which lead to the creation of tear faults. They suggest that an upper crustal stress regime that is higher than average in comparison to other fold-and-thrust belts may be one of the reasons for the tear faulting at Wheeler Ridge. Slip events along-strike in the thrust underneath the fault-bend fold cause shortening. After a number of earthquake cycles, enough displacement is accumulated for the thrust to move laterally and form a new tear fault (Mueller & Talling, 1997).

Pore fluid pressure plays an important role in faulting during sub-horizontal thrusting. Regional low pore fluids pressure can make it difficult for the continuous propagation of the fault, and thus tear faults are created to accommodate the increase in uplift at Wheeler Ridge (Mueller & Talling, 1997). A similar scenario can be envisioned where low pore fluid pressure halts the forward propagation of a thrust sheet in an area, and tear faults form to allow areas with higher pore fluid pressure to continue their forward movement. Tear faults can also form if there is an increase in rock strength due to lithology-changes, for example, if the sand/shale ratio in the detachment zone increases. Such differences in rock strength can additionally lead to variations of pore fluid pressure in an area (Mueller & Talling, 1997).

In the field, tear faults are identified by their steep dip, strike-slip movement, and their relationship in geometry and timing with the surrounding compressional structures. A thrust fault terminating against a sub-vertical strike-slip fault is evidence of the presence of a tear fault (Twiss & Moores, 1992). Likewise, if a fold is present in a thrust sheet near a tear fault, the fold axis usually terminates against the lateral ramp (Benesh et al., 2014). A tear fault will be active at the same time as the youngest thrust fault in a duplex or imbricate zone. It will not cut through the footwall of the thrust, and only the hanging-wall will be impacted by the tear fault (Twiss & Moores, 2006). This can help determine whether faults in the duplex or imbricate zone have developed in sequence or out of sequence. If the tear fault cuts through to the foremost ramp, the structure is in sequence, and if the tear fault terminates against a thrust at the back of the structure, the horse or imbricate unit in the front are out of sequence.

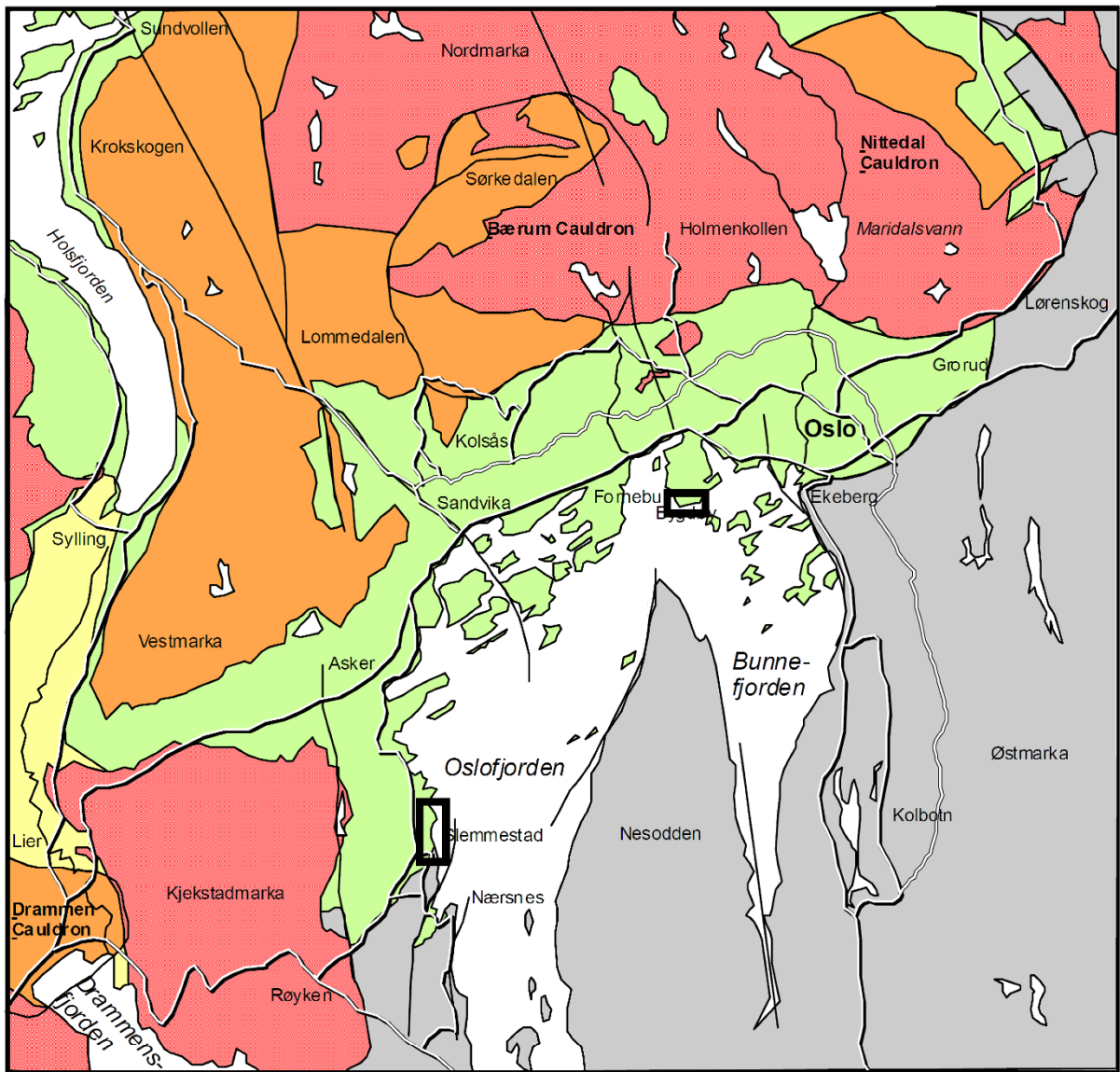
## 4. Regional Geology

### 4.1 Introduction

This chapter will give an overview of the palaeogeography, the geological structures, and the Lower Palaeozoic stratigraphy of the Oslo Region, as well as short summary of the magmatic evolution of the Oslo Rift. First, an overview of the depositional environment of the Lower Palaeozoic is presented. This is followed by an explanation of the nomenclature of the Ordovician successions and a short summary of the Ordovician lithostratigraphy pertaining to the study areas. Then the evolution of the Caledonian orogeny is presented, with an emphasis on the palaeo-continent and terranes involved. Lastly, a description of the Caledonian and Permian structures found in the Oslo Region today is given.



The two study areas of the thesis, Slemmestad and Bygdøy, lie within the Oslo Region (Fig. 4.1.1 and Fig. 4.1.2). The Oslo Region spans approximately 230 km from Langesund in the south to Ringsaker in the north (Fig. 4.1.1). The region covers an area of about 10 000 km<sup>2</sup> and comprises the front of the Caledonian fold and thrust belt with its Lower Palaeozoic sediments that are down-faulted and preserved within the Permian Oslo Rift (Størmer, 1953; Dons, 1978; Bockelie & Nystuen, 1985; Nordgulen, 1999, Bruton et al., 2010). The Oslo Rift is the result of late Carboniferous to Permian extension (Ramberg & Larsen, 1978; Olausen et al., 1994; Larsen et al., 2008).



## GEOLOGISK OVERSIKTSKART OVER OSLO-OMRÅDET

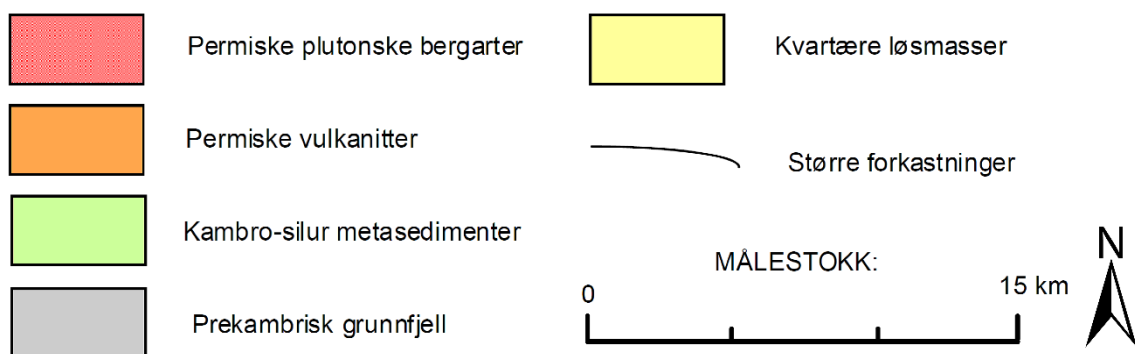


Figure 4.1.2: Overview of Oslo and surrounding areas. Black boxes indicate the study areas of Slemmestad and Huk. Figure modified from Bjørlykke (2004).

## 4.2 Lower Palaeozoic Depositional Environment

By the beginning of the Palaeozoic era, the crystalline basement of southern Scandinavia had been eroded to a low-relief surface known as the Sub-Cambrian peneplain. This erosional surface causes an angular unconformity or a nonconformity between the Pre-Cambrian rocks of the basement and the sediments deposited on top (Gabrielsen et al., 2015). The peneplain in the Oslo Region was submerged during the middle Cambrian transgression. The rising sea levels led to the formation of a shallow epicontinental sea covering a shallow depression in the Baltic craton. Middle Cambrian to Lower Ordovician sediments were deposited in a deep-water environment with near stagnant conditions, which is reflected in organically rich, black shales with beds and concretions of bituminous limestone (Bjørlykke 1974; Bockelie & Nystuen, 1985; Larsen & Olaussen, 2005; Bruton et al., 2010).

The Ordovician period was marked by high sea levels with repeated transgressions and regressions, which led to cyclic deposition of mud and limestone (Larsen & Olaussen, 2005; Bruton et al., 2010). Due to this, the Lower to Upper Ordovician successions are easily recognisable by their alternating beds of grey or black shales and light grey limestones. There are only a few distinct siltstone beds in the Early to Middle Ordovician succession (e.g. the Håkavik Member (Mb.) of the Elnes Formation (Fm.); Owen et al., 1990; Larsen & Olaussen, 2005). The Lower Ordovician beds were deposited in the Baltic epicontinental sea (Bruton et al., 2010). Multiple Ordovician formations are characterised by a cyclic variation in sedimentation rate and sediment composition (Bjørlykke, 1974; Owen et al., 1990; Ballo et al., 2019). Ballo et al. (2019) use high-precision age dating to support the interpretation that such rhythmic alternations in the Arnestad Fm. reflect Milankovitch cycles (astronomically controlled changes in Earth's long-term climate), and that Milankovitch cycles may explain the cyclicity in other parts of the Ordovician strata too, such as in the Vollen Fm.

The Upper Ordovician saw an increase in sedimentation rate with more siliciclastic material and alternation between fine grained mud- and limestones and coarser silt- and sandstones (Bockelie & Nystuen, 1985; Owen et al., 1990; Larsen & Olaussen, 2005; Bruton et al., 2010). The boundary between the Late Ordovician and early Silurian is marked by a marked regression and deposition of sandstone (Owen et al., 1990; Bruton et al., 2010) followed by a large-scale transgression, which led to the deposition of a shale-dominated sequence with thin beds of siltstone. The interbedded siltstones are interpreted as storm deposits (Worsley et al., 1983; Bruton et al., 2010). The Early Silurian saw an alternation of transgressive and

regressive events. The transgressions led to the deposition of shales and carbonate-rich units, whilst periods of clastic sedimentation reflect the regressive events (Worsley et al., 1983; Larsen & Olausson, 2005; Bruton et al., 2010).

As the collision between Laurentia and Baltica progressed, the epicontinental sea of the Oslo Region gradually changed during the middle to late Silurian into a foreland basin. The change was accompanied by an increased rate in sedimentation, as the erosion of the growing mountain chain led to an influx of coarse, clastic material to the basin. The late Silurian is dominated by fluvial red-bed facies sandstone deposition (Worsley et al., 1983; Bockelie & Nystuen, 1985; Larsen & Olausson, 2005; Bruton et al., 2010).

During the Scandian phase, the final emplacement of the Caledonian nappes led to compression of the sedimentary successions in the Oslo Region. Folds, ramps, internal flats, and listric reverse faults were amongst the structures that formed above basal detachment faults within the shale-rich units of the region. (Nystuen, 1981; Bockelie & Nystuen, 1985; Morley, 1987; Bruton et al., 2010).

### 4.3 Stratigraphy of the Lower Palaeozoic Successions

When doing research on the Oslo Region and its Lower Palaeozoic sedimentary units, one will often come across different unit names depending on the age of the source material one is perusing. A short overview of the history of the Ordovician and Silurian nomenclature for the Oslo Region will therefore be presented in this subchapter. A comprehensive table comparing the old and new Ordovician nomenclature is included (Fig. 4.3.1).

## The Ordovician System Period

		Chronostratigraphy				Local Stratigraphic Nomenclature				
		Post - 2000		Ca 1980		Lithostratigraphy, Oslo - Asker  (Following Owen et al. 1990)	Traditional Norwegian Nomenclature  (Informal)	Old Stage Code		
		Global (ICS)	British	British	British					
Ma	Series/ Epoch	Stage/Age	Series/ Epoch	Stage/Age	Series/ Epoch	Stage/Age				
443.8	Upper	Hirnantian	Upper	Ashgill	Upper	Ashgill	Langøyene Fm.	Kalksandstein	5b	
							Langåra Fm.	Gastropodekalk	5a,b	
							Husbergøya Fm.	Gastropodekalk	5a	
							Skogerholmen Fm.	Isoteluslag	4d	
							Skjerholmen Fm.	Øvre Tretaspisskifer	4cy	
							Grimløya Fm.	Tretaspiskalk	4cβ	
		Katian					Venstøp Fm.	Undre Tretaspisskifer	4ca?	
		Sandbian		Caradoc	Caradoc		Hiatus			
			Solvang Fm.			Øvre Chasmopskalk	4bδ1-2			
			Nakkholmen Fm.			Øvre Chasmopsskifer	4bγ			
			Frognerkilen Fm.			Undre Chasmopskalk	4bβ			
							Arnestad Fm.	Undre Chasmopsskifer	4ba	
	458.4	Middle	Darwillian	Middle	Llanvirn	Middle	Llandeilo	Vollen Fm.	Ampyxkalk	4aβ
Llanvirn							Elnes Fm.	Håkavik Mbr.	Ogygia zone (pars)/Trinucleus bronni zone	4aa4
							Engervik Mbr.	Ogygiocarisskifer	4aa3	
							Sjøstrand Mbr.	Øvre Didymograptusskifer	4aa1-2	
							Helskjær Mbr.	(Megistaspis gigas zone)	3cδ	
Lower		Floian	Lower	Arenig	Lower	Arenig	Huk Fm.	Svartodden Mbr.	Orthocerkalk	3cy
							Lysaker Mbr.	Asaphusskifer	3cβ	
							Hukodden Mbr.	Megistaspiskalk	3ca	
							Tøyen Fm.	Golgeberg Mbr.	Undre Didymograptusskifer	3bβ-ε 3ba (pars)
								Hagastrand Mbr.		3ba (pars)
470.0		Dapingian				Bjørkåsholmen Fm.	Ceratopygekalk	3aγ		
		Tremadocian		Tremadoc	Tremadoc	Alum Shale Fm. (Upper Part)	Ceratopygeskifer	3aa-β		
						Dictyonemaskifer	2e			
485.4										

Figure 4.3.1. Compilation based on Cohen et al. (2013; 2016), Stamm (2014), Owen et al. (1990), and Henningsmoen (1977). Included for lithostratigraphic formations present at the study areas of Huk and Slemmestad. Figure modified from Ryen (2017).

The Lower Palaeozoic sequence in the Oslo Region has been categorised and defined using a few different systems. Theodor Kjerulf, “The founder of modern geology in Norway” (Larsen & Olausen, 2005), introduced in 1857 a stratigraphical system consisting of eight “Etagen”, or stages. Waldemar C. Brøgger and Johan Kiær, both students of Kjerulf and renowned Norwegian geologists, published studies which expanded upon the different “Etagen” (Brøgger 1882, 1887 in Larsen & Olausen, 2005; Kiær 1897, 1902, 1908 in Larsen & Olausen, 2005; Owen et al., 1990; Larsen & Olausen, 2005). For example, Kiær added “Etagen” 9 and 10 to Kjerulf’s system (Worsley et al., 1983).

Each of the ten “Etagen” were defined on either a bio- or lithostratigraphic basis, or sometimes a mixture of the two. The stages were sorted numerically and divided into different



subcategories using Latin letters, Greek letters, and numerical subscripts. Stages and subgroups were also given descriptive names that reflected the particular unit's fossil content or lithological composition (Henningsmoen, 1982; Worsley et al., 1983). For example, the black shales and limestone nodules of today's Engervik Mb. of the Elnes Fm. was formerly known as *Ogygiocaris* Shale 4α<sub>1</sub> (Owen et al., 1990).

The work done by Kjerulf, Brøgger, and Kiær is still considered invaluable, and a solid foundation for later research on the Oslo Region. However, the "Etagé" scheme proved imprecise and difficult to apply to geological settings in the Oslo Region outside of the Oslo-Asker district (Størmer, 1953; Worsley et al., 1983). The consensus was that there was a need for an updated and modernised lithostratigraphic scheme which encompassed the successions of the entire Oslo Region (Worsley et al., 1983; Owen et al., 1990). A revision of the Silurian stratigraphical scheme was published in 1983 (Worsley et al., 1983), and a similar work on the Ordovician successions was published in 1990 (Owen et al., 1990). The successions are today divided into lithostratigraphic units, which all have been formally defined (Worsley et al., 1983; Owen et al., 1990).

#### 4.4 Lithostratigraphy of the Study Areas

A comprehensive overview of the Lower Palaeozoic successions of the Oslo-Asker district presented using the nomenclature and definitions put forth by Owen et al. in their 1990 publication *The Ordovician Successions of the Oslo Region, Norway* can be found in Appendix 1. These are the definitions of formations and members that have been used during detailed mapping at Huk and Slemmestad.

The study areas of this thesis, Slemmestad and Bygdøy, both contain well-exposed outcrops of Lower Palaeozoic successions in road cuts and along the coastline. On Bygdøy, several repetitions of strata, from the Lower Ordovician Tøyen Fm. up to the Upper Ordovician Arnestad Fm., are visible in outcrops. The late Cambrian Alum Shale Fm. and overlying Lower Ordovician Bjørkåsholmen Fm. are found at Killingen, a smaller island to the west of Bygdøy. At Slemmestad, similarly, repetitions through thrusting and folding is seen to involve successions from the Alum Shale Fm. up to the Middle Ordovician Elnes Fm. As no formations younger than the Arnestad Fm. have been studied in the field or included when creating maps or profiles, no younger formations have been described in detail in Appendix 1.

All formations of Ordovician age are presented in a simplified stratigraphic column (Fig. 4.3.1).

The different formations all show local variations in thickness. In addition to sedimentological factors (such as differences in sedimentation rates and the duration of particular depositional conditions), Caledonian folding and thrusting as well as Permian extension have played a part in modifying the local thickness of the beds. This post-depositional deformation can thicken a unit due to repetition or by the creation of ramps during the Caledonian contractional regime, or make it appear thinner as parts may have been cut out or displaced by Permian steep normal faulting (Owen et al., 1990). This means that the thicknesses presented in the literature is not always reflected in outcrops.

#### 4.5 The Caledonian Orogeny and the Plate Tectonic Framework

The Scandinavian Caledonides were formed as a result of the closing of the latest Proterozoic – early Palaeozoic Iapetus Ocean from the Ordovician to the end of the Silurian. The closing of the ocean involved the plate tectonic convergence of several lithospheric plates. These plates were carrying the large palaeo-continent bounding the Iapetus Ocean, as well as island arcs and micro-continent within the ocean. As the plates converged, several orogenic phases at the plate margins were caused by collisions with micro-continent and island arcs (Jakob et al., 2019), before the collisions between the large palaeo-continent at the final closing of the Iapetus Ocean (Roberts and Gee, 1985; Scotese & McKerrow, 1990; Torsvik et al., 1996; Torsvik & Cocks, 2016). The major palaeo-continent involved were Baltica, Laurentia, Avalonia, and Gondwana.

Baltica comprised a large part of today's northern Europe. (Fig. 4.1.1 and Fig. 4.5.1; Scotese & McKerrow, 1990; Torsvik & Cocks, 2016) Baltica became an independent continent during the Early Cambrian when it separated from Gondwana due to the opening of the Ran Ocean. It stayed independent until Late Ordovician when it collided with Avalonia (Cocks & Torsvik, 2002; Torsvik & Cocks, 2016).

Laurentia had been a separate continent since Proterozoic times, and remained so until the middle Silurian when it was involved in the collision with Avalonia-Baltica, which was the main phase of the Caledonian Orogeny (Cocks & Torsvik, 2005; Torsvik & Cocks, 2016).

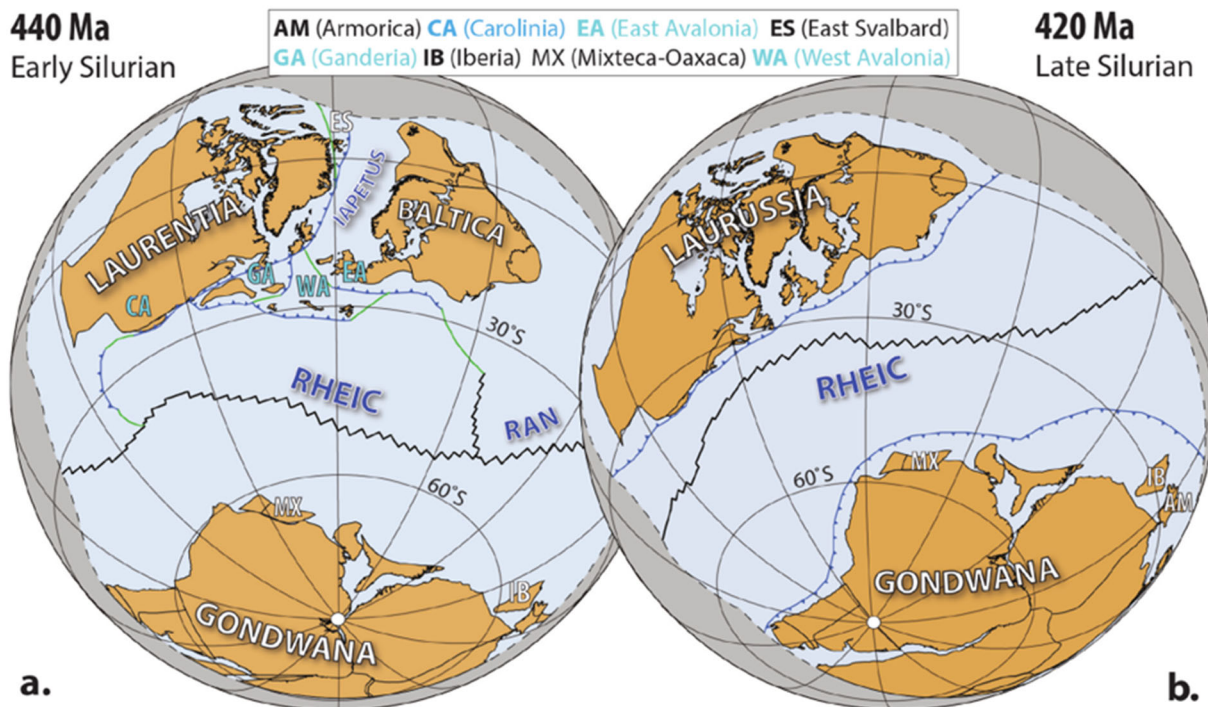


Figure 4.5.1. Palaeogeographic reconstructions from early to late Silurian. a) Early Silurian (440 Ma), with Laurentia approaching Baltica during the closing of the Iapetus Ocean, with an expanding Rheic Ocean to the south. b) late Silurian (420 Ma), with Laurentia and Baltica merged during the Silurian Caledonian Orogeny as the Iapetus closed. Blue lines represent subduction zones, green lines represent the margins of transform plates, and black lines represent spreading centres. The dashed lines at the edges of the globes mark a chosen outer limit of the Iapetus and Rheic-Ran domains (Domeier, 2015). Figure from Torsvik and Cocks (2016).

In the Late Ordovician, Baltica and Avalonia approached each other as the Tornquist Sea closed. At 443 Ma, an oblique docking of the two continents resulted in the creation of Avalonia-Baltica. Laurentia and Avalonia-Baltica were brought together by the closing of the Iapetus Ocean, which caused collisions of island arc chains and microcontinents found between the two continents (Torsvik & Cocks, 2016; Jakob et al., 2019). The complete closure of the Iapetus Ocean happened in the middle Silurian, and the resulting continental collision created the superterrane Laurussia (Fig. 4.5.1; Cocks & Torsvik, 2002). This merger, completed at about 420 Ma, is called the Caledonian Orogeny. On the Baltic continent, this event is referred to as the Scandian Orogeny, or the Scandian phase of the Caledonian Orogeny (Roberts & Gee, 1985; Andersen, 1998). During the collision, tectonic units, or nappes, originating from the margins of Baltica and Laurentia, as well as terranes from Iapetus, were thrust eastwards/southeastwards onto the Baltic Shield (Bockelie & Nystuen, 1985; Roberts & Gee, 1985).

The tectonostratigraphy of the Scandinavian Caledonides has traditionally been divided into autochthonous units, parautochthonous units, and allochthonous units. The allochthonous units were subdivided into the Lower Allochthon (late Proterozoic to early Palaeozoic sediments of generally low metamorphic grade), Middle Allochthon (Strongly deformed Precambrian crystalline basement from the Baltic margin), Upper Allochthon (Iapetus-derived), and Uppermost Allochthon (originating from the margin of Laurentia; Roberts & Gee, 1985). Several recent studies have called for a revision of this tectonostratigraphic scheme, as it does not reflect the true complexity of the nappe pile (e.g. Corfu et al., 2014). As this thesis mainly concerns units within the lowermost allochthonous units and the parautochthonous foreland fold and thrust belt, I will, for simplicity, refer to the Lower, Middle, Upper and Uppermost Allochthons in the following.

In the Devonian, late- to post-orogenic extensional collapse of the Caledonian Orogen resulted in the formation of several supra-detachment sedimentary basins, as well as exhumation of high-pressure and ultra-high-pressure rocks in the Western Gneiss Complex of western Norway. (Andersen, 1998; Fossen, 2010; Corfu et al., 2014).

#### 4.6 Caledonian Structures in South Eastern Norway and the Oslo Region

The Osen-Røa Nappe Complex in the Lower Allochthon is found in the Sparagmite Region in Southern Norway, northwest of the Oslo Region (Fig. 4.1.1). The nappe complex comprises sheets of crystalline basement and the Precambrian Hedmark Group (“sparagmite”, or arkose) with a 5-150 m thick unit of parautochthonous to autochthonous Lower Palaeozoic sediments at the nappe front (Nystuen, 1981, 1983; Bockelie & Nystuen, 1985, Nordgulen, 1999). The nappe complex overlies a thin unit of autochthonous Cambro-Silurian sediments, which in turn overlies Precambrian crystalline basement. The autochthonous to parautochthonous sedimentary cover at the nappe front thickens considerably southeastwards into the Oslo Region (Nystuen 1981, 1983; Bockelie & Nystuen, 1985), reaching a final thickness of about 1 km (Owen et al., 1990).

Nystuen (1983) states that in the Mjøsa area, the Osen-Røa thrust meets, and “*continues into*” (Nystuen, 1983, pp.70), the sole thrust underlying the Cambro-Silurian strata of the Oslo Region, and Bockelie and Nystuen (1985) mark the Osen-Røa thrust at the northern part of Lake Mjøsa. They further state that in the northernmost part of the Oslo Region, the Cambro-

Silurian successions make up the front of the Osen Nappe, which in turn make up the front of the Osen-Røa Nappe Complex. In this definition, the Osen-Røa Nappe Complex is separate from the parautochthonous units of the Oslo Region (Fig. 4.1.1). Today, however, it is generally agreed that the Osen-Røa Nappe Complex includes the Lower Palaeozoic successions of the Oslo Region (Fig. 4.1.1; Oftedahl, 1943; Morley, 1986a; Nordgulen, 1999; Bruton et al., 2010; Lutro et al., 2017). Bruton et al. (2010) refer to the décollement zone of the Oslo Region as an equivalent to the Osen-Røa detachment, but states that this basal detachment zone can be referred to as the Osen-Røa thrust “as far south as it is traceable”. It is thought to terminate in a blind thrust near Langesund, at the southern end of the Oslo Region (Fig. 4.1.1; Morley, 1986a, 1987; Bruton et al., 2010, Corfu et al., 2014)

The Lower Palaeozoic successions of the Oslo Region are categorised as autochthonous to parautochthonous with the décollement zone mentioned above as the main, flat, basal thrust located within the Alum Shale Fm. (Bockelie & Nystuen, 1985; Kumpulainen & Nystuen, 1985; Owen et al., 1990; Corfu et al., 2014). Splay faults from the décollement zone have caused several local detachment zones at higher stratigraphic levels, creating ramp-flat geometries throughout the region (Morley, 1986a; Owen et al., 1990; Bruton et al., 2010). A myriad of different contractional structures are found associated with the detachment zones, such as imbricate fans, duplex structures, backthrusts, thrust-related folds, and both harmonic and disharmonic folding (Bockelie & Nystuen, 1985; Morley, 1986a; Bruton et al., 2010; Graversen, 2015). The formation of ramps within the strata has allowed for accommodation of shortening at different stratigraphic levels. Oblique, lateral, and transverse ramps are all part of the geometry of the Oslo Region (Bruton et al., 2010). On Bygdøy and in Slemmestad, local detachment zones and ramp structures are evident in the black shale-dominated Tøyen, Elnes, and Vollen formations. The accompanying contractional structures involve the Mid-Cambrian to Mid-Ordovician successions in both areas (this study; Morley, 1986a; 1994).

The deformation of the autochthonous/parautochthonous units within the Oslo Region has been interpreted to not involve the basement (Bockelie & Nystuen, 1985; Morley, 1987; Graversen, 2015), and the style is therefore categorised as thin-skinned deformation.

Throughout the region, strain intensity and transport length decreases southeastwards towards the thrust front. There is also a noticeable decrease in strain intensity and shortening up-section from the décollement zone. This vertical change in style of deformation is due to a contrast in both competence and thickness between the different Lower Palaeozoic lithologies (Bockelie & Nystuen, 1985; Morley 1986a, 1987; Bruton et al., 2010). The upper Cambrian to

Mid-Ordovician successions are poor in siliciclastic material, consisting of mostly incompetent beds (with the exception of the massive limestone formations of Bjørkåsholmen and Huk, and the limestone-dominated Vollen Fm.), as opposed to the coarser, siliciclastic beds of the Upper Ordovician and Silurian (Worsley et al., 1983; Morley 1987; Owen et al., 1990). The latter also consist of much thicker units, with the Ringerike Sandstone as a 500-1000 m thick cap at the top (Bockelie & Nystuen, 1985; Morley, 1987).

The change in competence between the Cambro-Ordovician and Silurian successions leads to a structural style in the Cambro-Ordovician successions that consist mainly of thrusts and thrust-related folds. The Silurian strata, on the other hand, are dominated by broad buckle folding. The Silurian beds show little variation in style of shortening across the Oslo Region, rarely deviating from buckle folding as the preferred contractional structure (Morley, 1986a, 1987). Morley (1987) estimates a lateral change in deformation in the late Cambrian-Ordovician sediments from about 60% shortening through imbrication in the north to approximately 20% shortening by imbricate zones and pop-up structures further south, to finally 0% shortening where the basal thrust front terminates close to Langesund. This boundary between thrust-dominated and fold-dominated deformation lies between the Middle and Upper Ordovician in the north of the Oslo Region (Morley, 1987).

#### 4.6.1 Structural style of folds and thrust faults

Morley (1986a) describes the behaviour and vertical development of thrust faults in the Lower Palaeozoic successions in the Oslo Region. He estimated that faults with less than 50 metres throw generally die out in either the dark shales of the Elnes Fm., or when they reach the boundary between the Elnes Fm. and the limestone-dominated Vollen Fm. Thrusts die in the shaly Elnes Fm. because the low competency of the unit allows for the creation of multiple splays from a single fault. The slip on the original fault is then divided across the many splays and finally becomes too small to displace the higher-competency limestone of the Vollen Fm. Morley (1986a) notes that faults that are seen to continue through the Vollen Fm. and into the shale-dominated Arnestad Fm. do so with a stratigraphic displacement of 80 metres or more.

The data collected and interpreted by Morley (1986a) show that thrusts usually originate in shale-dominated units, and that splays form as the thrust propagates through the shale. In the case where a thrust fault survives a shale/limestone boundary, it will usually continue through

the limestone without forming any new splays. Morley (1986a) explains how less competent units can accommodate the strain at the fault tip by forming splays, bedding-parallel local detachment zones, or fault-propagation faults, whereas competent beds such as limestone break rather than fold. However, folds relating to faults are not limited to the dark shale units. If a thrust with a large amount of displacement encounters a thick limestone bed, the limestone can buckle and create a fault-propagation fold (Morley, 1986a).

Based on data collected at Slemmestad, Morley (1986a) states that folds involving the Huk Fm. limestone commonly have a second order thrust displacing the forelimb of the fold. The limestone imbricates of the Huk Fm. tend to form anticlines in the hanging-wall, and synclines in the footwall. Morley (1986a) concludes that the hanging-wall anticline/footwall syncline geometry means that folds and thrusts tend to accompany each other in the Huk Fm. Morley presents two possible explanations for the fault/fold relationship of the Huk Fm. One is that as the limestone of the Huk Fm. buckles, a fault develops from the closest detachment zone and creates a fault-propagation fold. Alternatively, as the Huk limestone starts to buckle, a fault develops *above* the closest detachment zone, and propagates upwards and downwards from within the fold. In both cases, faulting happens simultaneously as folding. Cases where faulting occurred post-folding are also seen, where the thrust cuts both limbs of the fold (Morley, 1986a).

#### 4.7 Late Carboniferous to Permian extension and rifting

Following the compressional regime of the Caledonian Orogeny, the folded and thrustured Cambro-Silurian sediments were eroded to a peneplain. A thin succession of late Carboniferous continental deposits known as the Asker Group are the only sediments preserved in the Oslo Region between the orogeny and the rifting. The sediments were deposited on the erosional surface, and were covered by lavas during rifting (Henningsmoen, 1978; Ramberg & Spjeldnæs, 1978; Sundvoll et al., 1992; Larsen et al., 2008). Extensional faulting from the late Carboniferous to Permian led to the formation of the Oslo Rift. The rift basin contains a large amount of volcanic rocks (Olaussen et al., 1994; Larsen & Olaussen, 2005).

The Oslo Rift is a continental magmatic rift consisting of different segments – four half grabens with main faults of alternating polarity. The segments are linked up through transfer

zones (Fig. 4.7.1). The northernmost segment is the Rendalen Graben with a westwards-dipping master fault and the southernmost segment is the offshore Skagerrak Graben with an eastwards-dipping master fault. The Skagerrak Graben terminates against the Sorgenfrei-Tornquist Zone in the south. The onshore Oslo Graben is situated in the middle of the Oslo Rift comprises two half grabens – the Akershus Graben to the north of Oslo with an east-verging master fault along the western flank, and the Vestfold Graben to the south of Oslo with a west-verging master fault on the eastern flank (Olaussen et al., 1994; Larsen et al., 2008). These two graben segments are connected by a transfer zone and the NW-SE- striking Krokkeiva-Kjaglidalen Transform Fault (KKTF), which is located NW of Oslo, running approximately from Sandvika to Sundvollen (Olaussen et al., 1994; Sundvoll and Larsen, 1994; Heeremans et al., 1996; Larsen & Olaussen, 2005; Larsen et al., 2008). When describing the KKTF as a transfer fault, Larsen and Olaussen (2005) and Larsen et al. (2008) refer to Heeremans et al. (1996). In their paper, Heeremans et al. (1996) use the name *Isidalen-Krokkeiva Transfer Fault* (IKTF), and the transfer zone appears in multiple figures marked on the same place on the map as the Krokkeiva-Kjaglidalen Transfer Fault (Fig. 4.7.1). The transfer zone between the two graben segments is unnamed when it is described by Olaussen et al. (1994), but it is marked in the same place as the KKTF. Sundvoll and Larsen (1994) refer to the Bærum-Øyangen accommodation zone, which they describe as the accommodation zone between the Akershus and Vestfold graben segments. This is most likely an earlier name for the Isidalen-Krokkeiva Transfer Fault, as it is described to have developed from the NNW-SSE to N-S oriented Langlia and Isidalen transfer fault zones (Sundvoll & Larsen, 1994). Faults that run parallel to, and are interpreted as part of the transfer zone, can be found in and around the Oslo area. One example is a NNW-oriented fault which runs from Bygdøy through Sørkedalen northwest of Oslo (Nordgulen & Dehls, 2003; Lutro et al., 2017).

A recent master thesis on the Krokskogen Lava Plateau found very little displacement along the KKTF, concluding that it cannot represent the main transfer zone (Køber, 2019). Køber proposes that the transfer zone between the two graben segments is located somewhere to the north of the KKTF, closer to Sørkedalen, and that the location of the transfer zone was influenced by the presence of a Precambrian shear zone, the Ørje mylonites zone (Nordgulen, 1999).



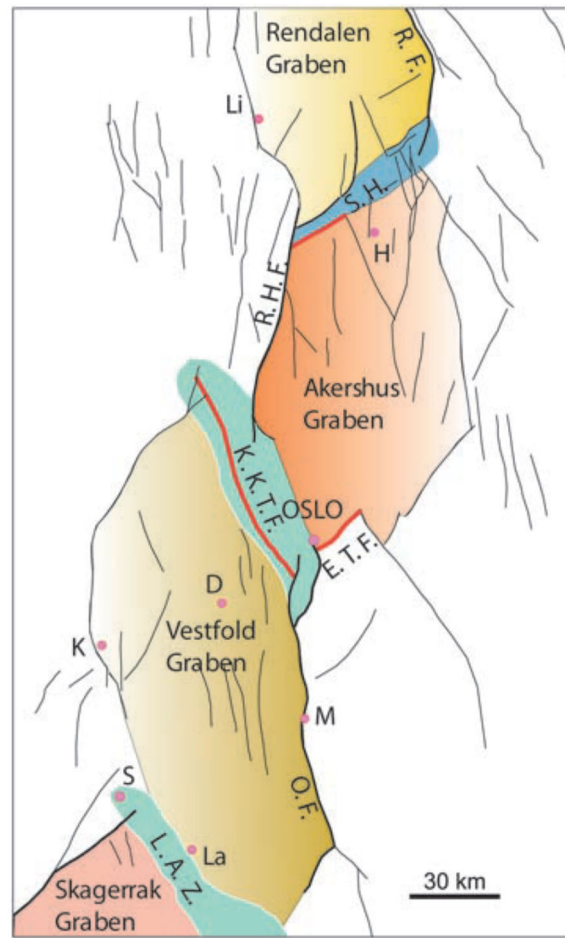


Figure 4.7.1. The different graben segments of the Oslo Rift in a simplified model. Yellow colour indicates west-verging master faults, orange colour indicates east-verging master faults, and green colour indicates transfer zones. The abbreviations used are R.F.: Rendalen fault, S.H.: Solberg Horst, R.H.F.: Randsfjorden-Hunnsvelv Fault, K.K.T.F.: Krokkleiva-Kjaglidalen Transfer Fault, E.T.F.: Ekeberg. Transfer Fault. O.F.: Oslofjord Fault, and L.A.Z.: Langesund Accommodation Zone. Li: Lillehammer, H: Hamar, D: Drammen, K: Kongsberg, M: Moss, S: Skien, La: Larvik. Figure from Larsen et al. (2008).

#### 4.7.1 Theory of passive rifting

There are two main theories for what initiated the extension of the area; active rifting due to a mantle plume beneath today's north-western Europe (Torsvik et al., 2008), and passive rifting as a result of the Variscan orogeny (Timmerman, 2004).

At the late stage of the Variscan orogeny (Western Europe), the Sorgenfrei-Tornquist Zone was reactivated at the Variscan front, between the Scandinavian Peninsula and continental Europe (Michelsen & Nielsen, 1993; Larsen et al., 2008). This WNW-ESE-oriented lateral fault system (with partly dextral strike-slip movement) was the largest of several that were active around this time. Strike-slip faulting paired with the late stage of the ongoing orogeny

is suggested to have led to the creation of an extensional stress field north of the Sorgenfrei-Tornquist Zone (Ramberg & Larsen, 1978; Olaussen et al., 1994, Heeremans et al., 1996, Larsen et al., 2008). This extensional stress regime was, furthermore, suggested to have caused rifting in the Variscan foreland during late Carboniferous to Early Permian, with the largest rift structure being the Oslo Rift. Extension and associated decompressional melting led to the high volcanic activity in the Oslo Rift and the large volume of volcanic rock found in the rift basin (Ramberg & Larsen, 1978; Olaussen et al., 1994; Larsen et al., 2008).

#### 4.7.2 Theory of active rifting

An alternative interpretation is that a Large Igneous Province (LIP) in north-western Europe was the driving force behind creation of the Oslo Rift. Magmatism in north-western Europe affected a large area and produced a large volume of mostly mafic volcanic material. The magmatic event took place over a short amount of time in most of north-western Europe, excluding the Oslo Rift (Neumann et al., 1992; Heeremans et al., 2004; Heeremans, 2005; Larsen et al., 2008). The early existence of a mantle plume has also been suggested due to the alkaline character of early basaltic magmatism, with the alkaline character of the magmatism being a primary feature from a mantle plume (Neumann, 2019). These factors support the presence of a deep-seated mantle plume. A deep-seated mantle plume can also explain the lack of a hot spot track (Torsvik et al., 2008). Torsvik et al. (2008) name this proposed LIP the Skagerrak-Centred Large Igneous Province (SCLIP).

#### 4.7.3 The six stages of the Oslo Rift

A six phase scheme for the tectonomagmatic development of the Oslo Graben was put forth by Ramberg & Larsen (1978), and later revised by Larsen and Sundvoll in 1983 and 1984 (Olaussen et al., 1994; Larsen et al., 2008). Olaussen et al. (1994) elaborated on the infill of the rift basin through the six stages (or phases as they refer to them in their paper).

Stage 1 is defined as the pre-rift phase. This stage is defined by the deposition of post-devonian sediments (The Asker Group) and by syenitic (mænaites) and basic sills (Neumann et al., 1992; Sundvoll et al., 1992; Larsen et al., 2008). Stage 1 took place before the formation of a rift basin, and due to the presence of sills, it has been proposed that the shallow

crust at this time was dominated by compression. This assumption is based on the theory that fractures open parallel to the minimal principal stress ( $\sigma_3$ ). For horizontal sills, the minimal principal stress should therefore be oriented vertically. Thus, horizontal sills can result from a compressive stress regime, and their presence is often thought to indicate such a stress regime (Hubbert & Willis, 1957 *in* Galland et al., 2018; Sundvoll et al., 1992; Olausson et al., 1994; Galland et al., 2018). However, sill emplacement when the minimal principal stress ( $\sigma_3$ ) is horizontal, rather than vertical, is not uncommon. For example, sills related to LIPs usually form before the initiation of rifting when the area is dominated by lithostatic stress, with a horizontal  $\sigma_3$ , and there are instances of sill emplacement in active rifts where extension is parallel to the horizontal  $\sigma_3$  (Galland et al., 2018). Galland et al (2018) state that compressional regimes might favour the emplacement of sills over dykes, but sills are likely not dependent on a compressional regime to form.

Sills are generally emplaced parallel to the layers of the host rock, leading to both horizontal and inclined sills depending on the orientation of the underlying and overlying layers. According to Galland et al. (2018), the preference for strata-concordant emplacement suggests sills are a result of magma feeders reaching a layer where it is easier for the magma to flow alongside the layer than to continue through it. This preference might be because of elastic properties of the host rock, such as a contrast in rigidity between layers, where the layer below an interface is less rigid than the layer above, or it might be that the interface between elastic rock layers is weak (Galland et al., 2018).

Sills are commonly found within shale units. Since shale tend to deform in an inelastic manner, ductile and brittle deformation are important factors in sill emplacement in shale formations (Spacapan et al., 2017; Galland et al., 2018). Pore fluid pressure might be another important factor in sill emplacement. Maturing organic material within a shale formation can in time lead to pore overpressure within the shale unit (Gressier et al., 2010; Galland et al., 2018). Experiments performed by Gressier et al. (2010) indicate that an overpressured host rock consisting of alternating layers of different competence proved ideal for strata-concordant sill emplacement.

Stage 2, the initial rifting, is defined by the first normal faulting and basaltic lava flows. Stage 3 saw the rift climax, with an increase in volcanic eruptions and fault activity, and the introduction of rhomb porphyry lava. The master faults of the Oslo Graben experienced large amounts of vertical displacement, and by the beginning of stage 4, a rift valley had formed (Ramberg & Spjeldnæs, 1978; Sundvoll et al., 1990; Neumann et al., 1992; Olausson et al.,

1994; Larsen et al., 2008). Bimodal central volcanoes developed in different parts of the rift during stage 4. The central volcanoes later collapsed to create calderas (Sundvoll et al., 1990; Larsen et al., 2008). Syenitic to granitic batholiths intruded the region during stage 5, before smaller intrusions of granite marked the termination of the rift at stage 6 (Larsen et al., 2008).

The stages were active at different times and for different durations in the Vestfold and Akershus Graben segments, starting in the SSW of the Oslo Graben and spreading towards NNE (Ramberg & Spjeldnæs, 1978; Sundvoll et al., 1990). In the LIP model proposed by Torsvik et al. (2008), stage 4 and 5 are not considered to be due to the deep-seated mantle plume.

#### 4.7.4 Palaeostress reconstructions from kinematic indicators

Heeremans et al. (1996) and Heeremans (1997) presents a system of different kinematic stages of the Oslo Region. The system set out to explain how the changing stress regimes from the Caledonian Orogeny and during the formation of the Oslo Rift relate to the different geological events of the Oslo Region. In a 2010 paper titled *Paleostress field reconstruction in the Oslo region* Sippel et al. (2010) re-evaluate some of the data and conclusions presented by Heeremans et al. (1996) on the evolution of the stress field in the Oslo Region.

For the 1996 study (Heeremans et al., 1996), data were collected from 50 stations in the Oslo Region, with 33 of them at outcrops of Precambrian or Cambro-Silurian rocks. Kinematic indicators from outcrops, as well as data collected from sills and dykes, were used to calculate five reduced stress tensors from the given data set (using the TENSOR program of Delvaux, 1993). The palaeostress tensors were sorted into groups based on the orientation of the principle stress axes and the ratio between them. Whether or not the phases represented by the stress tensors were present in syn- or pre-rift rocks was also taken into consideration when creating the groups. As Heeremans et al. (1996) had observed “*no conclusive overprinting relations*” (Heeremans et al., 1996, pp.62) in the sampled outcrops, the correlation of palaeostress tensor and geological event was done mainly based on the orientations of maximum principal stress ( $\sigma_1$ ) and minimum principal stress ( $\sigma_3$ ).

The first phase constitutes pure to radial NW-SE compression of late Silurian age. This is thought to be a Caledonian imprint as the stress tensors were found exclusively in the Lower Palaeozoic successions, and the minimum ( $\sigma_3$ ) and maximum ( $\sigma_1$ ) principal stresses

correspond with the Caledonian stress regime. Sippel et al. (2010) upholds this interpretation in their paper.

The second kinematic phase is N-S compression and was interpreted to be a Hercynian imprint. Heeremans et al. (1996) state that the data set for phase 2 is of poor quality, and that it is composed of kinematic indicators (faults and slickensides) found exclusively in Ordovician-Silurian strata. They suggest a correlation with the proposed compressive stress regime during sill intrusion in the region (Ramberg & Larsen, 1978; Sundvoll & Larsen, 1993), and therefore assign this phase a late Carboniferous age. Sippel et al. (2010) do not mention this kinematic phase in their paper, and the only compressional stress state discussed in their paper is the Caledonian imprint termed kinematic phase 1 by Heeremans et al. (1996).

The third phase is suggested by Heeremans et al. (1996) to represent a strike-slip stress regime that rapidly changes from NW-SE compressional strike-slip to NE-SW extensional strike-slip. The changing strike-slip regime is postulated to mark the transition from the compressional stress regime of kinematic phase 2 to an extensional regime (Heeremans et al., 1996).

Phase 3 is postulated to have occurred during late Carboniferous to Early Permian, and is divided into three sub-categories based on the orientation of maximum principal stress ( $\sigma_1$ ). The first of the three subcategories constitute pre-rift tensors, and the remaining two represent the initial rifting stage (Heeremans et al., 1996). These kinematic phases correlate with the two first stages of rifting coined by Ramberg and Larsen (1978).

Phase 3A is, as with the Hercynian imprint of phase 2, exclusively present in pre-Carboniferous rocks. The reduced stress tensors of phase 3A are based on measurements of faults and slickensides, and at four out of seven sites used, the kinematic indicators revealed WNW-ESE compressional strike-slip. Heeremans et al. (1996) state that the age of the rocks and the orientation of their deformation “*correspond to a Caledonian stress tensor*” (Heeremans et al., 1996, pp. 67). Yet, they assign the phase a post-Carboniferous age to match the interpretation proposed by Olaussen et al. (1994) where  $\sigma_1$  approximate a NW-SE orientation at the initial stage of rifting. According to Olaussen et al. (1994) the WNW-ESE – striking Sorgenfrei-Tornquist Zone was reactivated along the Fennoscandian Border Zone due to dextral strike-slip movement at this time.

Phase 3B is present in one station located in rocks of Precambrian age, seven stations in outcrops of Cambro-Silurian age, and one in an outcrop of late Carboniferous age (sills). Five

out of nine of these sites (including sills) contain kinematic indicators (faults and slickensides, as well as dyke orientations) that indicate NE-SW extensional strike-slip. The remaining four locations suggest compressional to pure strike-slip. Phase 3B was interpreted to be of post-Carboniferous age due to the late Carboniferous age of the sills at one of the locations (Heeremans et al., 1996).

Heeremans et al. (1996) refer to the proposition of Sundvoll et al. (1992) that the transition from a contractional regime to an extensional regime might be expressed by a period of strike-slip deformation. According to Heeremans et al. (1996), the “*predominantly pure to compressive phase 3A*” (Heeremans et al., 1996, pp.70) is an older kinematic phase than the extensional phase 3B, and the change from a transpressional regime to a transtensional one, as expressed by phase 3A and 3B, may support the hypothesis of Sundvoll et al. (1992).

Four outcrops, two of Precambrian age and two of Early Permian age, constitute phase 3C. As the youngest rocks of kinematic phase 3C are of Early Permian age, Heeremans et al. (1996) suggest the phase is of Early Permian age. Two of the four locations yielded extensive strike-slip stress tensors, and 3C was therefore interpreted to mark the end of the strike-slip transition period between the compressional and extensional regimes.

Kinematic phase 4 includes ENE-WSW to NW-SE pure extension according to Heeremans et al. (1996). They suggest that this phase might represent stress tensors of different ages, as the NW-SE-oriented  $\sigma_3$  is only seen in Precambrian-Silurian rocks, whilst the E-W to WSW-ENE-oriented  $\sigma_3$  is confined to the Permian outcrops.

Kinematic phase 5 is a phase of radial extension. The palaeostress tensors of this phase was reported from 28 stations, with outcrops showing rocks ranging in age from Precambrian to Permian. Data collected from the Brumunddal Sandstones and the alkali granites corresponding to stage 5 according to Ramberg and Larsen (1978) solely include stress tensors of phase 5. Based on this, Heeremans et al. (1996) propose kinematic phase 5 to be the youngest palaeostress phase.

Sippel et al. (2010), on the other hand, state that their field data do not support the multiple different phases of extensional deformation in the Oslo Region, although it cannot be excluded. They therefore decide against sorting the extensional stress tensors into groups based on the orientation of maximal principal stress ( $\sigma_1$ ).

## 5. Results

### 5.1 Introduction

This chapter will introduce the two study areas, Bygdøy and Slemmestad, and present the lithostratigraphic and structural data collected there. The chapter will focus on southwestern Bygdøy where the bulk of the fieldwork was done, and a large number of potential tear faults were uncovered.

The Bygdøy study area contains outcrops with well-exposed structures. There are also stretches of tilted beds that appear to reflect the thickness of the geological formations of the area without. In addition, there are multiple structures that are not immediately visible in the field. These only became apparent once the field data had been analysed. Here I have divided the Bygdøy study area into 8 sub-areas that all relate to the identified tear faults of the area (Fig. 5.2.1). A broad overview of the geology of southern Bygdøy as revealed by field mapping will be followed by a description of the different sub-areas. Cross-sections, field photos, and figures with step-by-step illustrations will be utilised to give an impression of the structures and to present the structural style of the area.

As the Slemmestad area has been the subject of detailed mapping on several previous occasions (for example by Bockelie & Bockelie (1970-1976a, 1970-1976b, 1970-1976c, 1970-1976d), Morley (1986a), and Graversen (2015)), descriptions of structures, bedding, and structural style in this area will only be briefly summarised. The focus will lie on the identified tear faults and the evidence of their presence.

#### 5.1.1 On choosing the study areas

In all likelihood, Caledonian tear faults will exist throughout the Cambro-Silurian sediments of the Oslo Region. One would expect to identify such faults by detailed mapping of any given area of reasonable size and suitable geological exposures. For this thesis, two study areas were chosen for such detailed mapping, Bygdøy and Slemmestad. They were deemed appropriate candidates for the project as they have a good amount of exposed Lower Palaeozoic strata, and are known to contain both Caledonian and Permo-Carboniferous deformation (Henningsmoen, 1977; Morley, 1986a, 1987; Larsen et al., 2008; Bruton et al., 2010; Graversen, 2015; Lutro et al., 2017).

Slemmestad has been the subject of detailed mapping by several studies (e.g. Bockelie & Bockelie 1970-1976a; 1970-1976b; 1970-1976c; 1970-1976d; Morley, 1986a; Naterstad et al., 1990; Graverson, 2015; and Lutro et al., 2017), and is the area for a Master's field course in structural geology at the University of Oslo (GEO4850). As a student on the master's course, I identified two faults as candidates for being Caledonian tear faults. As a student in, and later a teaching assistant on the field course GEO3010, I also noticed potential tear faults in the Huk area at Bygdøy. With its very good outcrops along the coast, and much less history of extensive geological mapping (lack of structural geology mapping in particular), this area was chosen as the main focus of this thesis.

## 5.2 Southern Bygdøy – Huk

The Bygdøy peninsula (Fig. 4.1.2) is located in the western part of Oslo. It is largely a residential area with hardly any outcrops, except for at the coastline where excellent exposure of Cambro-Silurian rocks is provided. Therefore, detailed mapping was done along the seaside, whereas the geology of the interior of the peninsula mostly had to be inferred from extrapolation from the outcrops on the coast. Bygdøy is a popular destination for outdoor activities and attracts many beach goers in the summer months. Huk, the southern tip of Bygdøy, has multiple well-kept communal bathrooms, lifeguards on duty at the Hukodden beach, and a separate naturist beach to the north of Hukodden at Maurtubukta (Fig. 5.2.1).





Figure 5.2.1: Geological map of the Huk area of southern Bygdøy. A major, vertical, NNW-SSE trending syenite porphyry dyke of Permian age cuts through the area. Sub-areas are marked by encircled numbers. Black box marks detailed map of Sub-area 6 (Fig. 5.2.7.1). Colours and symbols explained in legend found in Figure 5.2.2. The map is also found in Appendix 3 (Plate 1), where more measurements are included.

# Legend for maps and profiles

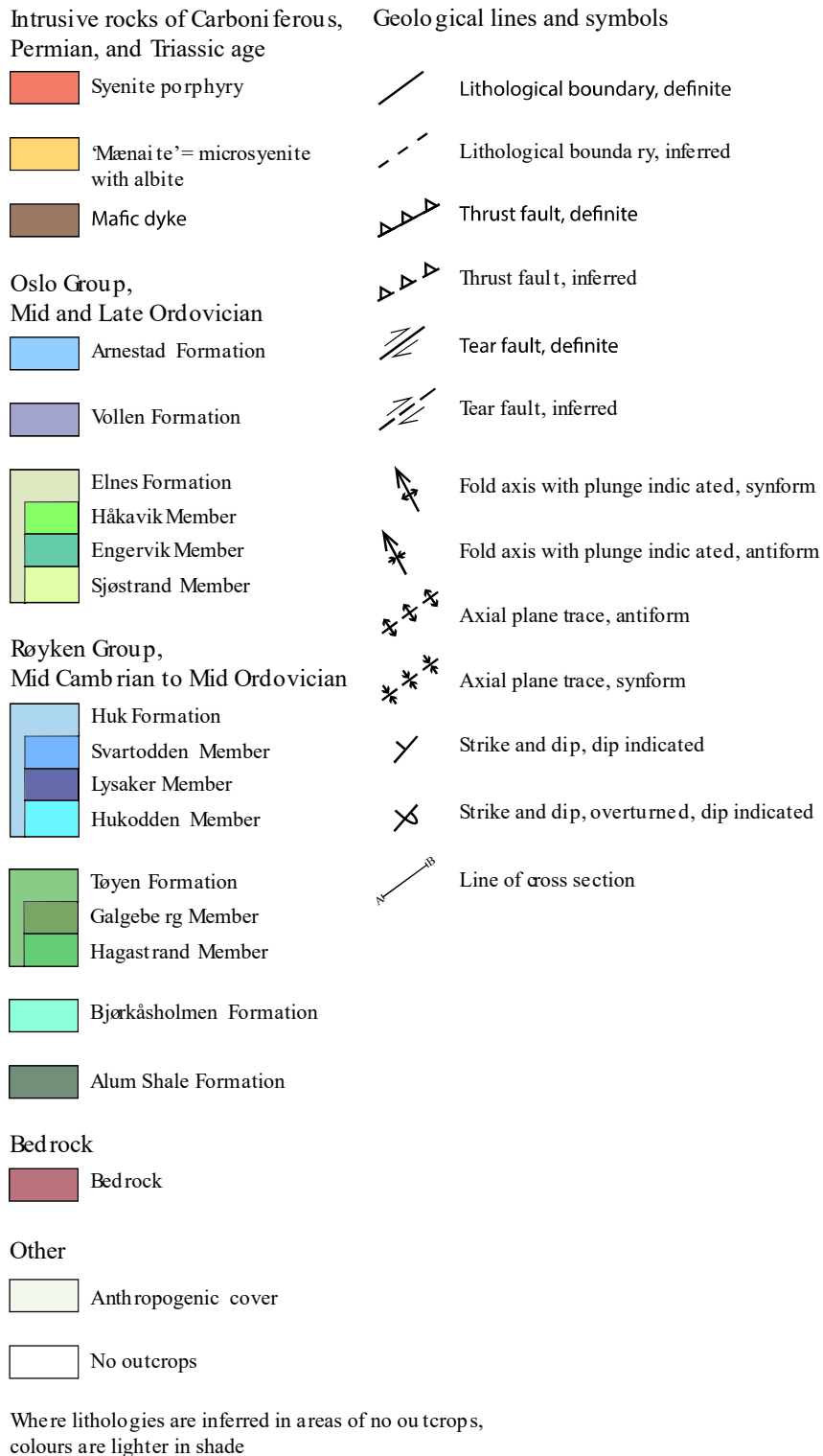


Figure 5.2.2: Legend for all geological maps and cross-sections constructed for this thesis. Figure can also be found in Appendix 3 (Plate 4).

Huk is characterised by Lower Ordovician sedimentary rocks with Caledonian deformation and Permo-Carboniferous intrusions and faults.

The Lower Palaeozoic formations comprise alternating units of dark shale and limestone. The oldest unit present in outcrops is the black shale Galgeberg Mb. of the Tøyen Fm. It usually accompanies repetitions of the overlying Huk Fm. and Elnes Fm., which are found at three of the study area's sub-areas (Sub-area 1, 5, and 6 on Fig. 5.2.1). The youngest sedimentary unit at Huk is the shale-dominated Arnestad Fm. It appears in the centre of a syncline with the Vollen Fm. on either side in sub-areas 2, 3, and 7 (Fig. 5.2.1). It also crops out in Sub-area 8 together with the underlying Vollen Fm. in the south. A residential area obscures potential outcrops of either formation to the north of Bekkebukta bay (Sub-area 8). It is thus uncertain whether the Arnestad Fm. comprises the hinge of a syncline in this sub-area (Fig. 5.2.1). The strike of the inclined beds at Huk keeps a SW-NE general trend.

The heterogeneous nature of the rocks is an important factor in the structural style of the area. Some structures, such as imbricate fans, fault-propagation folds, duplexes, and other ramp-flat geometries form due to variations in competence between layers. Other structures, such as small-scale folding, appear to pertain to one or more lithological units at any one place due to that particular unit's low competency. Multiple top-to-the-southeast thrusts, as well as one top-to-the-northwest backthrust, have been recorded in the black and dark grey shale formations. The thrust planes are all oriented approximately SW-NE parallel to the inclined beds, no matter if the thrusts are foreland-dipping or hinterland-dipping. These match the typical orientations of Caledonian thrusting (Bruton et al., 2010).

## 5.2.1 Cross-sections at Huk

### 5.2.1.1 Depth to Basement

The thickness of the Cambro-Silurian sedimentary cover in the Oslo Region has previously been estimated based on the thickness of the complete sedimentary succession as summarised by Owen et al. (1990). The assumption being that the depth to detachment equals the thickness measured from the bottom of the Alum Shale Fm. to the top of the lithostratigraphic formations exposed in outcrops in a particular area, and accounting for observed tectonic thickening of the formations. This has yielded depth to detachment thicknesses between 130-

250 m on Bygdøy (Morley, 1986a, 1994) and 150-250 in the Slemmestad area (Morley 1986a; Graversen, 2015; Lutro et al., 2017). In these cases, the depth to detachment (Osen-Røa detachment zone) and depth to basement (Precambrian crystalline basement) were assumed to coincide. However, when consulting recent geophysical data from the Oslo Region it becomes clear that this estimated depth to basement might not be entirely accurate. In a report on geothermal resources, Pascal et al. (2010) presented a new estimate on the thickness of the sedimentary cover. Gravimetric, petrophysical, and magnetic data, as well as lithological data from three boreholes, one from Arnestad, just north of Slemmestad, one from Rikshospitalet in the city of Oslo, and one from Hamar, in the Mjøsa Region, were used to create a 3D model (Pascal et al., 2010). The Arnestad borehole reveals highly deformed Cambro-Silurian sediments down to a vertical depth of 450 m. The sediments directly overlie the Precambrian basement with no Permian intrusions in between. The original report on the Arnestad borehole lists approximately 125 metres of Alum Shales between the crystalline basement and an overlying 300 m thick succession of Cambro-Silurian shales and limestones (Elvebakk, 2011, 2012). This succession of Cambro-Silurian strata corresponds well with the expected thickness of the geological formations found at this location (Owen et al., 1990; Hansen & Harper 2006), taking into account the folding and thrusting of the rocks in the borehole. The Rikshospitalet borehole reveals Cambro-Silurian sediments reaching a depth of approximately 880 m. This is not the true thickness of the sedimentary cover as vertical depth is unknown. Drill cuttings from the borehole suggests *at least* 70 metres of what is presumably Alum Shale directly overlying the Precambrian basement. Unfortunately, the next 740 m lack data from drill cuttings. At 60 metres depth, greenish shales of an unknown formation appear (Pascal et al., 2010). The Hamar borehole reveals Cambro-Silurian sediments reaching a depth of approximately 770 m with the bottom 230 m or so comprising Alum Shales (Elvebakk & Lutro, 2008; Elvebakk, 2012).

In addition, a 200 m deep borehole at the Geological Museum at Tøyen reveals Alum Shale down to a depth of 96 m, below which the Alum Shale is heavily intruded by syenite and maenaite intrusion. The alternating layers of Alum Shale and intrusions continue to 200 m depth without the borehole reaching basement (Elvebakk, 2013).

The thickness map included in the report by Pascal et al. (2010) reveal a sedimentary thickness of approximately 1 km in the Oslo Fjord between Bygdøy and Slemmestad, and a sedimentary thickness of approximately 900 m in the city of Oslo northeast of Bygdøy.

The report includes a map showing the thickness of the Cambro-Silurian sediments throughout the Oslo Region constructed from the 3D crustal model. It is accompanied by three cross-sections that are oriented perpendicular to the Oslo Graben. The map and southern cross-section indicate an approximately 250 m thick sedimentary cover at Slemmestad. The northern cross-section demonstrates a 500 m thick sedimentary sequence in Oslo north-east of Bygdøy. The map shows the sedimentary cover thinning slightly southwestwards, indicating a thickness of about 450 m in the Bygdøy area.

The 450 m thick sedimentary cover at Bygdøy is approximately 200 m thicker than previously assumed. Considering the data available from the boreholes (Elvebakk & Lutro, 2008; Pascal et al., 2010; Elvebakk, 2011; Elvebakk, 2012) the bottom 70-200 m might consist of Alum Shale, with the remaining 250-350 m comprising Cambro-Silurian shales and limestone. The lack of data between 740-60 m depth from the Rikshospitalet borehole means that the exact lithologies and structural geology of these Cambro-Silurian rocks are uncertain. The exposed geological formations at Huk have an undeformed thickness of approximately 160 m. This thickness has been calculated from the geological map created for this thesis (Fig. 5.2.1), and is based on bedding normal formation thickness measured in the field (for more information on the formations, included thickness, see Appendix 1). Assuming 150 m of Alum Shale directly overlying the Precambrian basement, it leaves 140 m of unknown lithologies resting atop the Alum Shale Fm. at Huk.

One possible explanation is that several repetitions of Lower to Middle Ordovician formations are present due to folding and thrusting, and that the structures and lithologies at depth are a reflection of the those at ground level. If so, ramps between detachment zones in dark shale lithologies might have created several storeys of repeating duplexes and other ramp-flat structures consisting of the Tøyen, Huk, and Elnes formations.

A second possibility is that the unaccounted-for strata is simply Alum Shale or Alum Shale intruded by maenaite and/or syenite. An argument in favour of this explanation is that repetitions of Alum Shale are observed on Bygdøy east of the Killingen island and on Killingen island. This suggests that the black shales are close enough to crop out nearby the study area. Cross-sections in the area of Maurtubukta and the naturist beach (Fig. 5.2.5.1 and Fig. 5.2.6.2) reveal that the large anticline observed here requires Alum Shale (and consequently also the Bjørkåsholmen Fm. limestone) to underlie the Tøyen Fm. shales. Without the added volume of the Alum Shale in the fold hinge, the size of the fold inferred from field data cannot easily be explained.

The boreholes and studies of Pascal et al. (2010) discussed above point to the existence of large thicknesses of Alum Shale at depth. The strata of the upper Cambrium – Middle Ordovician that outcrop in the inner Oslo Fjord from Slemmestad to Oslo City show no thickness variation that could explain these lateral changes in thickness. There is also no drastic change in topography that can explain the added sedimentary thickness in the Oslo Fjord and Oslo City compared to Slemmestad and Bygdøy. However, the variation in thickness might be due to the basement topography, in that the depth extremes in the Oslo Fjord and the city of Oslo might be natural inclines of the seafloor of the epicontinental sea where the Alum Shales were deposited. If this is the case, the unaccounted for strata at depth might be Alum Shale, with the Osen-Røa décollement cutting straight through the thicker parts of the shale, above the depths, and not following the undulating surface of the crystalline basement.

#### 5.2.1.2 Balanced cross-sections

In all of these scenarios, constructing a balanced cross-section where the autochthonous structural basement coincides with the autochthonous crystalline basement would involve a lot of guesswork. The interpretation of structures and lithologies found in the unaccounted for 140 m of sediments would invite a lot of unnecessary inaccuracy into the cross-section. I therefore decided to construct a balanced cross-section where the footwall of the local detachment within the Tøyen Shale constitutes the allochthonous structural basement (Woodward et al., 1989). The Alum Shale and Bjørkåsholmen formations have been added beneath the local detachment in the cross-sections (Fig. 5.2.5.1, Fig. 5.2.6.2, Fig. 5.2.7.4, and Fig. 5.2.7.5), as the two formations are needed to balance the cross-section at the naturist beach (Fig. 5.2.5.1, see also Fig. 5.2.6.2). The remaining 200 m above the Precambrian basement have not been attempted balanced, and is left blank.

The geological map (Fig. 5.2.1) clearly shows lateral displacement of several geological formations, as well as different kinds of compressional structures located right next to each other along-strike. These along-strike breaks in lateral continuity of the Caledonian deformation are interpreted to be caused by tear faults (see Fig. 5.2.6.2 and Fig. 5.2.6.3 in section 5.2.6, Fig. 5.2.5.1 in section 5.2.5 vs Fig. 5.2.7.4 in section 5.2.7, Fig. 5.2.7.7 in section 5.2.7, and section 5.4). Four of the cross-sections from Huk (Fig. 5.2.5.1, Fig 5.2.6.2, and Fig. 5.2.7.4) illustrate the results of large-scale tear faulting.

A fifth cross-section (Fig. 5.2.7.5) was constructed at Sub-area 6 to illustrate tear faulting at a smaller scale (Fig. 5.2.7.7). Here, a lateral ramp involving only a single thrust sheet in an imbricate fan structure lies between the fifth cross-section (Fig. 5.2.7.5) and one of the cross-sections also involved in illustrating the effects of a larger scale tear fault (Fig. 5.2.7.4).

The tectonic interpretations presented in the cross-sections represent only one of several possible solutions to accommodate the surface field observations. Permo-Carboniferous intrusions have not been included as the focus lies on Caledonian deformation of Lower Palaeozoic strata.

### 5.2.2 Sub-area 1: Hukodden, the headland west of the bay

In Sub-area 1, parallel, northwards-dipping beds of the Lower Ordovician succession from the Galgeberg Mb. (Upper Tøyen) to the Vollen Fm. crop out along a small headland. This locality does not show any repetition of units (Fig. 5.2.1). At low tide, the black shales of the Galgeberg Mb. (Upper Tøyen) are visible on the southeastern side of the headland. The shales directly underlie the massive limestone of the Hukodden Mb. (Lower Huk) with the depositional boundary intact. *Cycloendoceras commune* fossils in the Svartodden Mb. (Upper Huk) reveal right way up towards NNW (Fig. 5.2.2.1).



Figure 5.2.2.1: *Cycloendoceras commune* fossils in the Svartodden Mb. (Upper Huk). Right way up towards NNW is indicated by the light blue arrow. As the compass is not in a level position, the north arrow displayed in the photo should be disregarded.

The beach northwest of the Huk Fm. comprises black shale of the Elnes Fm., with the primary, depositional boundaries between formation members visible in the outcrops. The calcareous silt beds of the Håkavik Mb. (Upper Elnes) show right way up towards NNW (Fig. 5.2.2.2) which is consistent with the right way up indicators in the Huk Fm. The beds visible in outcrops along the beach of Sub-area 2 dips approximately 50-60° towards NNW. This part of the succession is mostly undeformed and thus represents the sedimentary thickness of the Huk and Elnes formations at the study area.



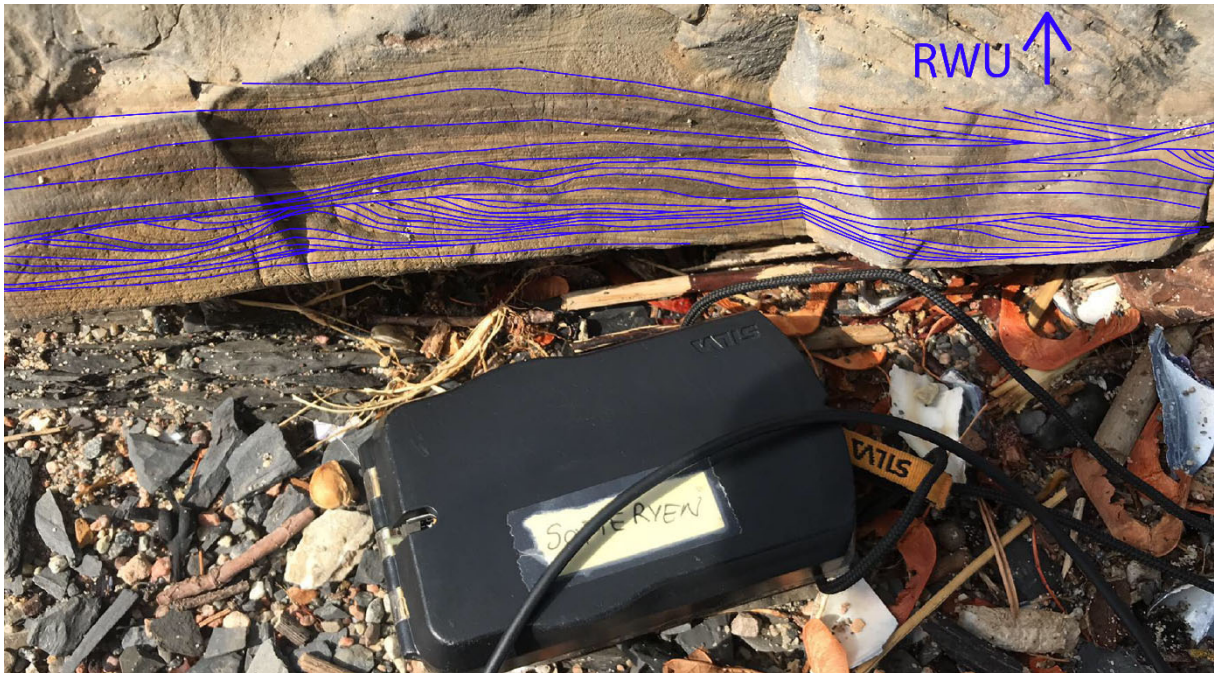


Figure 5.2.2.2: Cross-stratification in the Håkavik Mb. (Upper Elnes). The cross-cutting relationship of the silt beds indicate right way up towards NNW.

The skerries SSE of the headland (Fig. 5.2.1) comprise the three members of the Huk Fm., and *Cycloendoceras commune* in the Svartodden Mb. (Upper Huk) reveal right way up for the unit to be towards NNW and represent a repetition of the Huk Fm. This repetition is interpreted to be caused by thrusting and formation of fault-propagation folds (Fig. 5.2.5.1). If the unit had been overturned, Sub-area 1 would have been interpreted as an anticline with the two Huk Fm. repetitions comprising the two fold limbs.

There are three mafic sills in Sub-area 1. They are all emplaced in the shale of the Elnes Fm. and are oriented parallel to the beds of limestone and calcareous silt. One of the sills is located by the restaurant and although it is discontinuous at ground level, the end wedges of its two parts overlap in an *en echelon* way, and most likely, these two parts join up to make one continuous sill in the sub-surface. Due to lack of outcrops, it is uncertain whether the two remaining sills are two separate sills also are parts of one single sill.

### 5.2.3 Sub-area 2: The restaurant at Hukskjærgrunnen and northwards approaching Maurtubukta

On the western side of the restaurant at Hukskjærgrunnen, the interbedded calcareous silt layers of the Håkavik Mb. (Upper Elnes) gradually become less frequent as the member gives way to the Vollen Fm. Following the beach northwards, the beds become richer in shale as they approach the depositional boundary between the Vollen and Arnestad formations. The shale-dominated Arnestad Fm. overlies the Vollen Fm. The beds have a general NNW dip of approximately 40-50° between the restaurant and Maurtubukta bay, where they dip towards SE with the Vollen Fm. underlying the Arnestad Fm. in the NW (Fig. 5.2.1). The change in dip and configuration of the formations is explained by a syncline with the younger Arnestad Fm. in its centre (Fig. 5.2.5.1).

There are multiple low-angle, SW-NE striking thrust faults in the Vollen and Arnestad formations, and most of them show little to negligible fault movement. These faults are evident due to the calcite infill on the fault plane, which often provides good kinematic indicators such as slicken fibres. An example of internal thrusting of the Vollen Fm. is a small-scale duplex structure to the west of the restaurant at Hukskjærgrunnen, which is visible from two angles in the outcrop (Fig. 5.2.3.1 and Fig. 5.2.3.2)



Figure 5.2.3.1: Small-scale duplex in the Vollen Fm. west of the restaurant at Hukskjærgrunnen. Three horses can be seen separated by fault planes with calcite infill. Compass for scale, marked by red box.

In addition to the thrust faults, there are multiple NNW-SSE oriented sub-vertical faults with little throw, most displacing the stratigraphy by no more than 5-20 cm. A number of these faults can be seen close by the duplex structure west of the restaurant (Fig. 5.2.3.1 and Fig. 5.2.3.2). The steep faults all terminate against one of the thrust faults of the duplex structure, and most of them flatten out as they approach the underlying thrust fault plane (Fig. 5.2.3.2). Due to weathering of the calcite infill, slicken fibres are preserved in only one of the sub-vertical faults. The slicken fibres shows sub-horizontal movement along the fault plane, but there is no apparent cross-fault displacement of stratigraphy. These faults are interpreted as small-scale Caledonian tear faults, as they are confined to a horse within a Caledonian duplex structure (Table 5.4.2 and Table 5.4.3).



Fig. 5.2.3.2: Small-scale tear faults cutting through the hanging-wall of the upper horse of the duplex structure by the restaurant. The sub-vertical faults terminating against, or flattening out to merge with, the thrust fault plane. Backpack for scale.

A repetition of the Vollen and Arnestad formations can be seen to overlie a synform in the Arnestad Fm. halfway between the restaurant (Sub-area 2) and Maurtubukta (Sub-area 3; repetition seen in Fig. 5.2.1 and repetition and synform seen in Fig. 5.2.3.3). This, along with the small-scale internal thrusting of the Vollen and Arnestad formations (e.g. Fig. 5.2.3.1 and Fig. 5.2.3.2), is interpreted as part of a pop-up structure in the fold hinge of the larger syncline (Fig. 5.2.5.1). Continuous compression from the NNW without the ability to move further southeastwards on existing fault planes is interpreted to have led to out-of-sequence deformation in the low-competency units in the fold hinge.



Figure 5.2.3.3: A synform within the Arnestad Fm. underlies a repetition of the Vollen Fm. The northwestern limb of the Arnestad Fm. syncline is steeper than the southwestern limb, possibly due to drag against the fault plane that separates the two units. Backpack for scale.

#### 5.2.4 Sub-area 3: Maurtubukta

The southeastern beach of the Maurtubukta bay comprises SW-NE striking beds of the Vollen Fm. In the nook of the bay, an antiform in the Vollen Fm. along with a top-to-the-northwest backthrust and a top-to-the-southeast thrust are visible in outcrops (Fig. 5.2.1, Fig. 5.2.4.1, Fig. 5.2.4.2 and Fig. 5.2.5.1). Both thrusts are accompanied by drag folds (Fig. 5.2.4.1 and Fig. 5.2.4.2). The backthrust is interpreted to have formed either as a response to the termination of a ramp-flat structure in the sub-surface of Sub-areas 2 and 3 (Fig. 5.2.5.1 and Fig. 5.2.6.2) or in response to the floor thrust of the imbricate fan in the sub-surface of Sub-area 1 becoming stuck and initiating out-of-sequence deformation (Fig. 5.2.5.1). A suggestion for the order of events is presented in Appendix 2.

The top-to-the-southeast thrust along with the floor thrust of the ramp and the backthrust form a triangle zone in the sub-surface (Fig. 5.2.5.1 and Fig. 5.2.6.2). According to Morley (1987), triangle zones and pop-up zones form where the sole thrust becomes stuck and thus create a local area with a high concentration of strain. This may happen when a sole thrust of a ramp structure terminates against a backthrust; a part of the displacement along the sole thrust is not translated into deformation along the fault before it reaches termination. The remaining displacement is transferred from the dying sole thrust to the backthrust, resulting in added displacement along the backthrust's fault plane (Jamison, 1993)

The backthrust at Maurtubukta is also involved in the pop-up zone in the fold hinge of the syncline in Sub-area 2 (Fig. 5.2.5.1 and Fig. 5.2.6.2).

An approximately 14 m thick NNW-SSE oriented syenite porphyry dyke cuts in the Vollen Fm. (Fig. 5.2.1 and Fig. 5.2.4.1; see also description in sections 5.2.8 and 5.2.10). The outcrop provides a good view of the contact between the dyke and the sedimentary rocks southwest of the dyke (Fig. 5.2.4.1). A few poor quality outcrops to the northeast of the dyke reveal beds of the Vollen Fm., but potential structures are obscured by vegetation and paths. The dyke cannot be followed further northwest of the Maurtubukta beach in the study area, where it disappears under piers and a residential area. The syenite porphyry dyke can be observed to continue northwest of the residential area (outside the Huk study area).

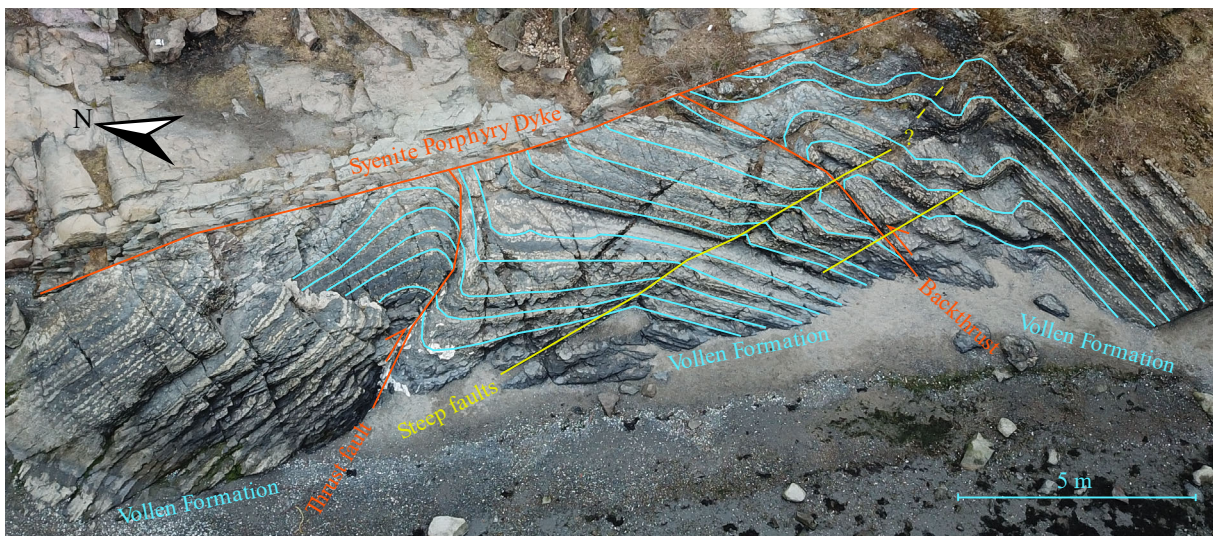


Figure 5.2.4.1: Drone photo of an outcrop at Sub-area 3. A thrust fault and backthrust visible in an outcrop at Maurtubukta bay. The outcrop also reveals an antiform in the Vollen Fm. Both thrusts show drag folds in the hanging-wall. Stratigraphic offset at either fault is difficult to determine by observing the outcrop, as the cyclical limestone-and-shale beds of the Vollen Fm. are hard to tell apart. Displacement along these faults are therefore unknown, but the presence of the drag folds indicate more slip than most of the other thrust faults observed in the Vollen Fm. in Sub-area 3. Two steep, NNW-SSE striking faults run parallel to the syenite porphyry dyke. An interpretation of the geology at depth is illustrated in Figure 5.2.5.1

Two NNW-SSE striking sub-vertical faults run parallel to the syenite porphyry dyke (Fig. 5.2.4.1). The faults show only a few cm offset, but calcite infill on the fault planes shows sub-horizontal lineations indicating strike-slip to oblique-slip movements. It is uncertain where one of the faults terminate as vegetation obscures the strata away from the beach, but the other fault appears to die out in the drag folds of the backthrust. If the syenite porphyry dyke has been emplaced in a Caledonian tear fault, it is possible that the sub-vertical strike-slip faults

are two accompanying smaller-scale tear faults that developed syn- or post-backthrusting (Table 5.4.2 and Table 5.4.3).



Figure 5.2.4.2: Close-up of the backthrust at Maurtubukta bay, backpack for scale. The drag folds indicate reverse movement along the fault plane. Backpack for scale.

#### 5.2.5 Sub-area 4: Eastern side of the Huk naturist beach headland

Sub-area 4 comprises the southeastern side of the naturist beach headland, which is also the northwestern side of the Maurtubukta bay (Fig. 5.2.1). Vegetation and concrete structures cover most of the headland, but outcrops of SW-NW oriented beds of the Elnes Fm. are visible along the coastline at low tide. The complete Elnes Fm. sequence is inverted and dips to the north with the Sjøstrand Mb. (Lower Elnes) in the NE, the Engervik Mb. (Middle Elnes) in the middle, and the Håkavik Mb. (Upper Elnes) in the SW (Fig. 5.2.1). The inversion of the sequence is also evident from the cross-stratification in the silt beds of the Håkavik Mb., which show right way up to the SSE.

The inverted Elnes Fm. sequence is interpreted as the SE fold limb of an overturned anticline (Fig. 5.2.5.1 and Fig. 5.2.6.2). The fold hinge and the NW fold limb is not visible due to lack of outcrops away from the coastline.

The tip of the headland comprises beds of the Vollen Fm., which are separated from the structurally overlying Elnes Fm. succession in the NE by a break in the outcrop that has been filled with loose rocks. A distinct difference in orientation of the beds on either side of the break indicate the presence of a thrust fault (Fig. 5.2.1, Fig. 5.2.5.1, and Fig. 5.2.6.2).

The Vollen Fm. contains two folds, an antiform in the NE and a synform in the SW. The folds are constrained to the Vollen Fm. and separated by a top-to-the-northwest backthrust (Fig. 5.2.1, Fig. 5.2.5.1, and Fig. 5.2.6.2). The backthrust in Sub-area 3 (Fig. 5.2.1, Fig. 5.2.4.1 and Fig. 5.2.4.2) across the bay aligns with the backthrust in the Vollen Fm. in Sub-area 4, and they are therefore interpreted as parts of one thrust (Fig. 5.2.1).

The antiform in Sub-area 4 is interpreted as the continuation of the antiform visible in the Vollen Fm. across the bay in Sub-area 3 (Fig. 5.2.1 and Fig. 5.2.4.1). Likewise, the synform in Sub-area 4 is interpreted as the continuation of the syncline in Sub-area 2 that involves the Vollen and Arnestad formations (Fig. 5.2.1 and Fig. 5.2.5.1). At the naturist beach headland, the fold hinge is visible in the Vollen Fm. and the fold axis plunges towards SE, which explains why the fold hinge is found in the Vollen Fm. at the naturist beach headland in Sub-areas 4 and 5, and in the Arnestad Fm. across the bay in Sub-area 2 (Fig. 5.2.1).



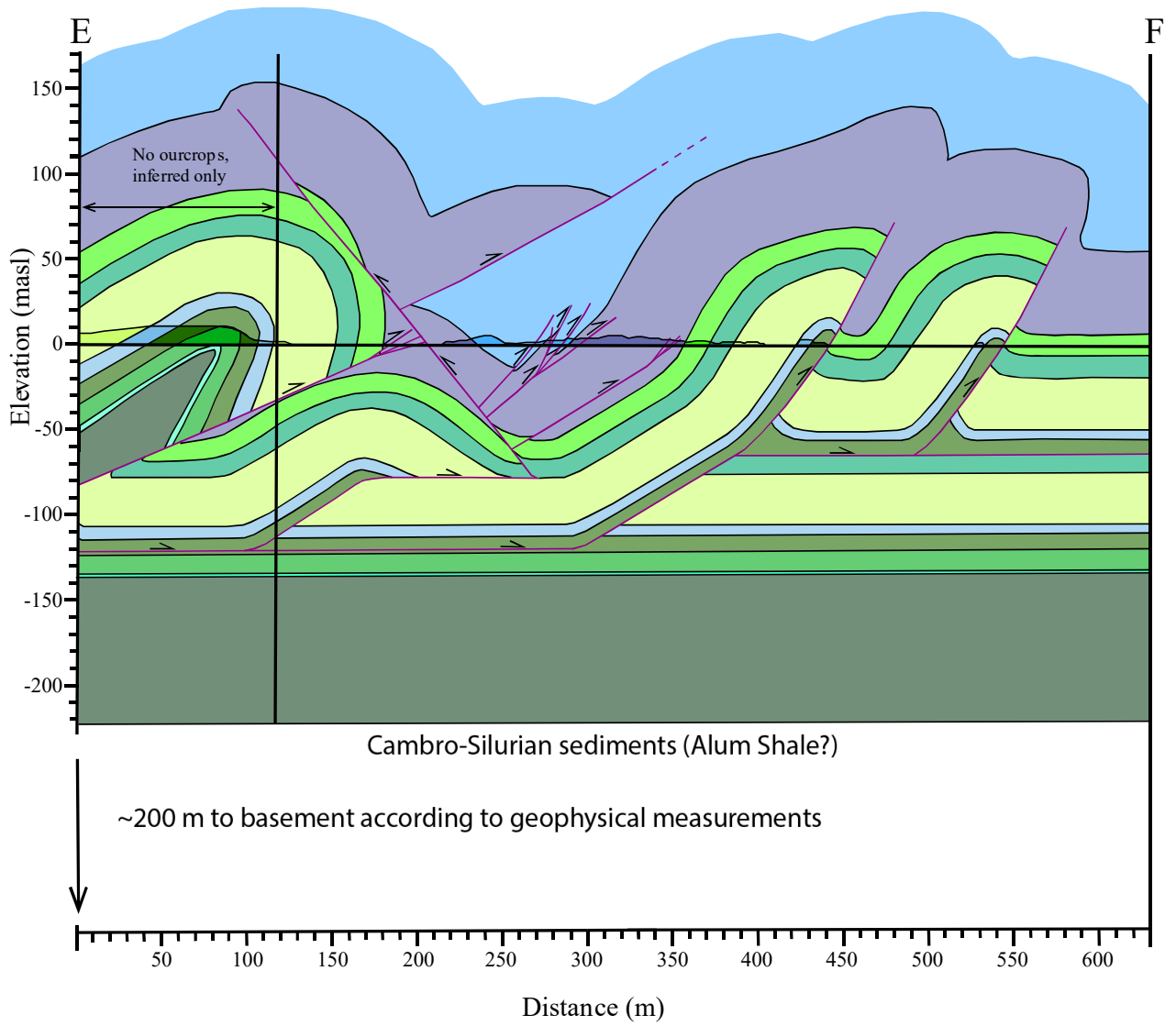


Figure 5.2.5.1: Figure text on next page

Figure 5.2.5.1: Balanced cross-section EF illustrating the geology of sub-areas 1, 2, 3, and 4 at depth. Legend can be found in Figure 5.2.2. Cross-section EF runs from the eastern shore of Maurtubukta bay (Sub-area 3) in the north to south of the Hukskjæra skerries (Sub-area 1) in the south. The headland to the west of Maurtubukta bay and consists of the full sequence of the Elnes Fm. separated from the underlying Vollen Fm. by an inferred thrust fault. The beds of the Elnes Fm. dips to the north with the Sjøstrand Mb. (Lower Elnes) overlying the Engervik Mb. (Middle Elnes), which in turn overlies the Håkavik Mb. (Upper Elnes). Kinematic indicators in the Håkavik Mb. (Upper Elnes) show right way up towards SE. The inverted Elnes sequence is interpreted as a limb of an overturned anticline. At the headland east of Maurtubukta bay, the Vollen Fm. and the overlying Arnestad Fm. are involved in top-to-the-southeast thrusting and one instance of top-to-the-northwest backthrusting. These structures are interpreted to be related to the development of a ramp structure and a related triangle zone in the sub-surface. The layering of the Vollen Fm. and the Arnestad Fm. show a general southeastwards dip in the north by Maurtubukta bay (Sub-area 3) which changes to a general northwestwards dip by Sub-area 2 in the south. This implies the Vollen and Arnestad formations sit in a syncline structure. Continuous compression from NNW as the active thrust sheet had slowed down or halted completely caused out-of-sequence deformation in the form of a pop-up structure in the hinge of the syncline involving the Vollen and Arnestad formations. The northwestern limb of the syncline is explained by the sub-surface ramp structure, and the southeastern limb is explained by a fault-propagation fold involving the Tøyen, Huk, and Elnes formations at Hukodden (Sub-area 1). Another repetition of the Huk Fm. is apparent in the skerries south of Hukodden (Sub-area 1), and has been interpreted as second fault-propagation fold. Another ramp structure underlying the fault-propagation folds is needed to accommodate (?) the stratigraphic thickness and dip of the strata involved in the syncline. Figure can also be found in Appendix 3 (Plate 6).

### 5.2.6 Sub-area 5: Western side of the Huk naturist beach

Sub-area 5 comprises the shoreline along the southwestern side of the headland that is the naturist beach. The synform and antiform in Sub-area 4 are observed to continue in the Vollen Fm. beds in Sub-area 5 (Fig. 5.2.1). The continuation of the backthrust from Sub-area 4 is present, but more difficult to observe in Sub-area 5 due to poor outcrops, and the break between the Elnes and Vollen formations is wider and more eroded here.

The full Elnes Fm. sequence is separated from the underlying Vollen Fm. by a break in the outcrop. Whereas the Elnes Fm. sequence in Sub-area 4 showed a general dip towards SE, the same sequence in Sub-area 5 dips towards NW (Fig. 5.2.1). At the northwestern end of Sub-area 5, four repetitions of the Huk Fm. are visible in outcrops. The southernmost of these is the core of an upright anticline where the Elnes Fm. sequence along the naturist beach comprises the southeastern fold limb. Three other repetitions of Huk Fm. and Galgeberg Mb. (Upper Tøyen) are separate thrust sheets overriding the northwestern fold limb of the anticline (Fig. 5.2.1 and Fig. 5.2.6.2).



Fig. 5.2.6.1: Small-scale folding in the Håkavik Mb. (Upper Elnes). Backpack for scale.

The Håkavik Mb. (Upper Elnes) that structurally overlies the Vollen Fm. is almost twice as thick in the outcrop as its calculated vertical thickness at Huk (Appendix 1), and the shale is intensely deformed by small-scale folds (Fig. 5.2.6.1 and Fig. 5.2.6.2). The preferred explanation is that a syncline-anticline pair in the Håkavik Mb. was created when the larger anticline of Sub-area 5 was thrust over the ramp in the sub-surface (Fig. 5.2.6.2 and Fig. 5.2.6.3). The small-scale folds are interpreted as parasite folds associated with the fold hinge of the syncline-anticline pair.

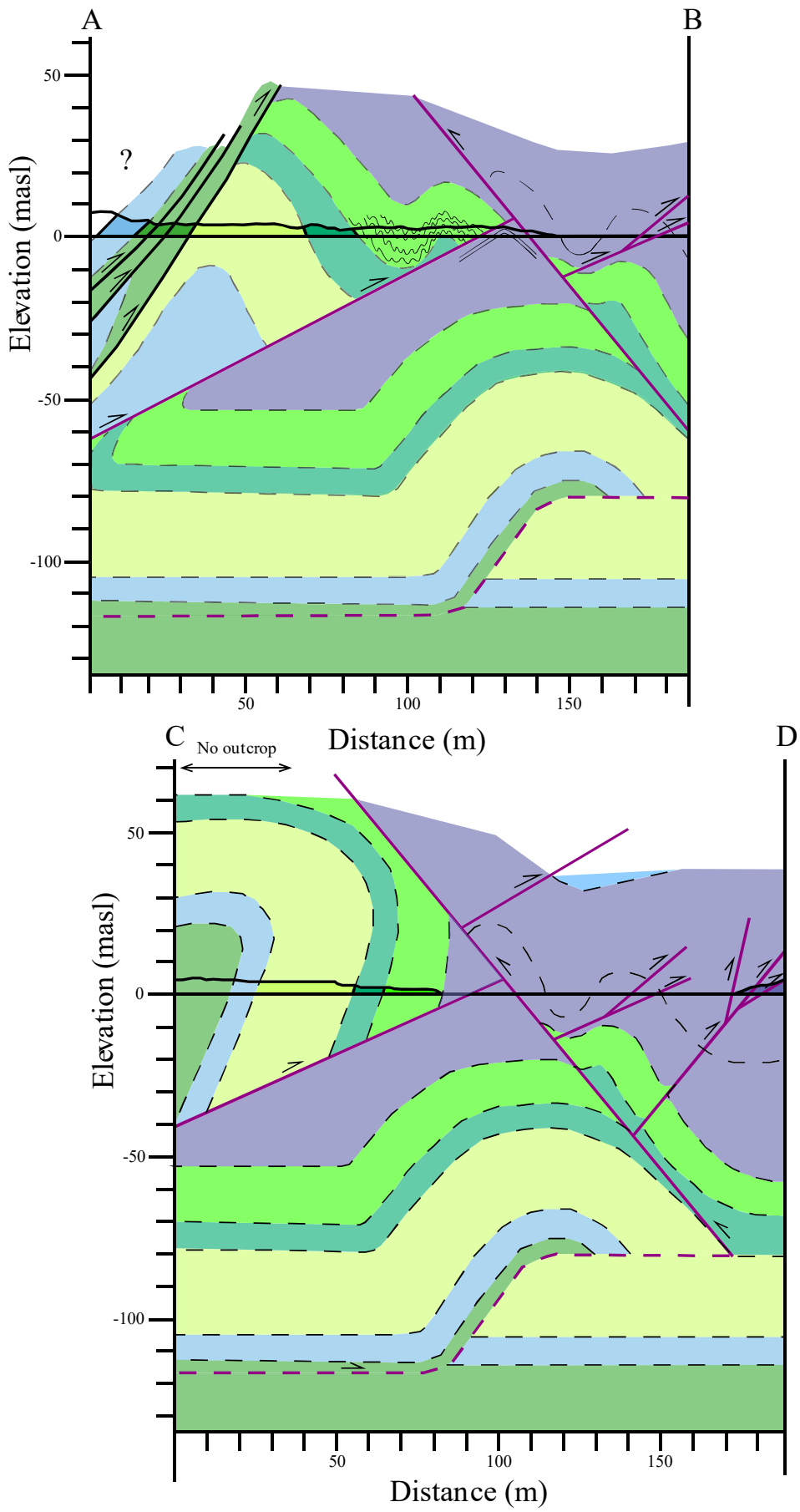


Figure 5.2.6.1: Figure text on next page

Figure 5.2.6.1: Cross-sections AB and CD, not balanced. Legend can be found in Figure 5.2.2. The two profiles, AB and CD, are aligned according to their mutual location on the map. This way, the cross-fault juxtaposition of the features in the profiles is retained by moving vertically from one profile to the other in the figure.

Cross-section AB shows the southwestern side of the headland (Sub-area 5) interpreted as an anticline that has been thrust over a ramp structure in the sub-surface. The northwestern fold limb contains three thrust faults that have caused repetitions of the Tøyen and Huk formations to be visible in the surface at ground level. The southeastern fold limb contains parasite folds in the shale of the Elnes Fm., and the fold limb is folded so the Håkavik Mb. is almost doubled in thickness in the outcrop along the beach.

Cross-section CD shows a section of Sub-area 4 parallel to the northwestern part of balanced cross-section EF. The northeastern side of the headland (Sub-area 4) is interpreted as a simple overturned anticline that has been thrust over ramp structure in the sub-surface.

Beds of the Vollen Fm. comprise the tip of the headland SE of the folded beds of the Elnes Fm. at both Sub-area 4 and 5. The two formations are separated by an inferred thrust fault, with the folded Elnes Fm. overlying an anticline in the Vollen Fm. The lateral break in fold geometry in the Elnes Fm. folds on either side of the headland can be explained by a Caledonian tear fault that cuts through the headland and terminates in the inferred thrust fault that separates the Elnes and Vollen formations. This is illustrated in Figure 5.2.6.3. Figure can also be found in Appendix 3 (Plate 5).

The break in lateral continuity between the northwestern and southeastern sides of the headland can be explained by a Caledonian tear fault that cut through the anticline as it formed, allowing the southeastern side to become overturned whilst the northwestern side stayed upright (Fig. 5.2.6.2, Fig. 5.2.6.3, Table 5.4.2, and Table 5.4.3). The inferred thrust that separates the Elnes and Vollen formations at the tip of the headland is interpreted as the active thrust fault on which the two tear blocks moved (Fig. 5.2.6.2 and Fig. 5.2.6.3)

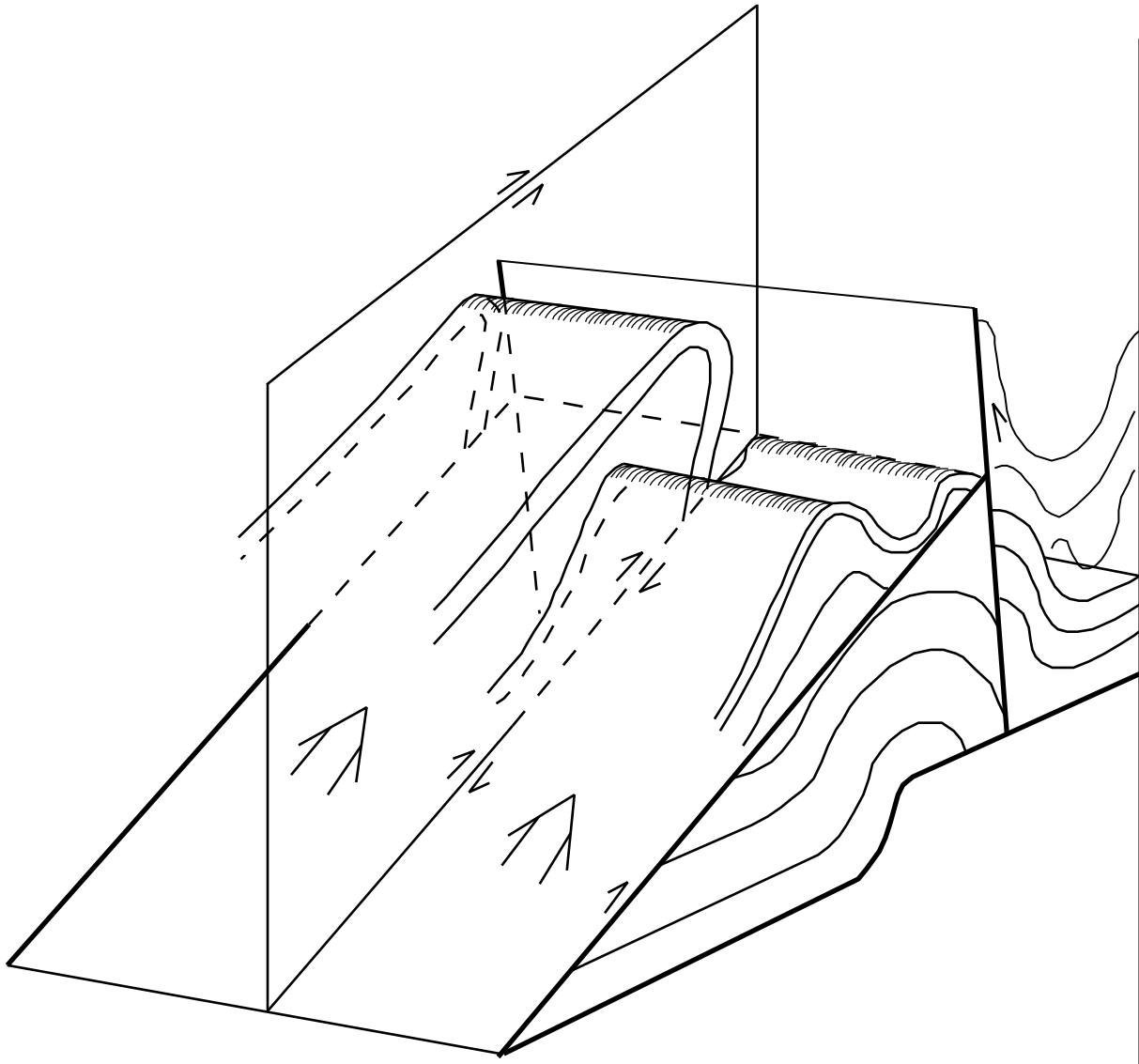


Figure 5.2.6.3: The structural interpretation shown in Profiles AB and CD from Figure 5.2.6.2 sketched in 3D perspective.

### 5.2.7 Sub-area 6: Hukodden, the headland east of the bay

Sub-area 6 comprises the headland east of the Hukodden bay. The large structure that stands out against the low topography of the beach is hereafter informally referred to as the Hukodden imbricate system (Fig. 5.2.7.2 and Fig. 5.2.7.3). The Hukodden imbricate structure consist of three repetitions (imbricate units) of the Huk Fm., which in some places are accompanied by dark shales of the Elnes and Tøyen formations (Fig. 5.2.7.1, Fig. 5.2.7.2, and Fig. 5.2.7.3). Right way up directions for all three repetitions has been determined by examining *Cycloendoceras commune* fossils in the Svartodden Mb. (Upper Huk). The three shale-and-limestone imbricate units are separated by top-to-southeast thrusts that are visible in

outcrops on the western and eastern side of the structure, but are covered by debris in the middle. Due to the complicated nature of the Hukodden imbricate structure, the mapping of Sub-area 6 was carried out in great detail as shown in the map in Figure 5.2.7.1. The map is at a scale that makes it possible to differentiate between the different members of the Huk Fm., something that is vital for understanding the geometry of this structure (Fig. 5.2.7.1, Fig. 5.2.7.2, and Fig. 5.2.7.3).

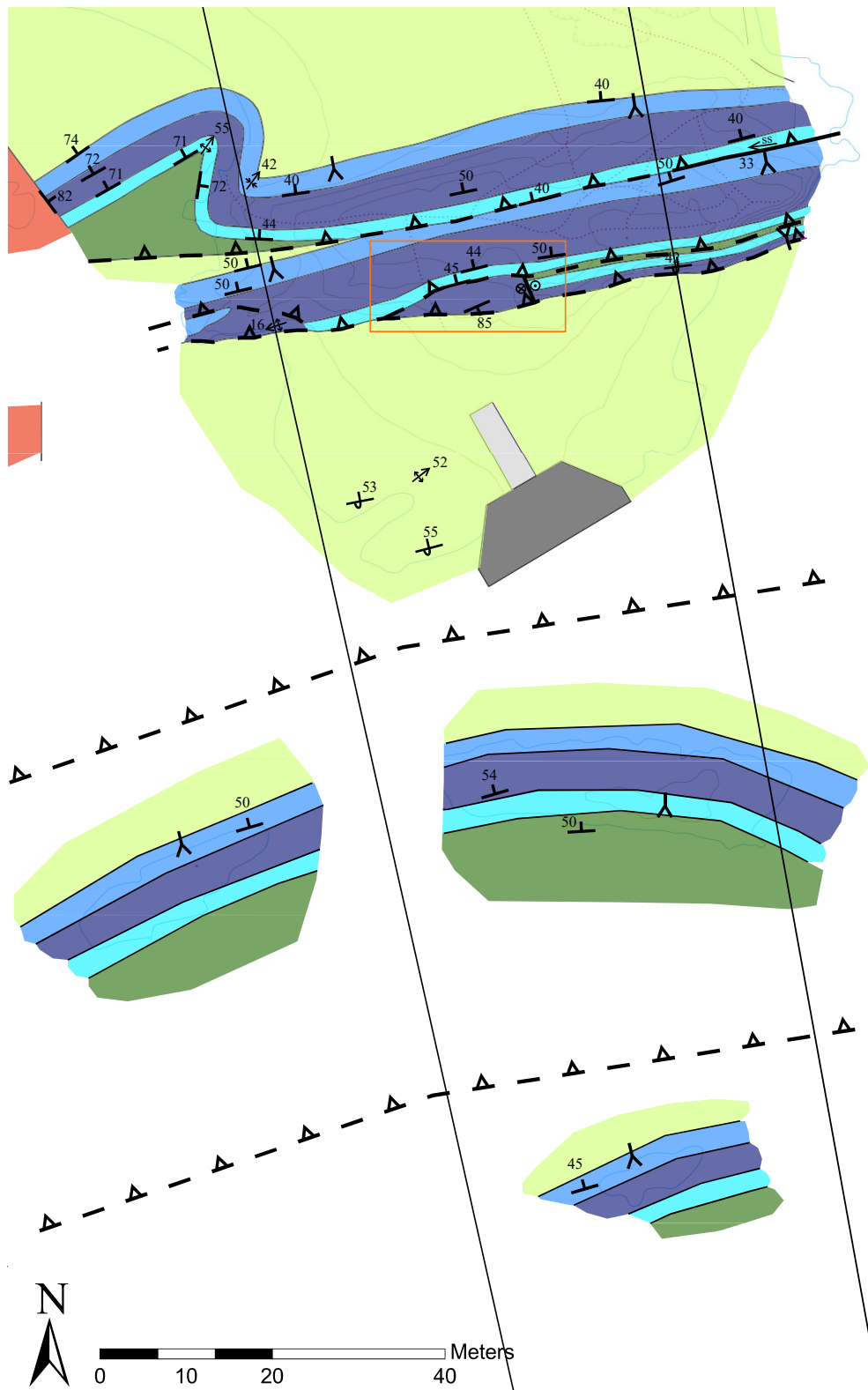


Figure 5.2.7.1: Detailed map of Sub-area 6, the headland east of Hukodden bay. Legend can be found in Figure 5.2.2. Structures and lithologies visible at low tide has been included, even though the topography of the map reflects a time of high tide. The western line of section corresponds to the GH-line of the larger scale Huk map, and the eastern line of section corresponds to the IJ-line of the larger scale Huk map. Figure can also be found in Appendix 3 (Plate 2).





Figure 5.2.7.2: Drone photo of the Hukodden imbricate structure. The boundaries between lithological units, as well as the name of the units have been marked in dark blue. Right way up indicators are included in orange, but faults, other structures, and measurements have not been marked on the figure. Figure can also be found in Appendix 3 (Plate 12).



Figure 5.2.7.3: Photo of the Hukodden imbricate structure taken from SW to give a view of the structure from the southwestern side.

Bedding in the northernmost (upper) imbricate unit dips towards the NNW, and lies in a right way up position according to the *Cycloendoceras commune* fossils in the Huk Fm. The Sjøstrand Mb. of the Elnes Fm. (Lower Elnes) directly overlies the Svartodden Mb. (Upper Huk) in Sub-area 6. This can be seen in outcrops accessible at low tide. The on shore area north of the Hukodden imbricate structure is artificially covered by fine beach sand.

Low tide in the Hukodden bay also reveals a syncline-anticline pair of tight folds in the uppermost Huk Fm. repetition. The folds plunge towards NNE, and are only visible at ground level on the western side of the structure.

The depositional (stratigraphic) boundary between the Hukodden Mb. limestone (Lower Huk) and the black shales of the Tøyen Fm. in the upper imbricate unit can be observed in the little beach nook on the western side of the structure (Fig. 5.2.7.3). Here, the Tøyen shales structurally overlie dark Sjøstrand (Lower Elnes) shales, which in turn overlie massive limestone of the Svartodden Mb. (Upper Huk) in the middle imbricate unit. These two black shale units form a wedge that tapers off eastwards before reaching the middle of the outcrop where the Hukodden Mb. limestone (Lower Huk) of the upper imbricate unit directly overlies

the Svartodden Mb. limestone (Upper Huk) of the middle imbricate unit. The tectonic boundary between the Tøyen and Elnes shales and the two Huk limestones is mostly obscured by shrubbery and dirt, but the top-to-southeast thrust is visible with slicken fibres on the eastern side of the Hukodden imbricate structure.

At the western side of Sub-area 6, the middle imbricate unit of the Hukodden imbricate structure consists of the Sjøstrand Mb. shales (Lower Elnes) seen in the beach nook (Fig. 5.2.7.3), as well as the two upper members of the Huk Fm. The Hukodden Mb. (Lower Huk) is missing. The imbricate unit dips NNW in right way up position as indicated by the *Cycloendoceras commune* fossils in the Svartodden limestone (Upper Huk). The middle imbricate unit overlies a basal imbricate unit consisting of folded limestone of the Svartodden Mb. (Upper Huk) and nodular limestone of the Lysaker Mb. (Middle Huk). The fold hinge, exposed by the Lysaker Mb., plunges towards SW. The forelimb is steeply dipping to overturned, and the backlimb has a similar orientation to the two overlying thrust sheets (imbricate units). The fold has a SE vergence.

The boundary between the two lowermost imbricate units is an in part undulating thrust plane. Moving eastwards along strike, this undulating thrust plane makes a southward excursion and cuts out the Lysaker Mb. fold hinge in the basal imbricate unit (see Fig. 5.2.7.1 and Fig. 5.2.7.2). Continuing eastwards, the undulating thrust plane swings back northwards. This again exposes the folded Lysaker Mb. nodular limestone in the basal imbricate unit south of the Hukodden Mb. of the middle imbricate unit.

Further east, the Lysaker Mb. fold hinge abruptly stops at a fault contact against an overturned succession of a thin sliver of the Tøyen Fm. (top of the lower imbricate unit), Hukodden Mb. (Lower Huk), and the Lysaker Mb. (Middle Huk, base of imbricate unit). The fault plane of this contact is measured to 154/87 where it is seen to cut the massive limestone of the Hukodden Mb. (Lower Huk). The fault does not cut up into the overlying middle imbricate unit, nor does it cut down into the underlying Elnes Fm. There are no slickenlines or calcite infill present, but the differing geological units and structures on either side indicate that this is a minor tear fault within the Hukodden imbricate structure (Table 5.4.1, Table 5.4.2, and Table 5.4.3). The difference in geology on either side of this fault is apparent in the cross-sections (Fig. 5.2.7.4 and Fig. 5.2.7.5)

At the eastern side of the outcrop, the thrust plane of the middle imbricate unit has evened out and is no longer undulating. Immediately above it lies the black shales of the Tøyen Fm. with

the depositional boundary to the overlying Hukodden Mb. (Lower Huk). Thus, the thrust plane in this area separates the Tøyen Fm. in the right way up position in the middle imbricate unit above, from the Tøyen Fm. in inverted position in the basal imbricate unit below.

The middle and lower members of the Huk Fm. in the imbricate units along the southern side of the Hukodden imbricate structure directly overlie dark shales of the Sjøstrand Mb. (Lower Elnes) that form the beach in the southern part of the headland. This implies that the entire southern side of the Hukodden imbricate structure is bounded by a thrust fault. In some places, it is difficult to observe the contact due to artificial beach sand, shrubbery, or manmade dirt paths. No calcite infill or slickensides are observed along this thrust.

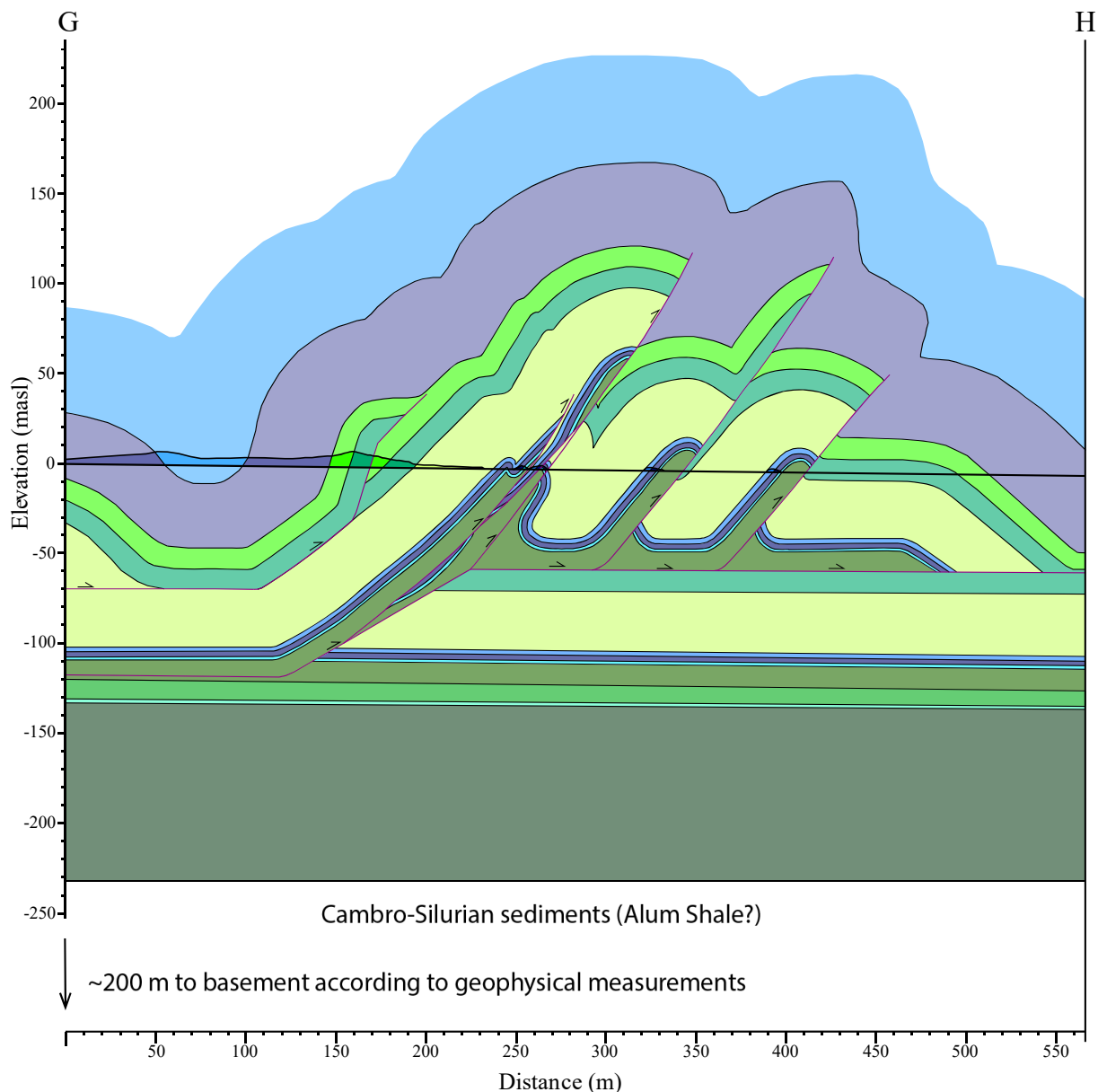


Figure 5.2.7.4: Balanced cross-section GH. Profile GH runs from east of Maurtubukta (Sub-area 3 and 7) in the north, to south of Hukskjæra in the south (Sub-area 6). Legend can be found in Figure 5.2.2. This cross-section illustrates the western side of Sub-area 6, where the basal imbricate unit consists of folded Lysaker Mb. (Middle Huk) at ground level. In the northern parts of this profile, the geology is not exposed, except for a minor outcrop of southwards dipping Vollen Fm. In the south, repetitions of the Tøyen, Huk, and Elnes formations are involved in a complicated imbricate fan. The imbricate fan is part of a larger ramp structure. To the north of the imbricate fan, there are repetitions of the upper part of the Elnes Fm. The imbricate fan seems to be developed on a detachment zone in the upper part of the Tøyen Fm., which is the oldest formation observed to be involved. Thus, the involvement of the Alum Shale Fm. is not called for. The development of the structure is further explained in Figure 5.2.7.9. Figure can also be found in Appendix 3 (Plate 7).

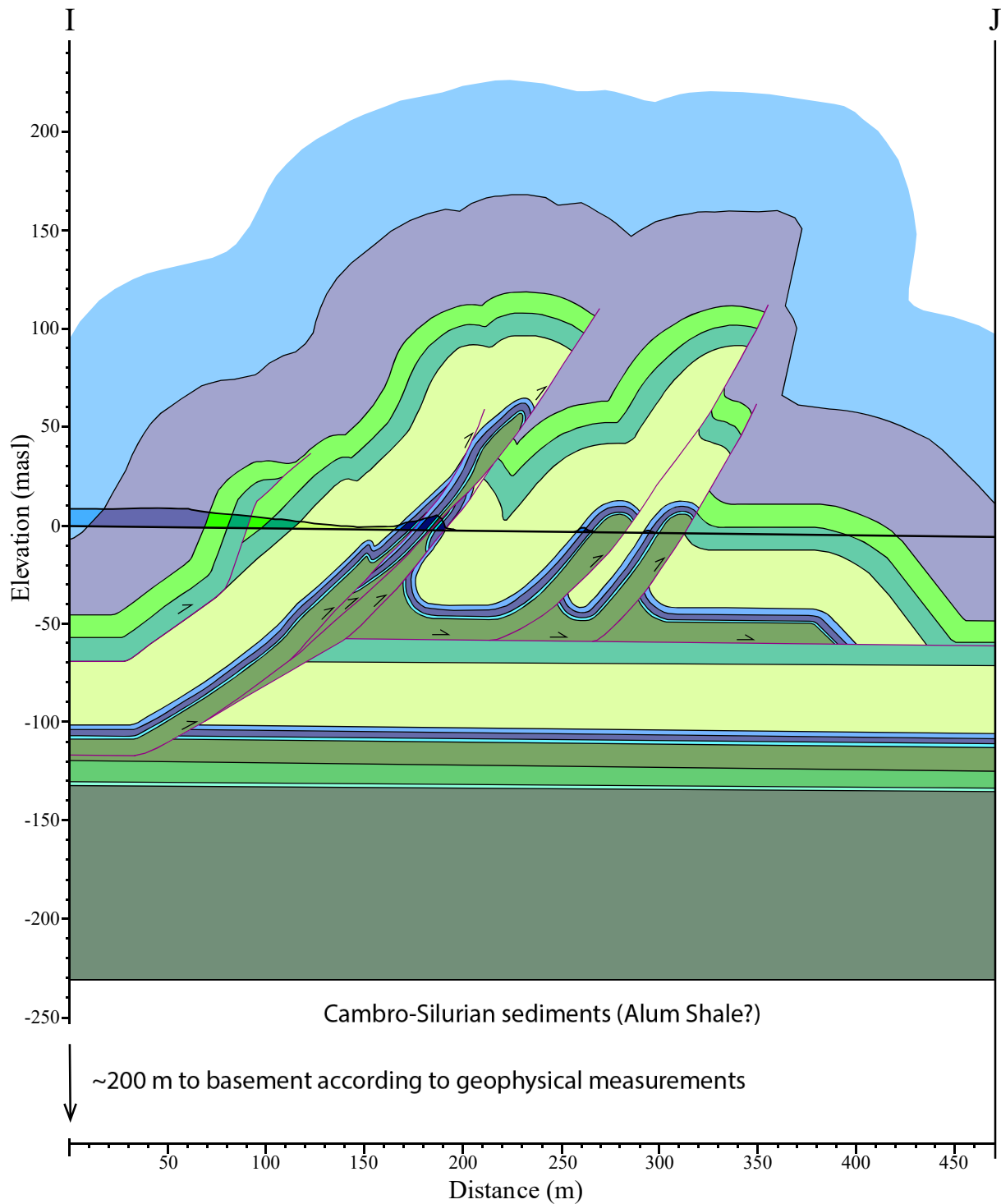


Figure 5.2.7.5: Balanced cross-section IJ. Legend can be found in Figure 5.2.2. This cross-section illustrates the eastern side of Sub-area 6, where the basal imbricate unit consists of overturned Tøyen and Huk formations in the outcrops. In the northern parts of this profile, the geology is not exposed, and is inferred from profile GH. The cross-section portrays the same imbricate fan as cross-section GH, with some local variations. In addition to the differences of the basal imbricate unit of the Hukodden imbricate structure, the syncline-anticline fold pair at the upper imbricate unit of the Hukodden imbricate structure does not breach the surface. The development of the structure is further explained in Figure 5.2.7.10. Figure can also be found in Appendix 3 (Plate 9).

In summary, the complex thrust system in Sub-area 6 consists of a SE verging fold split into three imbricate units. The two upper imbricate units consist of bedding right way up, and the bottom imbricate unit consists of the fold hinge of the fold in fault contact with overturned bedding of the Tøyen and Huk formations. The upper imbricate unit carries a SE-verging fold, which is only visible at the western end of the structure (Fig. 5.2.7.1, Fig. 5.2.7.2, Fig. 5.2.7.4, and Fig. 5.2.7.5).

A proposed model to explain this structure is a SE-verging fault-propagation anticline formed in the hanging-wall of a ramp structure and repeatedly cut and displaced by second and third order thrusts (splays from the detachment zone and splays from other splays). This interpretation can be seen in profiles GH (Fig. 5.2.7.4) and IJ (Fig. 5.2.7.5), each supported by a figure explaining the development of the structure through time by illustrating the steps in the palinspastic restoration of the balanced cross-sections (although only the part of the cross-section that covers the Hukodden imbricate structure; Fig. 5.2.7.9 and 5.2.7.10). The two cross-sections run on each side of the structure to illustrate the difference in geology on the western and eastern side of the postulated tear fault in the bottom thrust sheet (Fig. 5.2.1, Fig. 5.2.7.1, Fig. 5.2.7.6, and Fig. 5.2.7.7).

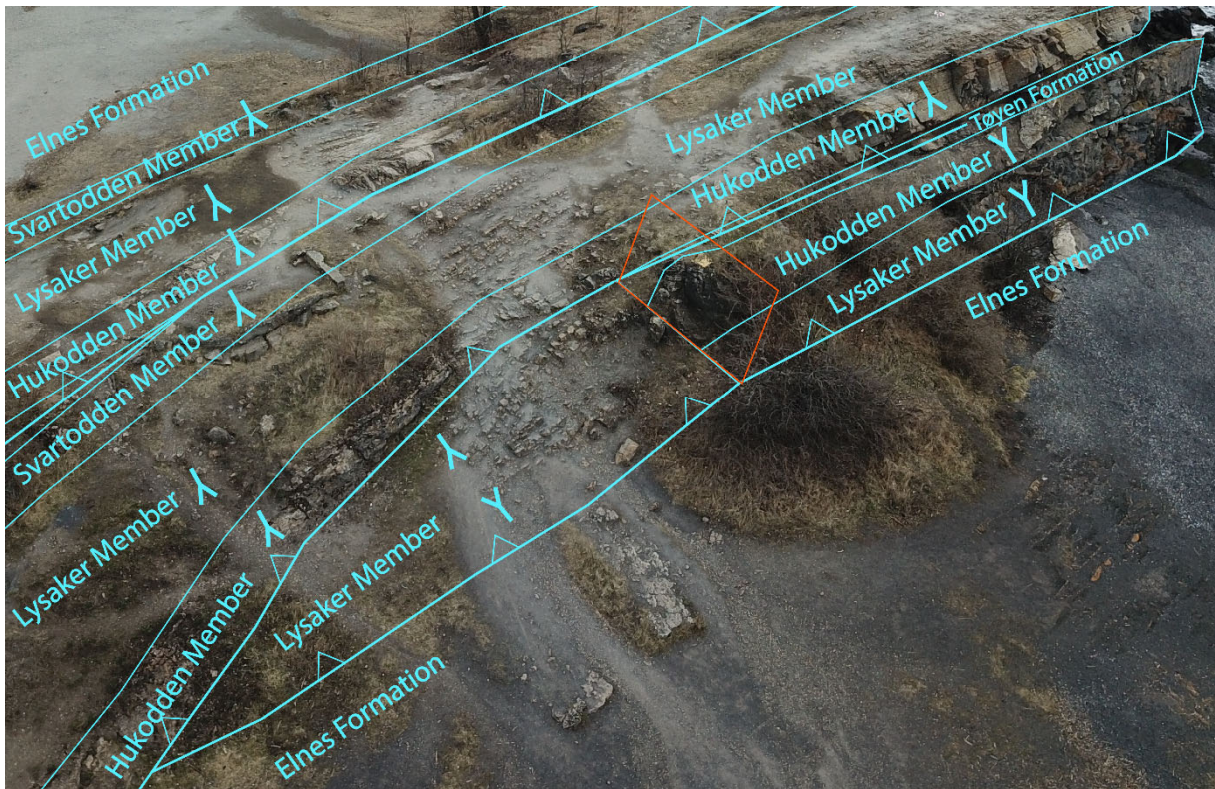


Figure 5.2.7.6: Drone photo of the Hukodden imbricate structure taken from SW. The boundaries between lithological units, as well as the name of the units have been marked in light blue. Right way up indicators are included, and the fault plane of the identified tear fault is marked in orange. The unmarked «rocks» that appear at the bottom of the photograph are pieces of concrete.

In the lower imbricate unit of the Hukodden imbricate structure, the section of the overturned forelimb of the fault-propagation fold (Fig. 5.2.7.5, east) is, by a minor tear fault, juxtaposed with the section of the fold hinge (Fig. 5.2.7.4, west). This relationship is illustrated in Figure 5.2.7.6 and Figure 5.2.7.7. The eastern tear block has most likely propagated forwards further than the western tear block. This lateral displacement, with no evidence of the deformation continuing into the overlying thrust sheet indicates a tear fault in an out of sequence thrust system. The lower imbricate unit was evidently split by tear faulting before the next imbricate unit of the sequence was emplaced on top of it (Fig. 5.2.7.7).



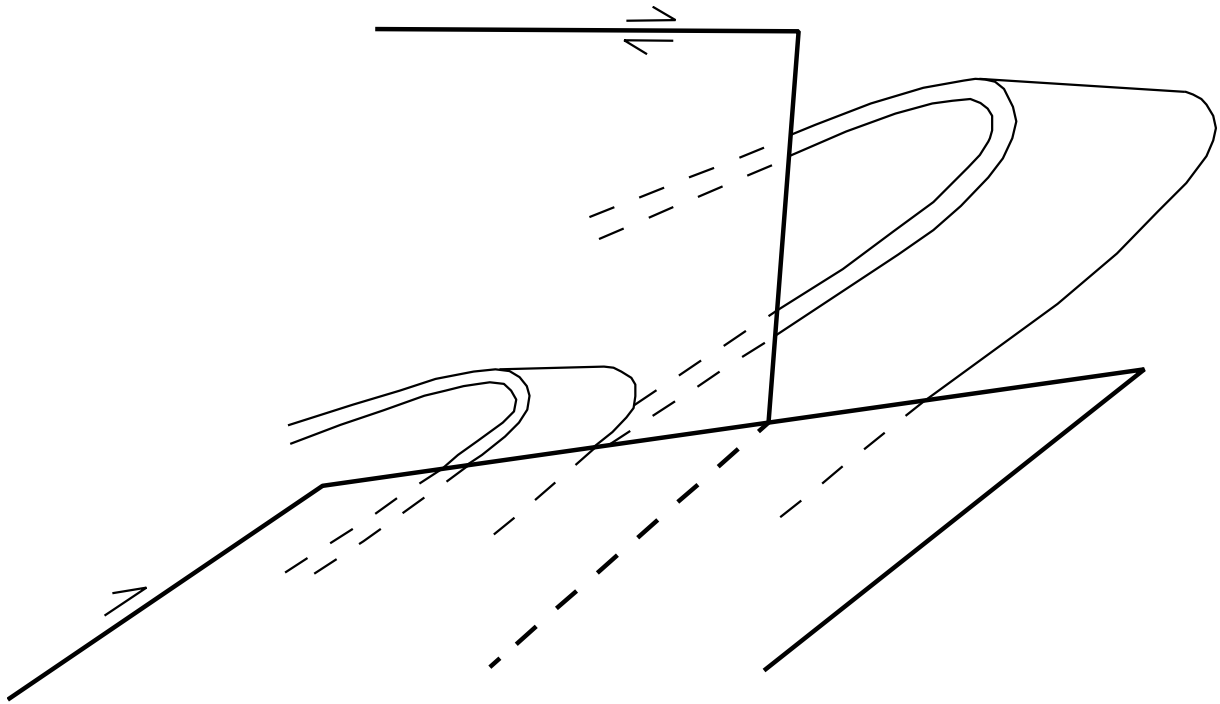


Figure 5.2.7.7: The structural interpretation of the tear fault shown in Figure 5.2.7.6 sketched in 3D perspective. Progressive deformation on either side of the fault is illustrated in Figure 5.2.7.9 and Figure 5.2.7.10.



Figure 5.2.7.8: Fold in the Sjøstrand Mb. (Lower Elnes) by the concrete quay. The quay can be seen in Figure 5.2.1, Figure 5.2.7.1, and Figure 5.2.7.2.

The Sjøstrand Mb. (Lower Elnes) that comprises the beach south of the Hukodden imbricate structure sits in the syncline formed between the Hukodden imbricate structure and the Hukodden skerries (Fig. 5.2.7.4 and Fig. 5.2.7.5). Folds can be observed in the dark shales close to the quay, and are thought to have formed as a result of the array of fault-propagation folds (Fig. 5.2.7.8). Due to its SE vergence, the fold in Figure 5.2.7.8 is thought to be a parasite fold on the backlimb of the middle fault-propagation fold.

Two repetitions of the Huk Fm. with Elnes Fm. shale above and Tøyen Fm. shale below are found in the skerries located in the sea some 60 meters south of the Hukodden imbricate structure (Figs. 5.2.1 and 5.2.7.1). The two repetitions are interpreted as two additional fault-propagation folds (Fig. 5.2.7.4 and Fig. 5.2.7.5). Together with the Hukodden imbricate structure fault-propagation fold, these make up an imbricate structure, either an imbricate fan or a duplex missing its roof thrust due to erosion. As any potential roof thrust lies above today's erosional level, it is not possible to say for certain. However, when balancing the profiles (Fig. 5.2.7.4 and Fig. 5.2.7.5), it became apparent that it was very difficult to follow the balancing guide of Woodward et al. (1989) and produce a duplex structure with a sub-horizontal roof thrust. Therefore, this structure is interpreted to be an imbricate fan, as illustrated in profiles GH (Fig. 5.2.7.4) and IJ (Fig. 5.2.7.5).

On drone photos, it looks like the NW skerries in Sub-area 6 have been cut in the middle, possibly by the syenite porphyry dyke and the postulated tear fault. However, there is no discernible change in dip of the beds or in deformation on either side of the skerries, and inspection of the break from canoe revealed no evidence of syenite porphyry dyke or faulting here (Fig. 5.2.1 and Fig. 5.2.7.1).

The sole thrust of the imbricate fan is postulated to run in the dark shales of the Galgeberg Mb. of the Tøyen Fm. The decision to place a local detachment zone in this lithological unit is based on field observations. Repetitions of the Huk Fm. appear in clusters in Sub-area 5 and 6, and the thrust displacing the limestone almost always runs within the underlying Tøyen shales. Lithological units older than the Tøyen Fm. are never observed to be included in these thrust systems. It is therefore reasonable to assume the thrusts displacing the Huk Fm. limestones are splays from a detachment zone within the Galgeberg Mb. (Upper Tøyen).

This conforms well with Bruton et al. (2010) who suggests there are local detachment zones within the black shales of the Lower to Middle Ordovician. The more competent units

between the black shales cause ramps to form between the flats. The ramps, in turn, form imbricate stacks.

Considering the stratigraphic thickness of the exposed lithologies (Appendix 1), and their dips of the beds, the presence of a ramp at depth is necessary in order to construct a balanced cross-section. Based on observations in the field, it seems most likely that the ramp is linked to flats in the shales of the Tøyen and Elnes formations. The development of the Hukodden imbricate structure from layercake stratigraphy to the structure observable in outcrops today can be seen in Figure 5.2.7.9 and 5.2.7.10.

# Illustration of the steps in the palinspastic restoration of the Hukodden imbricate structure in balanced cross-section GH

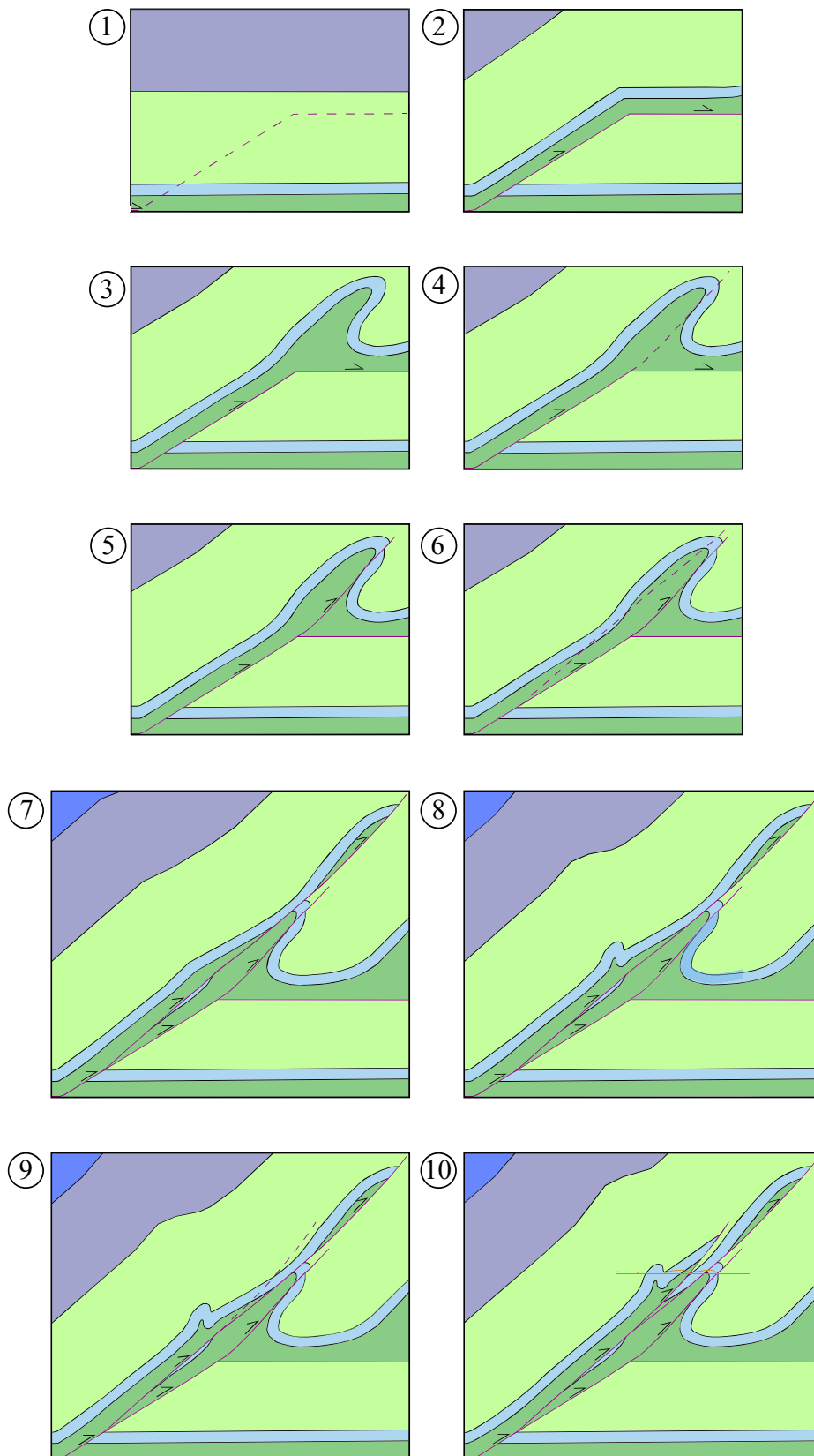


Figure 5.2.7.9: Figure text on next page

Figure 5.2.7.9: Figure illustrating the steps of the palinspastic restoration of the Hukodden imbricate structure in balanced cross-section GH (Fig. 5.2.7.4) at the western side of the Hukodden imbricate structure. Figure can also be found in Appendix 3 (Plate 8). Legend can be found in Figure 5.2.2. The figure is a cartoon that illustrates the progressive deformation of the Hukodden imbricate structure and each step illustrates either the formation of a new fault or fold, or the displacement along a fault. New faults forming are indicated by stippled lines, and arrows indicate movement along active faults. The figure is constructed along the same line of section as cross-section GH (Fig. 5.2.7.4) and is made to scale.

1: The layers are undeformed in a horizontal position, with a detachment zone within the Tøyen Fm. cutting towards to left of the figure. Stippled line indicates where the formation of a ramp will form.

2: A thrust fault cuts from the detachment zone in the Tøyen Fm. through the Huk Fm. and into the Elnes Fm., resulting in a ramp-flat structure.

3: As seen in Figure 5.2.7.4, multiple fault-propagation folds have formed in the hanging-wall of the ramp-flat structure, out of frame of this figure. As the hanging-wall of the ramp-flat structure is unable to propagate forwards (towards the left of the figure), a fold forms above the ramp. The structural relationship between lithologies of the Hukodden imbricate structure visible at ground level today relies on the fold shape seen in step 3.

4: A second order thrust (splay) branches off the detachment zone and cuts through the overturned forelimb of the fold just below to the fold hinge.

5: Displacement along the second order thrust juxtaposes the fold hinge within the Lysaker Mb. (Middle Huk) with the Elnes Fm., which corresponds to field observations (Fig. 5.2.7.1 and Fig. 5.2.7.2).

6: A new second order thrust forms and cuts through the Tøyen Fm. and Huk Fm. of the backlimb before cutting through the Tøyen Fm. and Huk Fm. of the fold hinge.

7: Displacement along the second order fault juxtaposes the Lysaker Mb. (Middle Huk) of the backlimb (middle imbricate unit) with the Lysaker Mb. of the fold hinge (bottom imbricate unit). This corresponds to field observations (Fig. 5.2.7.1 and Fig. 5.2.7.2). The backlimb sees a thick layer of Tøyen Fm. shale underlying the Huk Fm. in the hanging-wall flat of the ramp. The Tøyen Fm. layer thins along the splay to where the splay cuts through the Huk Fm.

8: As the hanging-wall of the detachment zone propagates forwards, a syncline-anticline pair forms in the backlimb of the fold where the layer of Tøyen Fm. starts to wedge out.

9: A third order thrust branches off the second order thrust from step 6. It cuts through the wedge of Tøyen Fm. and the overlying Huk Fm.

10: Displacement along the third order fault juxtaposes the Elnes Shale of the middle imbricate unit with the Tøyen Shale of the upper imbricate unit. This corresponds to field observations (Fig. 5.2.7.1, Fig. 5.2.7.2, and Fig. 5.2.7.3). Today's topography has been marked in orange. This 10<sup>th</sup> step corresponds to cross-section GH (Fig. 5.2.7.4). The Hukodden imbricate structure has been interpreted as a fault-propagation fold that has been cut through and displaced by two second order thrusts and one third order thrust. The Hukodden imbricate structure also has a syncline-anticline pair in its backlimb, which breaches the surface in the west. The interpretation presented in this figure and in cross-section GH (Fig. 5.2.7.4) is only one possible solution to the surface field observations on the western side of the Hukodden imbricate structure.

# Illustration of the steps in the palinspastic restoration of the Hukodden imbricate structure in balanced cross-section IJ

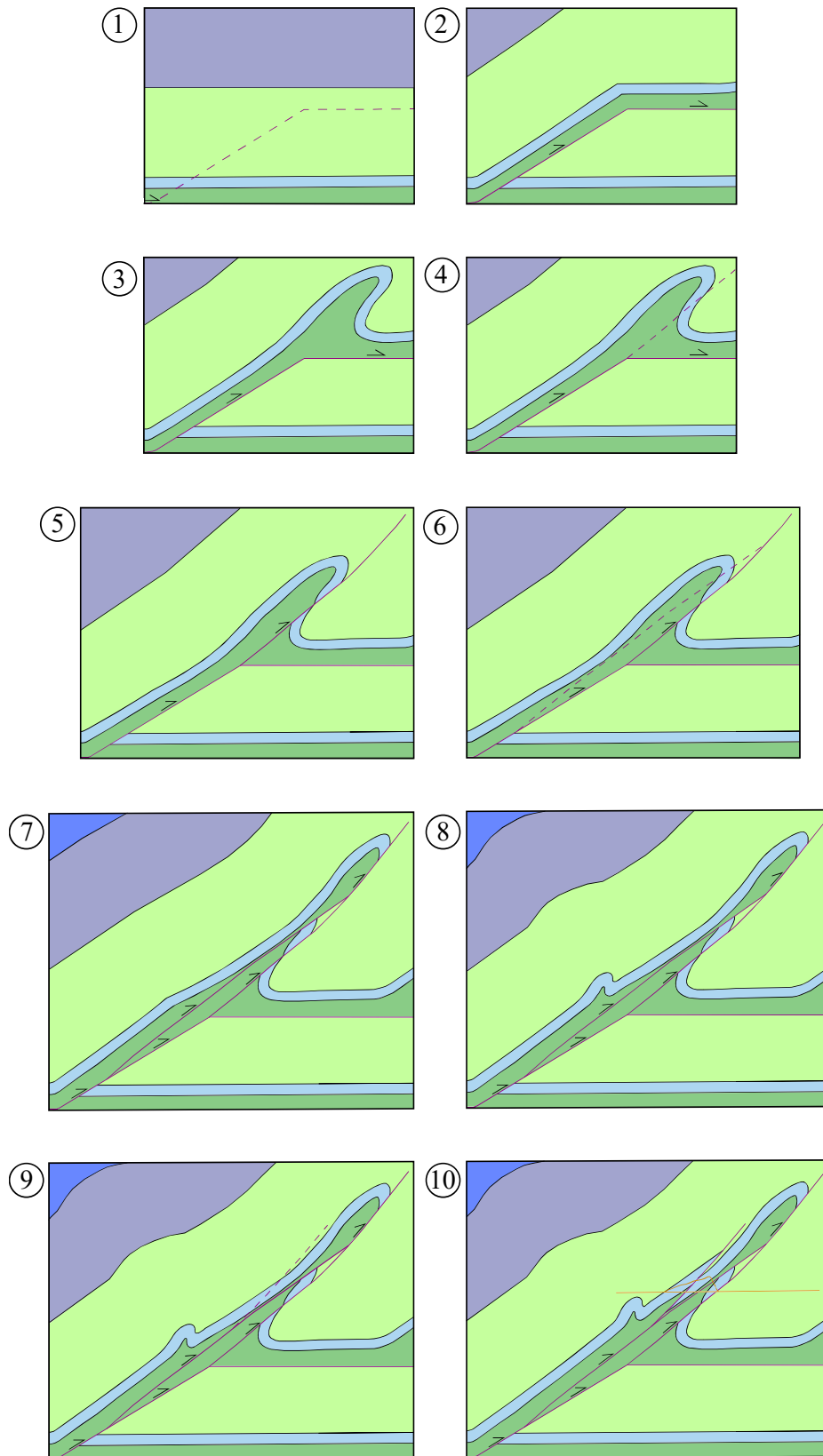


Figure 5.2.7.10: Figure text on next page.

Figure 5.2.7.10: Figure illustrating the steps of the palinspastic restoration of the Hukodden imbricate structure in balanced cross-section IJ (Figure 5.2.7.5) at the eastern side of the Hukodden imbricate structure. Figure can also be found in Appendix 3 (Plate 10). Legend can be found in Figure 5.2.2. The figure is a cartoon that illustrates the progressive deformation of the Hukodden imbricate structure and each step illustrates either the formation of a new fault or fold, or the displacement along a fault. New faults forming are indicated by stippled lines, and arrows indicate movement along active faults. The figure is constructed along the same line of section as cross-section IJ (Fig. 5.2.7.5) and is made to scale.

1: The layers are undeformed in a horizontal position, with a detachment zone within the Tøyen Fm. cutting towards to left of the figure. Stippled line indicates where the formation of a ramp will form.

2: A thrust fault cuts from the detachment zone in the Tøyen Fm. through the Huk Fm. and into the Elnes Fm., resulting in a ramp-flat structure.

3: As seen in Figure 5.2.7.5, multiple fault-propagation folds have formed in the hanging-wall of the ramp-flat structure, out of frame of this figure. As the hanging-wall of the ramp-flat structure is unable to propagate forwards (towards the left of the figure), a fold forms above the ramp. The structural relationship between lithologies of the Hukodden imbricate structure visible at ground level today relies on the fold shape seen in step 3. So far, the progression of the eastern side of the Hukodden imbricate structure has not diverged from the western side (Fig. 5.2.7.9)

4: A second order thrust (splay) branches off the detachment zone and cuts through the overturned forelimb of the fold below to the fold hinge. The splay cuts the forelimb further away from the fold hinge in the east than in the west (Fig. 5.2.7.9). An undulating thrust plane of the second order thrust cutting downwards towards the east can explain this. The presence of an undulating thrust plane cannot explain the juxtaposition of the Lysaker Mb. (Middle Huk) fold hinge and the overturned Hukodden Mb. (Lower Huk) illustrated in Figure 5.2.7.1, Figure 5.2.7.2, and Figure 5.2.7.6.

5: Displacement along the second order thrust juxtaposes the overturned Lysaker Mb. (Middle Huk) with the Elnes Fm., which corresponds to field observations (Fig. 5.2.7.1 and Fig. 5.2.7.2).

6: A new second order thrust forms and cuts through the Tøyen Fm. of the backlimb before cutting through the Tøyen Fm. and Huk Fm. just below the fold hinge. The fault has been interpreted to merge with the first second order thrust, but this is just one possible interpretation. It is also possible that the new second order thrust cuts upwards to create a more listric fault geometry. In this interpretation, the two second order thrusts encloses the middle imbricate unit, making the middle imbricate unit a horse in the Hukodden imbricate structure.

7: Displacement along new the second order fault from step 6 juxtaposes the Tøyen Fm. of the backlimb (middle imbricate unit) with the Tøyen Fm. of the overturned forelimb (bottom imbricate unit). This corresponds to field observations (Fig. 5.2.7.1 and Fig. 5.2.7.2). As with the western side of the Hukodden imbricate structure (Fig. 5.2.7.9), the backlimb of the eastern side sees a thick layer of Tøyen Fm. shale underlying the Huk Fm. in the hanging-wall flat of the ramp. The Tøyen Fm. layer thins along the splay to where the splay cuts through the Huk Fm.

8: As the hanging-wall of the detachment zone propagates forwards, a syncline-anticline pair forms in the backlimb of the fold where the layer of Tøyen Fm. starts to wedge out. The plunge of the syncline-anticline pair measured at ground level in the field suggests the fold pair forms at a greater depth on the eastern side of the backlimb than on the western side (Fig. 5.2.7.9). This explains why the fold pair

is only visible on the western side of the Hukodden imbricate structure (Fig. 5.2.7.1, Fig. 5.2.7.2, Fig. 5.2.7.4, and Fig. 5.2.7.5).

9: A third order thrust branches off the second order thrust from step 6. It cuts through the wedge of Tøyen Fm. and the overlying Huk Fm.

10: Displacement along the third order fault juxtaposes the Svartodden Mb. (Upper Huk) of the middle imbricate unit with the Hukodden Mb. (Lower Huk) of the upper imbricate unit. This corresponds to field observations (Fig. 5.2.7.1 and Fig. 5.2.7.2). Today's topography has been marked in orange. This 10<sup>th</sup> step corresponds to cross-section IJ (Fig. 5.2.7.5). The Hukodden imbricate structure has been interpreted as a fault-propagation fold that has been cut through and displaced by two second order thrusts and one third order thrust. The Hukodden imbricate structure also has a syncline-anticline pair in its backlimb, which does not breach the surface in the east. The interpretation presented in this figure and in cross-section IJ (Fig. 5.2.7.5) is only one possible solution to the surface field observations on the western side of the Hukodden imbricate structure.

## 5.2.8 Sub-area 7: Hukodden bay

Sub-area 7 comprises the beach at Hukodden bay. Most of the beach has been covered by artificial, white sand, but a few outcrops are still visible. A NNE-SSW striking syenite porphyry dyke cuts the Elnes Fm., which has resulted in the sedimentary rocks undergoing contact metamorphism (Fig. 5.2.8.1). At low tide, the dyke can be observed to crop out in the middle of the Hukodden bay between Sub-area 1 and 6. South of the normally submerged outcrop, the dyke changes direction westwards, and if one extrapolates the dyke out of the bay, it runs east of the Hukskjæra skerries in Sub-area 1 and west of the skerries in Sub-area 6 (Fig. 5.2.1). Due to lack of outcrops beyond the bay, it is unknown whether the dyke continues further into the sea.





Figure 5.2.8.1: A composite dyke at Hukodden where a mafic dyke cuts through a syenite porphyry dyke with an apophysis of mafic rock intruding the lighter syenite porphyry.

The dyke has been intruded by a smaller mafic dyke (Fig. 5.2.8.1), which does not continue into the outcrop in the Hukodden bay. Both dykes are discussed in more detail in Section 5.2.10 along with descriptions of other dykes and sills at this sub-area.

To the NE of the syenite porphyry dyke, a repetition of the upper two Elnes Fm. members can be seen. The outcrop to the SW of the syenite porphyry dyke, however, comprises beds of the Vollen Fm (Fig. 5.2.1). The repetition of the two upper Elnes members in Sub-area 7 is interpreted to be due to internal thrusting of the Elnes Fm. (Fig. 5.2.7.4 and Fig. 5.2.7.5).

The Galgeberg Mb. (Upper Tøyen), Huk Fm., and Sjøstrand Mb. (Lower Elnes) often accompany each other in thrust systems at Huk. This can be observed from the geological map of Huk (Fig. 5.2.1) and from cross-sections of Sub-area 1 (Fig. 5.2.5.1), Sub-area 5 (Fig. 5.2.6.2) and Sub-area 6 (Fig. 5.2.7.4 and Fig. 5.2.7.5). This suggest that ramps often form between flats in the Tøyen and Elnes shales as illustrated in Figure 5.2.5.1, Figure 5.2.7.4, Figure 5.2.7.5, Figure 5.2.7.9, and Figure 5.2.7.10.

The area between Sub-area 3 and Sub-area 7 contains no outcrops and is covered by paths and vegetation. However, by considering the outcrops in Sub-area 3, 6, and 7, the area has been

interpreted as a syncline (Fig. 5.2.7.4) similar to the one in the subsurface of Sub-area 2 (Fig. 5.2.5.1). The existence of the syncline is indicated by the NW dip of the layers in Sub-area 6, and 7, and by the SE dip of the layers at the northern end of Sub-area 7 (Fig. 5.2.1). There are no outcrops of the fold hinge and it is therefore uncertain if it mirrors the hinge of the syncline in Sub-area 2 in terms of deformational structures.

#### 5.2.8.1 The identified tear fault between Sub-areas 1 and 6

The differences in contractional tectonics on the southwestern (Sub-area 1, 2, and 7; Fig. 5.2.1 and Fig. 5.2.5.1) and northeastern (Sub-area 6 and 7; Fig. 5.2.1, Fig. 5.2.7.4) side of the Huk study area can only be explained by a Caledonian tear fault (Table 5.4.1, Table 5.4.2, and Table 5.4.3). The lithostratigraphic formations on either side of the fault are the same; it is only the expression of contractional deformation that differs. This indicates that the lateral breaks are not due to passive displacement of the strata, as one would expect from a Permian extensional or strike-slip fault. The Hukodden imbricate structure is not present anywhere on the southwestern side of the inferred tear fault, ruling out displacement due to a Permian strike-slip fault. Similarly, juxtaposing the structures in Sub-area 1 and 6 across-fault by Permian normal faulting is less likely than a thrust sheet undergoing tear faulting and the structures forming independently on either side of the fault.

This is supported by the fact that also the amount of compressional shortening is different on either side of the fault in this area (Sub-areas 1 and 6). The shortening of the Huk Fm. in the hanging-wall of the ramp-flat structure in Sub-area 1 and Sub-area 6 has been calculated from the balanced cross sections (Fig. 5.2.5.1 and Fig. 5.2.7.4) by using the start of the ramp-flat structure as the fixed reference point in each cross section (Table 5.2.8.1.1). This is because these points have not moved but stayed fixed both within and between both sections. In each cross-section, the shortening of the Huk Fm. has been calculated from the hanging-wall along a 330 m section from this fixed point, which is a minimum to capture the fault-propagation folds in both sections (Fig. 5.2.5.1 and Fig. 5.2.7.4). This way of calculation allows for a comparison between the amount of shortening on both sides of the fault (Table 5.2.8.1.1).

Table 5.2.8.1.1: Calculated shortening of the Huk Fm. along a 330 m section from the start of the ramp-flat structure in both balanced cross-section EF of Sub-area 1 (Fig. 5.2.5.1) and balanced cross-section GH (Fig. 5.2.7.4) of Sub-area 6.

	Balanced cross-section EF (between 300 m and 630 m along the x-axis)	Balanced cross-section GH (between 120 m and 450 m along the x-axis)
Original length of section (m)	485	610
Current length of section (m)	330	330
Shortening (m)	155	280
Shortening (%)	32	46

The two headlands are separated by the syenite porphyry dyke in Sub-area 7, which continues into the bay and changes direction westwards to cut between the skerries (Fig. 5.2.1). The dyke may have been emplaced in the former tear fault as it represent a structural, sub-vertical weakness in the rock. If this is the case, the orientation of the Caledonian tear fault can be estimated by measuring the orientation of the dyke. The fact that the dyke deviates from its NNW-SSE strike to cut between the skerries in Sub-area 1 and 6 rather than continuing its course may indicate that it was, at least in part, following a pre-existent weakness.

### 5.2.9 Sub-area 8: Bekkebukta bay

Following the shoreline eastwards from Hukodden, one walks along-strike through members of the Elnes Fm. Cross-stratification is visible in the silty beds of the Håkavik Mb. (Upper Elnes), and reveals the beds to dip NNW in right way up position (Fig. 5.2.1). The Elnes Fm. shale includes several asymmetric, tight folds that plunge gently in either NE or SW direction. The folds consistently include a steep southern limb and a more gently inclined northern limb, and have therefore been interpreted as possible parasitic Z-folds. At the bend in the shoreline at Bekkebukta bay, the depositional boundary between the silty shale of the Håkavik Mb. (Upper Elnes) and the cyclical beds of shale and knobby limestone of the Vollen Fm. can be observed. The exposed Vollen Fm. at Bekkebukta behave similarly to the outcrops in Sub-area 2, by the restaurant (Fig. 5.2.3.1 and Fig. 5.2.3.2). Clusters of thrust faults run within the thin shale beds, with a similar orientation to the bedding. It is not possible to measure the offset of these faults, but they do not carry enough displacement to cause repetitions of other formations to appear within the Vollen Fm. The Vollen Fm. contain several steep, NNW-SSE to NNE-SSW striking faults that cut perpendicular to the bedding. Some are seen to cut

straight through the sedimentary layers and every Caledonian thrust they encounter. These show sub-vertical slicken fibres and are interpreted as Permo-Carboniferous normal faults. A few other sub-vertical faults appear to run parallel to the Caledonian direction of transport. They appear to cause minimal displacement of the strata, and are seen to terminate in underlying and overlying thrust faults. These contained faults behave in a similar fashion to the ones observed in Sub-area 2, by the restaurant (Fig. 5.2.3.2), and have been categorised as small-scale Caledonian tear faults (Fig. 5.4.1 and Table 5.4.2).

When reaching the inner part of the bay, the lithology gradually changes from limestone-dominated to shale-dominated. This is the depositional boundary between the Vollen Fm. and the Arnestad Fm (Fig. 5.2.1). A few metres away from the shoreline, the geology is obscured by vegetation and a residential area which makes it impossible to continue mapping northwards. It is difficult to say for certain whether or not the formations in Sub-area 8 make up the southern limb of a great syncline, similar to the synclinal structure observed in Sub-area 6 and 7 (Fig. 5.2.7.4). A synform with its hinge in the Bekkebukta bay would be consistent with the orientation of the possible Z-folds observed in the Elnes Fm.

No repetitions were recorded when mapping the shoreline of Sub-area 8. All lithological units in this sub-area show a consistent NE-SW strike with beds dipping between 35° and 57° towards the NW. There is no discernible change in orientation when approaching the assumed fold hinge at Bekkebukta bay. Small, NE-SW striking top-to-southeast thrusts are common throughout the Elnes and Vollen formations.

#### 5.2.10 Permo-Carboniferous intrusive rocks and faults at Huk

The Cambro-Silurian strata at Huk is intruded by both sills and dykes. Mafic and syenitic dykes follow the general NNW-SSE trend of the brittle structures in the Oslo Rift, while a group of mafic intrusions assumed to be slightly older form bedding-parallel sills (Fig. 5.2.1). As the intrusive rocks are more resistant to erosion than the Cambro-Silurian sediments, they can be seen on the Hukodden beach where the outcrops are otherwise covered by artificial beach sand transported to the beach for recreational use.

The entire study area of Huk is cut by a large, NNW-SSE oriented syenite porphyry dyke, as illustrated in Figure 5.2.1. This dyke is visible in outcrops in Sub-area 3 by Maurtubukta (Fig. 5.2.4.1) and in Sub-area 7 by Hukodden (Fig. 5.2.8.1) as well as in a few highly weathered

and overgrown outcrops between Maurtubukta and Hukodden. It measures approximately 14 metres in width at Maurtubukta, and 12 metres in width at Hukodden (with the inclusion of a mafic dyke, as seen in Fig. 5.2.8.1). The dyke continues into the Hukodden bay and can be observed in the small outcrop visible in the middle of the bay (Fig. 5.2.1), where it only measures approximately 5 metres in width.

There are multiple thin mafic dykes intruding the area, measuring about half a metre to a metre in width. At Hukodden bay (Sub-area 7), a mafic dyke cuts through the middle of the syenite porphyry dyke along-strike (Fig. 5.2.8.1). The dyke-in-dyke relationship is accompanied by apophyses of mafic rock in the lighter syenite porphyry dyke. This cross-cutting relationship shows that the mafic intrusions are the younger of the two dyke generations. The syenite porphyry dyke is not intruded by the mafic dyke at Maurtubukta or in the small outcrop in the middle of the Hukodden bay.

The generational age relationship between the syenite porphyry dykes and the mafic sills can also be determined in the field. A few metres west of the composite dyke in Sub-area 7, a mafic sill is cut by an approximately 30 cm thick syenite porphyry dyke (Fig. 5.2.1) This indicates the mafic sills belong to a generation of intrusions older than the syenite porphyry dykes. A few metres north of the Hukodden bay, there is another possible case of cross-cutting relation with a mafic sill and the composite dyke in Sub-area 7 (Fig. 5.2.1). The outcrop is highly eroded, overgrown, and partly covered by a trail, so it is difficult to say whether the mafic sill reaches the syenite porphyry dyke, or if it dies out before that.

There are many sub-vertical fractures and normal faults of assumed Carboniferous or Permian age at Huk. The faults share a general NNW-SSE to N-S orientation, with calcite infill in some of the faults. When slickenlines are present, they reveal sub-vertical fault movement. The faults cut straight through outcrops with rocks of both Cambro-Silurian and Permo-Carboniferous age, and can be seen to cut across, and sometimes displace, Caledonian deformation in multiple sub-areas. Unlike tear faults, they do not terminate in overlying or underlying thrust faults. A majority of the normal faults show little to no discernible displacement, with maximum net slip being measured to about half a metre.

### 5.2.11 Summary of Huk

Detailed mapping has revealed that there is a clear break in the lateral continuity of the Caledonian (Silurian) compressional tectonic features in the Ordovician sequences on either side of the large syenite porphyry dyke that cuts across the field area (Fig. 5.2.1, Fig. 5.2.5.1, and Fig. 5.2.7.4). This lateral discontinuity cannot be explained by normal fault movement, and it is therefore unlikely that the two areas of differing geometry and displacement are separated by a Permo-Carboniferous normal fault. I therefore interpret that the dyke is emplaced in a former Caledonian tear fault. As the dyke deviates westwards from its on shore NNW-SSE orientation to cut between the Hukskjæra skerries in Sub-areas 1 and 6 may indicate that the dyke follows a pre-existent weakness. Likewise, there are clear differences in the Caledonian compressional tectonics between the eastern and western shores of the naturist beach that strongly indicates the existence of a Caledonian tear fault in the vegetation-covered interior of the headland (Fig. 5.2.6.2 and Fig. 5.2.6.3).

### 5.3 Slemmestad

Slemmestad (Fig. 4.1.2) is a residential area and the location of a large cement factory. The study area includes Proterozoic crystalline basement, Cambro-Ordovician sedimentary rocks from the Alum Shale Fm. to the Vollen Fm. and Carboniferous-Permian intrusive rocks. The Cambro-Ordovician sedimentary rocks display characteristic deformation by Caledonian compression (Fig. 5.3.1)

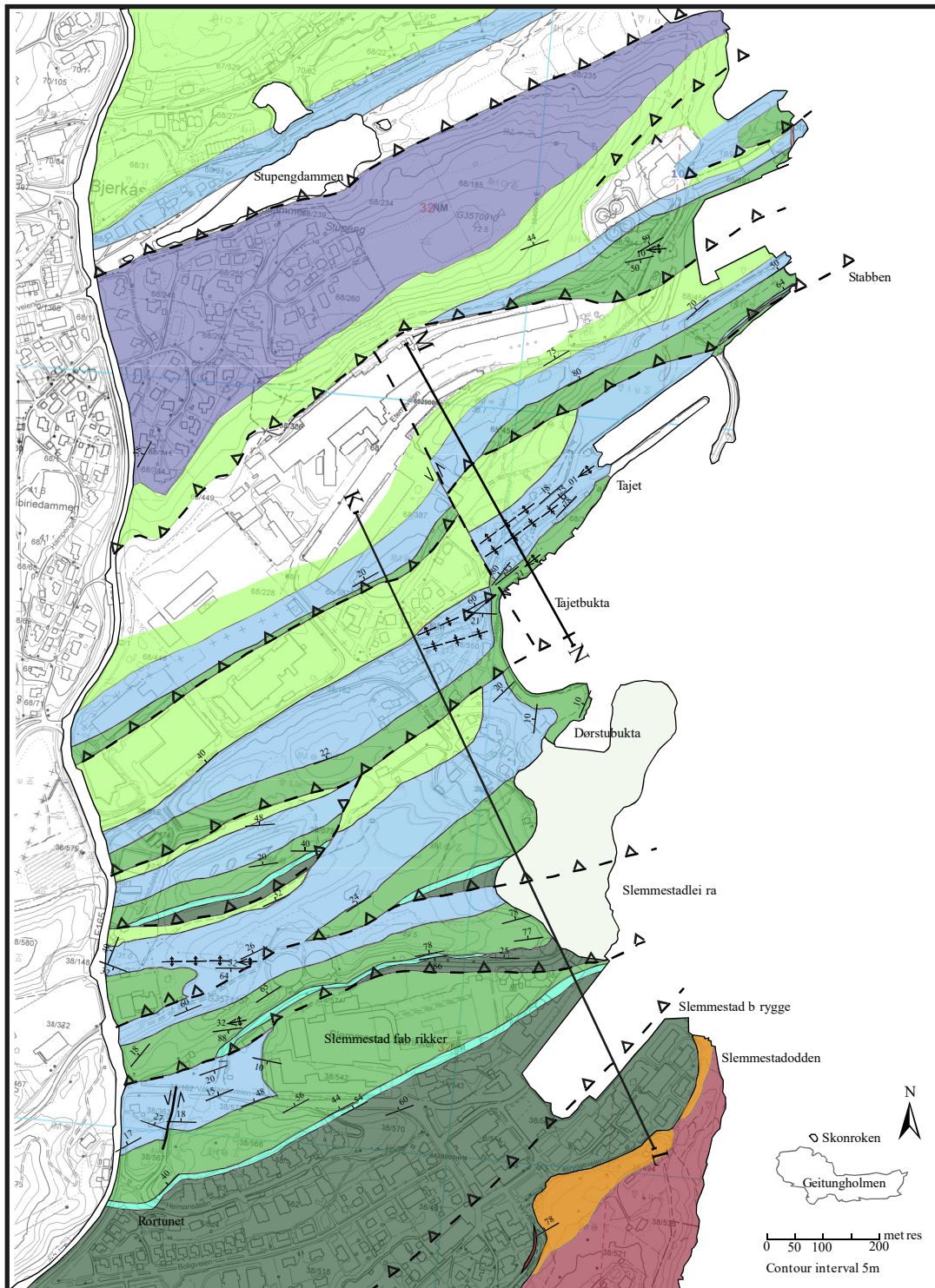


Figure 5.3.1: Geological map of Slemmestad. The south of the study area sees Precambrian bedrock, a maenite sill, and upper Cambrian Alum Shale. The stratigraphy becomes progressively younger when moving northwards with multiple repetitions easily identified in the field by the Huk Fm. limestones. “Slemmestad fabrikk” – the Slemmestad cement factory – marks a dip in the topography where presumably the Huk Fm. limestone has been removed to make room for the factory buildings. Similarly, the Huk Fm. repetition NW of the factories have a saddle-like appearance due to the topography where the Huk Fm. limestone has been removed to make room for buildings. Legend for map found in Figure 5.2.2: Map can be found in Appendix 3 (Plate 3).

The repetition of stratigraphy (Fig. 5.3.1) may be explained by multiple fault propagation folds, as illustrated in Figure 5.3.2. During the mapping of the area, two proposed tear faults exposed in road cuts were identified (Fig. 5.4.1, Table 5.4.2, and Table 5.4.3). The outcrops show that the dips of the Ordovician sequences on either side of the tear fault do not match. Cross-sections along the identified tear fault at Tajetbukta are presented in Figure 5.3.2 to demonstrate how the Caledonian tectonic structures and Ordovician sequences are disconnected and displaced along the identified tear fault (Fig. 5.3.1).

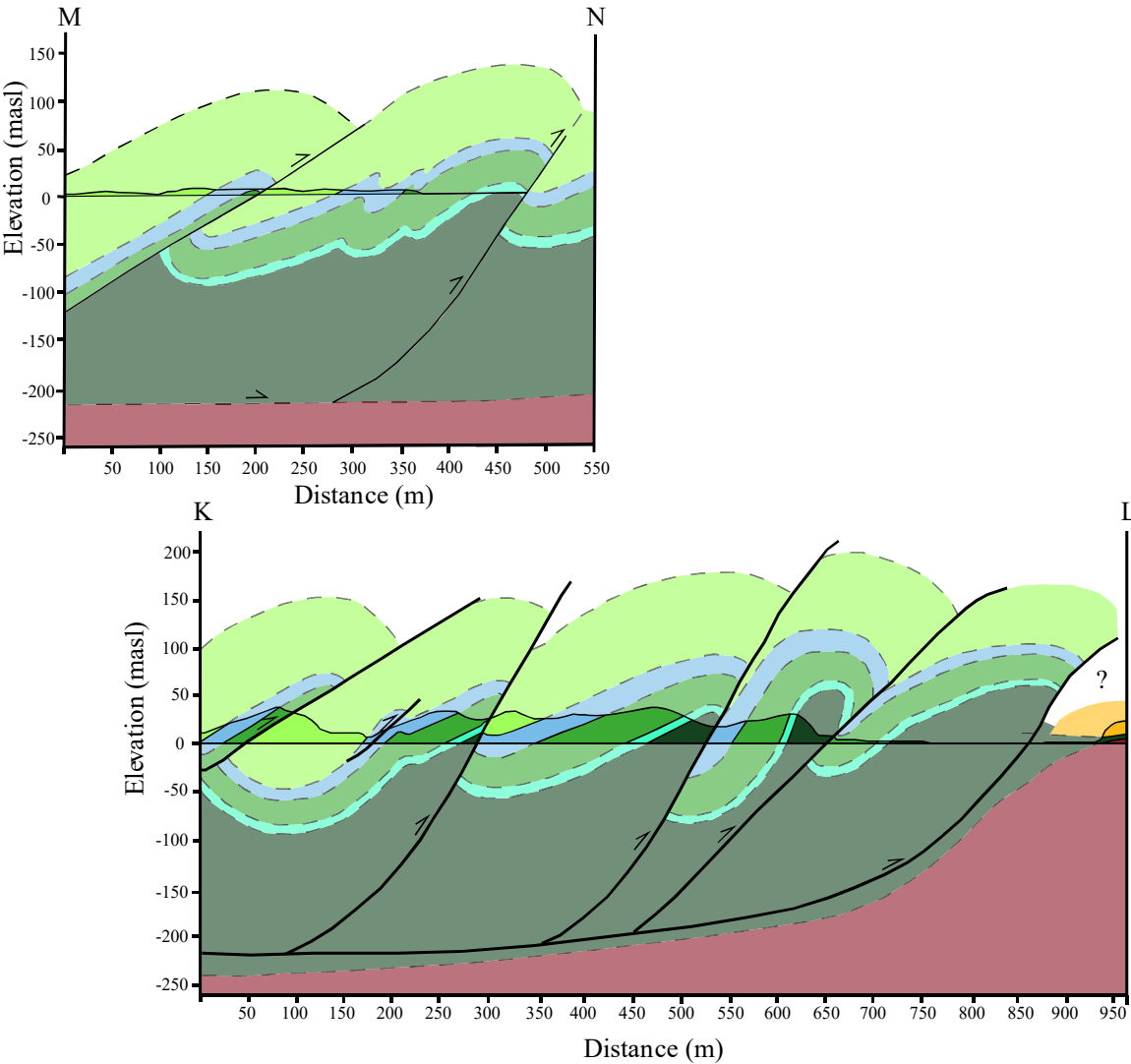


Figure 5.3.2: Cross-section KL and MN. The cross-sections run parallel to each other on either side of the postulated tear fault at Tajetbukta. Legend can be found in Figure 5.2.2. They display difference in deformation of the Huk Fm. within a thrust sheet. The Huk Fm. is deformed by internal small-scale folding in the east and internal small-scale faulting in the west. The two profiles, KL and MN, are aligned according to their mutual location on the map. This way, the cross-fault juxtaposition of the features in the profiles is retained by moving vertically from one profile to the other in the figure. Figure can also be found in Appendix 3 (Plate 11).



Cross-sections KL and MN (Fig. 5.3.2) of the Slemmestad map (Fig. 5.3.1) run alongside the identified tear fault at Tajetbukta to show lateral discontinuity of the Caledonian contractional structures. Cross-section MN (Fig. 5.3.2) shows that the Huk Fm. is deformed by smaller scale folds within a thrust sheet on the eastern side of Tajetbukta. Moving westwards, cross-section KL (Fig. 5.3.2) shows a small-scale thrust fault cutting through and displacing the Huk Fm. within the thrust sheet. The difference in shortening and structural style is accommodated by the tear fault.

A road with roadcuts on either side at Vaterlandsveien revealed another proposed tear fault. A folded repetition of the Huk Fm. can be seen in both road cuts, but there is a clear difference in fold geometry on either side of the road. The westernmost road cut section contains calcite-filled sub-vertical fault planes with slickenlines plunging 54 degrees. This is much steeper than what was initially expected for slickenlines associated with a tear fault. However, oblique-slip movement along a tear fault is theoretically possible and would explain the difference in fold geometry on either side of the road cut.

Southeast of the cement factory (Slemmestad fabrikk, Fig. 5.3.1), the Precambrian basement crops out. The outcrops show a maenaite sill emplaced sub-horizontally between the Precambrian crystalline basement and the Alum Shale Fm.

## 5.4 Tear fault identification

As a NNW-SSE to NNE-SSW striking strike-slip fault in the Oslo Region may in theory be the expression of either Permo-Carboniferous strike-slip faulting or Caledonian tear faults. Other indicators in addition to orientation and direction of fault movement must be considered to determine the age of the fault. Sub-vertical NNW-SSE to NNE-SSW striking Permo-Carboniferous extensional faults are plentiful in the Oslo Region, and should also be considered if fault movement is uncertain. A comprehensive list of criteria for identifying tear faults is presented in Table 5.4.1. The criteria for Caledonian tear faults is listed alongside criteria for Permo-Carboniferous strike-slip faults and Permo-Carboniferous extensional faults so it is possible to cross-reference the properties of a fault.

Table 5.4.1: Criteria for three types of sub-vertical faults one can expect to find in the Oslo Region. Criteria are listed by increasing significance; from indicative at top to definitive at bottom.

<b>Caledonian tear faults</b>	<b>Permian strike-slip faults</b>	<b>Permian extensional faults</b>
Sub-vertical structure, sometimes observed to become less steep and flatten out towards the underlying thrust plane.	Sub-vertical structure.	Sub-vertical structure to steeply dipping.
Strike generally perpendicular to the general Caledonian transport direction of the area with some deviation, presumably due to changes in propagation of the active thrust sheet.	Strike generally parallel to the strike of the Oslo Rift, with some deviation, as presented by Heeremans et al. (1996).	Strike generally parallel to the strike of the Oslo Rift, with some deviation.
Slickenlines show sub-horizontal to oblique movement along fault surface.	Slickenlines show sub-horizontal movement along fault surface.	Slickenlines show sub-vertical movement along fault surface.
Can be deformed or displaced by Permian and Carboniferous structures. Can also be deformed or displaced by Caledonian deformation.	Can be deformed or displaced by Permian and Carboniferous structures. Cannot be deformed or displaced by Caledonian deformation.	Can be deformed or displaced by Permian and Carboniferous structures. Cannot be deformed or displaced by Caledonian deformation.
Will not cut across Permian and/or Carboniferous structures.	Can cut across Permian and/or Carboniferous structures.	Can cut across Permian and/or Carboniferous structures.
Terminates in the underlying and/or overlying Caledonian thrust plane, depending on whether the contractional deformation is in-sequence or out-of-sequence. Deformation caused by the fault is contained within the hanging-wall of the active thrust fault.	Cuts across all Caledonian deformation it encounters.	Cuts across all Caledonian deformation it encounters.
Caledonian deformation structures have developed independently on each side of the fault and cannot be aligned to fit across the fault by reversing the strike-slip displacement. This is due to the nature of the tear fault, which accommodates differing contractional deformation in different parts of the thrust sheet.	Caledonian deformation structures are cut and separated by the strike-slip displacement along the fault. These structures may be re-aligned to fit across the fault by reversing the strike-slip displacement.	Caledonian deformation structures are cut and separated by the dip-slip displacement along the fault. These structures may be re-aligned to fit across the fault by reversing the dip-slip displacement.

Detailed mapping of Huk and Slemmestad reveal 15 faults as candidates for Caledonian tear faults (Table 5.4.2 and Fig. 5.4.1). The faults have affected the areas in different ways and at different scales. Some of the faults have only caused a few centimetres of displacement across-fault (e.g., Sub-area 2, 3, and 8 in Fig. 5.2.1). Other faults have caused displacement across-fault at a scale of 10s of metres, and accommodate considerable differences in shortening and in the development of geological structures on either side of the fault (e.g. Sub-area 6 at Huk and Vaterlandsveien at Slemmestad; Fig. 5.2.7.1, Fig. 5.2.7.7, and Fig. 5.3.1). Lastly, some faults represent displacements of a 100 metres or more. In these cases, the lateral breaks in structural style are identified through detailed mapping and the construction of geological maps and/or cross-sections (e.g. Sub-area 1 and 6 at Huk and Tajetbukta at Slemmestad; Fig. 5.2.1, and Fig. 5.3.1).

Table 5.4.2: Tear faults observed or inferred from field data and by applying the criteria presented above (see table Tables 5.4.1 and Table 5.4.3). The different scales are a measure of how much displacement each fault has caused within the active thrust. The scales only measure amount of displacement at a local scale, not regional. Small-scale means at most a 20 cm of displacement, no discernible difference in structures on each side of the tear fault. Intermediate-scale means displacement on a scale of 10s of metres with noticeable difference in structures on either side of the fault. Large-scale means 100s of metres of displacement with obvious differences in structures on either side of the fault.

Study area	Strike	Dip	Slicken-lines	Trend	Plunge	Scale	Location	#
Slemmestad	359	88	Yes	172	54	Intermediate	Hill by Vaterlandsveien	1
Slemmestad	329	88	No	-	-	Large	By Tajetbukta	2
Bygdøy	337	79	No	-	-	Large	Dyke at Maurtubukta (Sub-area 3)	3
Bygdøy	342	80	No	-	-	Large	Dyke at Hukodden (Sub-area 1, 6, 7)	4
Bygdøy	340	80	No	-	-	Large	Naturist beach (Sub-area 4 and 5)	5
Bygdøy	9	81	No	-	-	Small	Bekkebukta (Sub-area 8)	6
Bygdøy	13	73	Yes	53	39	Small	Bekkebukta (Sub-area 8)	7
Bygdøy	332	83	No	-	-	Small	Restaurant (Sub-area 2)	8
Bygdøy	9	82	No	-	-	Small	Restaurant (Sub-area 2)	9
Bygdøy	13	62	No	-	-	Small	Restaurant (Sub-area 2)	10
Bygdøy	341	88	Yes	333	20	Small	Restaurant (Sub-area 2)	11
Bygdøy	157	87	No	-	-	Small	Restaurant (Sub-area 2)	12
Bygdøy	154	87	No	-	-	Intermediate	Lower imbricate unit of the Hukodden imbricate structure (Sub-area 6)	13
Bygdøy	147	81	Yes	165	33	Small	Maurtubukta (Sub-area 3)	14
Bygdøy	152	76	Yes	161	21	Small	Maurtubukta (Sub-area 3)	15

Based on the detailed mapping in this thesis, the identification of the faults in Table 5.2.4 as tear faults have been confirmed by checking them against the criteria in Table 5.4.1. This is presented in Table 5.4.3.

Table 5.4.3: Faults identified as tear faults by the fieldwork (Table 5.4.2) are checked against the criteria for tear faults (Table 5.4.1). Green V means the faults fulfils the criteria, red X means the fault does not fulfil the criteria, black hyphen (-) means the outcrops did not reveal whether criteria was fulfilled or not.

<b>Criteria / fault #</b>	1	2	3	4	5	6	7	8	9	10	11	12	13	14	15
Sub-vertical	V	V	V	V	-	V	V	V	V	V	V	V	V	V	V
Strike approx. perpendicular to Caledonian transport direction	V	V	V	V	V	V	V	V	V	V	V	V	V	V	V
Sub-horizontal to oblique slickensides	V	-	-	-	-	-	V	-	-	-	V	-	-	V	V
Cut by Permian structures	X	X	V	V	-	X	X	V	V	V	X	X	X	X	X
Cut by Caledonian structures	X	X	X	X	-	X	X	X	X	X	X	X	X	X	X
Cuts through Caledonian structures, but not Permian structures	V	V	V	V	-	V	V	V	V	V	V	V	V	V	V
Terminates in a Caledonian thrust plane	-	-	-	-	V	V	V	V	V	V	V	V	V	V	-
Separates adjacent domains of different Caledonian structures	V	V	V	V	V	X	X	X	X	X	X	X	V	X	X

The identified tear faults (Table 5.4.2) are presented in a stereographic projection in Figure 5.4.1. The strike of the majority of the faults corresponds to the general Caledonian transport direction in the Oslo Region (NNW-SSE) with some of the faults striking N-S to NNE-SSW

(Fig. 5.4.1). The deviation from the general Caledonian transport direction is interpreted as local variation due to for example inhomogeneities in the rocks.

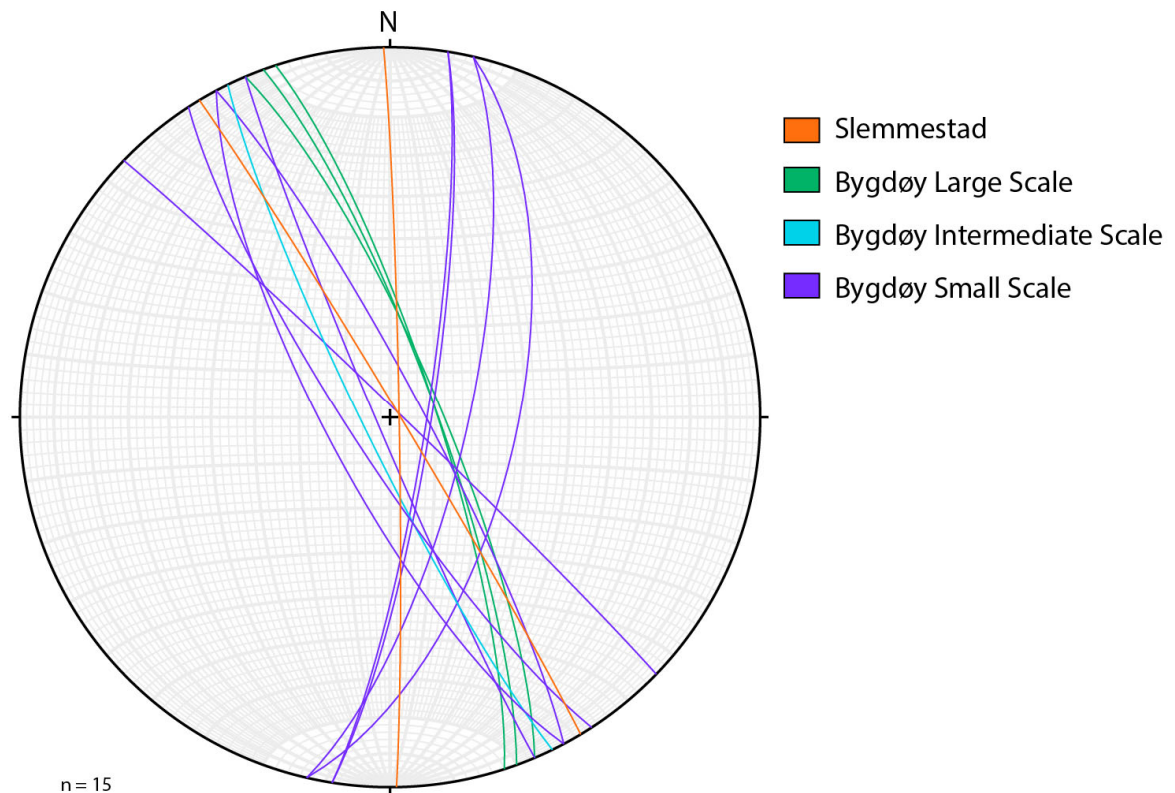


Figure 5.4.1: Stereographic projections of tear faults listed in Table 5.4.2. Does not include slickenside measurements (Table 5.4.2). The fault measurements have been divided into four groups based on study area and estimated displacement. In order to make the stereonet less cluttered, the two tear faults at Slemmestad have not been sorted by displacement in this projection.

## 6. Discussion

### 6.1 Introduction

The first aim of this study is to investigate the presence, extent and importance of Caledonian compressional tear faults in the Oslo Region through field mapping. The evidence for the existence and extent of these structures is presented in the previous chapter. In this chapter, the implications of Caledonian tear faults on a local and regional scale will be discussed with respect to the structural style of Caledonian deformation and the kinematic phases of the Permo-Carboniferous rifting in the Oslo Region proposed by e.g. Heeremans et al. (1996). Furthermore, the emplacement of sills will be discussed in relation to the proposed compressional regime preceding the rifting event in the Oslo Region.

### 6.2 Causes for tear faulting at Hukodden

Tear faults develop to compensate for differences in propagation on either side of the fault caused by lateral differences in properties that determine the amount of friction along a thrust plane, e.g. changes in pore pressure or lithological properties. It is unlikely that the identified tear fault at Hukodden was initiated by differences in pore fluid pressure in Sub-area 1 and 6. Faults and joints on both sides of the Hukodden bay are filled with calcite that sometimes contain slicken fibres, which indicate the presence of fluids in the calcareous sediments at the time of fault movement. There is no discernible difference in calcite infill on either side of the bay. One hypothesis is that tear faulting between the two headlands initiated because the sole thrust beneath the hanging-wall of the ramp-flat structure in Sub-area 6 (Fig. 5.2.7.4 and Fig. 5.2.7.5) cut up into the limestone-dominated Vollen Fm. from the dark shale-dominated Elnes Fm. As the thrust sheet became stuck or slowed down in the more competent Vollen Fm. in Sub-area 6, it continued its forwards propagation in the less competent Elnes Fm. in Sub-area 1, leading to tear faulting in the Hukodden bay between the two sub-areas (Fig. 5.2.1). A suggestion for the order of events related to the identified tear fault is included in Appendix 2.

### 6.3 Caledonian tear faults in the Oslo Region

The identified tear faults presented in the previous chapter (Table 5.4.2, Fig. 5.4.1) are generally oriented NNW-SSE to NNE-SSW, which is approximately perpendicular to the

strike of the Caledonian thrust faults they accompany. Direct observations consist of kinematic indicators on fault planes and strike-slip or oblique-slip displacement of the strata across the fault (Table 5.4.1). On a larger scale, the existence of tear faults are identified as breaks and inconsistencies between adjacent domains of Caledonian compressional structures. An important criterion for tear faults at any scale is that the deformation caused by the tear faults is constrained to a thrust sheet by an upper and a lower thrust fault (Table 5.4.1).

Tear faults as part of Caledonian compressional tectonics have received little to no attention in previous tectonic studies and are not explicitly mentioned in e.g. Morley (1986a, 1987, 1994) or Bruton et al. (2010). Earlier studies have mainly interpreted the Caledonian deformation through NW-SE oriented cross-sections, which focus on structures oriented parallel to the Caledonian thrust front. Consequently, structures that would become more apparent when studying the NE-SW sections may therefore have gone mostly unnoticed. The lack of references to such tear faults in the literature on the Oslo Region can easily give the impression that Caledonian tear faults are non-existent, and all strike-slip faults in the region seem to be assumed to belong to later deformation events (e.g. Heeremans et al., 1996; Bruton et al., 2010; Sippel et al., 2010). The numerous Caledonian tear faults in the detailed maps (Fig. 5.2.1 and Fig. 5.3.1) and cross-sections (Fig. 5.2.5.1, Fig. 5.2.6.2, Fig. 5.2.7.4, Fig. 5.2.7.5, and Fig. 5.3.2) presented in the previous chapter challenges this idea.

The displacement caused by Caledonian tear faults is substantial and clearly visible in the geological maps (Fig. 5.2.1 and 5.3.1) and cross-sections (Fig. 5.2.5.1, Fig. 5.2.6.2, Fig. 5.2.7.4, Fig. 5.2.7.5, and Fig. 5.3.2) from Huk and Slemmestad. Tear faults at Huk have been observed at different scales ranging from small displacements within a single thrust sheet only a couple of metres thick (Sub-area 2 and 8; Fig. 5.2.1) to hundreds of metres of displacement within a complex imbricate structure (Sub-area 1, 6, and 7; Fig. 5.2.1). The tear faults interact with, and have a noticeable effect on, the surrounding geological structures. The structures are prevalent in both the main study area at Huk and at Slemmestad. Since both of these areas appear to be lithologically and structurally representative of much of the Palaeozoic rocks in the Oslo Region, it is therefore assumed that detailed studies of other areas would reveal similar patterns. This study therefore suggests tear faults are an integral feature of the Caledonian structural style at a local scale in the Oslo Region.



## 6.4 Caledonian tear faults vs. Permo-Carboniferous strike-slip faults

Some previous studies have sorted strike-slip faults in the Oslo Region into three post-Caledonian fault sets. They have apparently not taking into account the possible existence of Caledonian tear faults during their data collection and processing. The three fault sets in question are strike-slip faults interpreted to relate to the Permian Kjaglidalen-Krokkleiva Transfer Fault (KKTF; Heeremans et al., 1996; Heeremans et al., 1997; Larsen et al., 2008), strike-slip faults that comprise the late Carboniferous to Permian kinematic phase 3 of Heeremans et al. (1996), and a Permian late- to post-rifting event as suggested by Sippel et al. (2010).

In the cases where the faults are not observed to cut Permo-Carboniferous strata, these studies assigned the faults post-Caledonian ages without direct age dating and without providing sufficient indirect proof, e.g. by detailed mapping to demonstrate the tectonic context of individual faults. (e.g. Heeremans et al. 1996; Sippel et al. 2010). Instead, age determination appear to have been made on the assumption that all faults that share a similar orientation hail from the same tectonic event. I would argue that if an outcrop contains strike-slip to oblique-slip deformation that does not interact with, or does not cut, rocks of post-Caledonian age, it should not be assigned a post-Caledonian age without first considering the criteria listed in Table 5.4.1, and a possible Caledonian origin. Misidentification of the age and nature of such faults may have caused Caledonian tear faults to be included as part of a different fault generation and may consequently have distorted the results of the studies. This may have repercussions for the interpretation of deformation in the Oslo Region at a regional scale. Caledonian tear faults should therefore be considered alongside Permian extensional faulting when encountering lateral breaks in structural geology or lithostratigraphy in the field.

### 6.4.1 Strike-slip faults and the Permian transfer zone

The transfer zone that accommodates lateral displacement between the Vestfold and Akershus graben segments was originally proposed to be centred around the KKTF (Heeremans et al., 1996; Larsen et al., 2008). Køber (2019) propose the transfer zone is more likely centred along Sørkedalen further north, as minimal displacement was estimated across the KKTF. The proposed transfer zone in Sørkedalen encompasses faults with displacements ranging from

10s of metres to kilometres, and its orientation aligns with the Precambrian Ørje shear zone (Nordgulen, 1999; Køber, 2019).

Bygdøy and Slemmestad are located within the proposed KKTF transfer zone, so one would expect the study areas of this thesis to contain deformation associated with it. The extension of the proposed Sørkedalen transfer zone potentially affects Bygdøy, but not necessarily. It depends on the width and length of the transfer zone, which has yet to be established.

Faults associated with a Permian transfer zone would necessarily fit the criteria for Permian strike-slip faults from Table 5.4.1, albeit potentially with a normal fault component as well. Caledonian tear faults in the transfer zone or in adjacent areas would therefore not be confused with this younger generation of faults as long as detailed mapping of the faults and the surrounding geology is performed, and sufficient exposures are present. The identified Caledonian tear faults in this study displace Lower Palaeozoic strata resulting in along-strike differences in geological structures that cannot be restored to align across the fault. This type of deformation cannot be achieved by Permian strike-slip to oblique-slip faulting. Thus, the detailed mapping in this thesis finds no evidence for strike-slip faults associated with a Permian transfer zone in the study area, even though both Huk and Slemmestad lie within the proposed KKTF transfer zone. This, and the observations by Køber (2019) call into question the importance of the KKTF as a zone transferring deformation between the different half graben segments, and support Køber's (2019) suggestion that the transfer zone has been misidentified and misplaced in previous studies (Heeremans et al. 1996; Larsen et al. 2008).

## 6.5 Late Carboniferous compressional stress regime and palaeostress reconstructions

Heeremans et al. (1996) presented a system of kinematic phases that detail the stress evolution of the Permo-Carboniferous Oslo Rift. The system is based on palaeostress reconstructions from kinematic indicators collected in and around the Oslo Rift as well as the tectono-magmatic model of the Oslo Rift described by Ramberg and Larsen (1978), Sundvoll et al. (1990), and Olausen et al., (1994). The different kinematic phases are related to the different tectonic events in the evolution of the Oslo Rift. The phases are explained in detail in section 4.5.4 of this thesis. Sippel et al. (2010) performed palaeostress reconstructions from kinematic

indicators collected at stations in the Oslo Region to expand on the study presented by Heeremans et al. (1996).

Heeremans et al. (1996) describe the data set of faults related to kinematic phase 2 as being of poor quality. It comprises three stations, one in an outcrop of Precambrian age, and two in outcrops of Ordovician-Silurian age. Kinematic phase 2 comprises compressive stress tensors that Heeremans et al (1996) suggest are linked to the emplacement of sills in the Oslo Region. The hypothesis that the emplacement of sills indicate a compressive stress regime is explained in section 4.7.3. As there are no cross-cutting relations with Permo-Carboniferous strata or structures, the inferred ages of these faults are based solely on the hypothesis of a late Carboniferous compressional regime related to the sill emplacement (Heeremans et al., 1996). Since they do not fulfil the criteria in Table 5.4.1, they may in fact be of Caledonian (or some other) age.

A sub-horizontal sill at Slemmestad is case in point. It has been emplaced between the Precambrian crystalline basement and the black shales of the Alum Shale Fm., which would be interpreted to reflect a regional compressive stress regime. However, there is a big difference in competence between the two lithologies, and that may be the reason why the feeder dyke rotated to a sill when it reached the interface between the bedrock and the sediments (Galland et al., 2018).

In comparison, the sills at Huk are strata-concordant but not sub-horizontal, with dips between 50°-75°. As the sill emplacement post-date the tilting of the strata the sills must have been emplaced in an inclined position rather than horizontally. For the sills to indicate a compressional tectonic regime, the minimal principal stress ( $\sigma_3$ ) must be vertical, and the sills must be emplaced horizontally. As this is not the case for the layer-parallel sills at Huk, they are by themselves not indicative of a compressional regime. The sills have similar orientations with the Caledonian thrust faults found within the shaly formations at Huk, so it is possible the sills have been partly emplaced along weaknesses created by Caledonian faulting.

Alternatively, the combination of shale-rich formations interbedded with limestone (i.e., strong mechanical contrast) and the high pore fluid pressure often found in organic rich shale may control the geometry of igneous intrusions in the Oslo Region. As explained in section 4.7.3, laboratory experiments performed by Gressier et al. (2010) illustrate how sill emplacement is favoured over dykes during such conditions.

Since this study suggests that sills were emplaced due to factors other than the presence of a compressional regime (see section 4.7.3), and since the fault population that was used to constrain kinematic phase 2 (Heeremans et al., 1996) is poorly constrained in age, the existence of kinematic phase 2 and a late-Variscan compressional regime is highly uncertain. Moreover, Sippel et al. (2010) did not identify any post-Caledonian compressional regime in their results when they performed palaeostress reconstructions of data from the Oslo Region, but assigned all the compressional stress tensors a Caledonian age.

## 6.6 Late Carboniferous to Early Permian strike-slip and palaeostress reconstructions

Kinematic phase 3 details a strike-slip regime that Heeremans et al. (1996) have linked to the late-Variscan reactivation of the Sorgenfrei-Tornquist Zone. The phase was divided into three sub-phases that demonstrate how the stress regime of the Oslo Region transitions from compressional (emplacement of sills) to extensional (rifting) through a shifting strike-slip regime (Fig. 6.6.1).

C: Phase 3A Holtbraten, Drøbak 1814 II

n=19

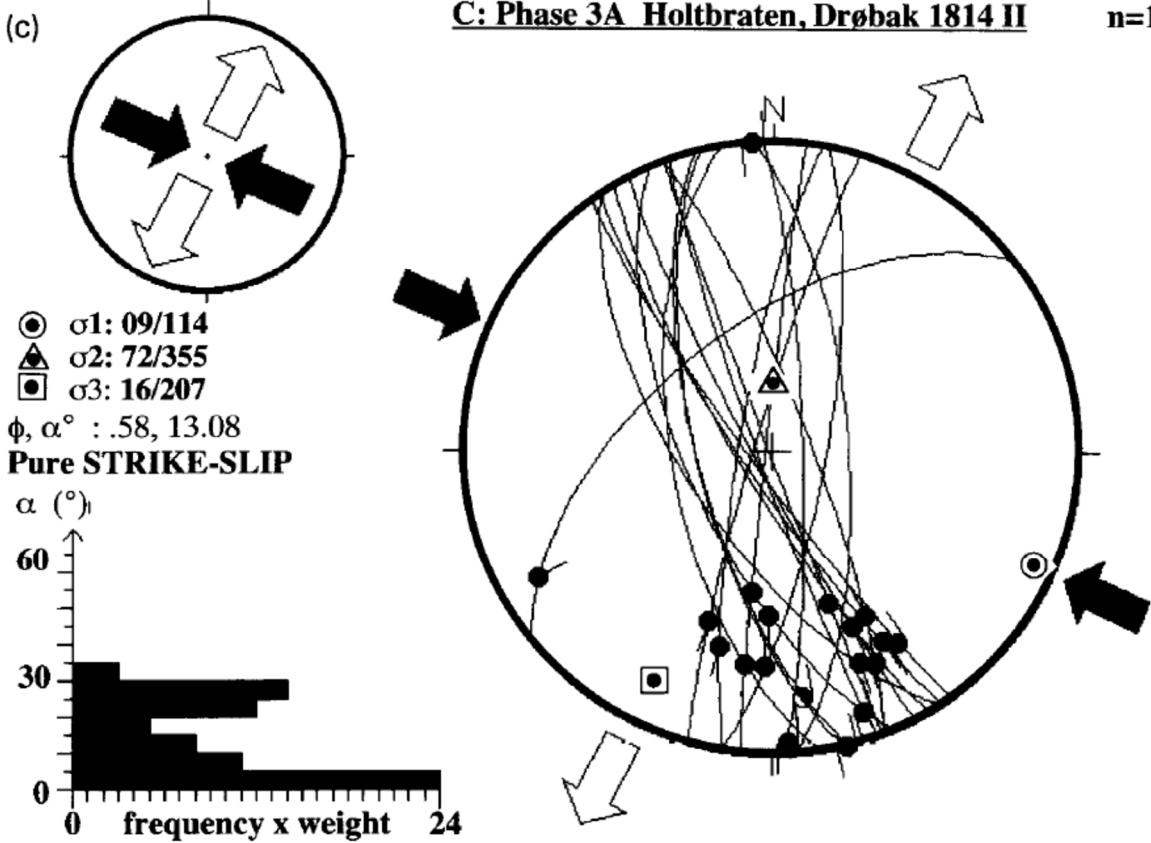


(Figure 6.6.1 continues on next page)

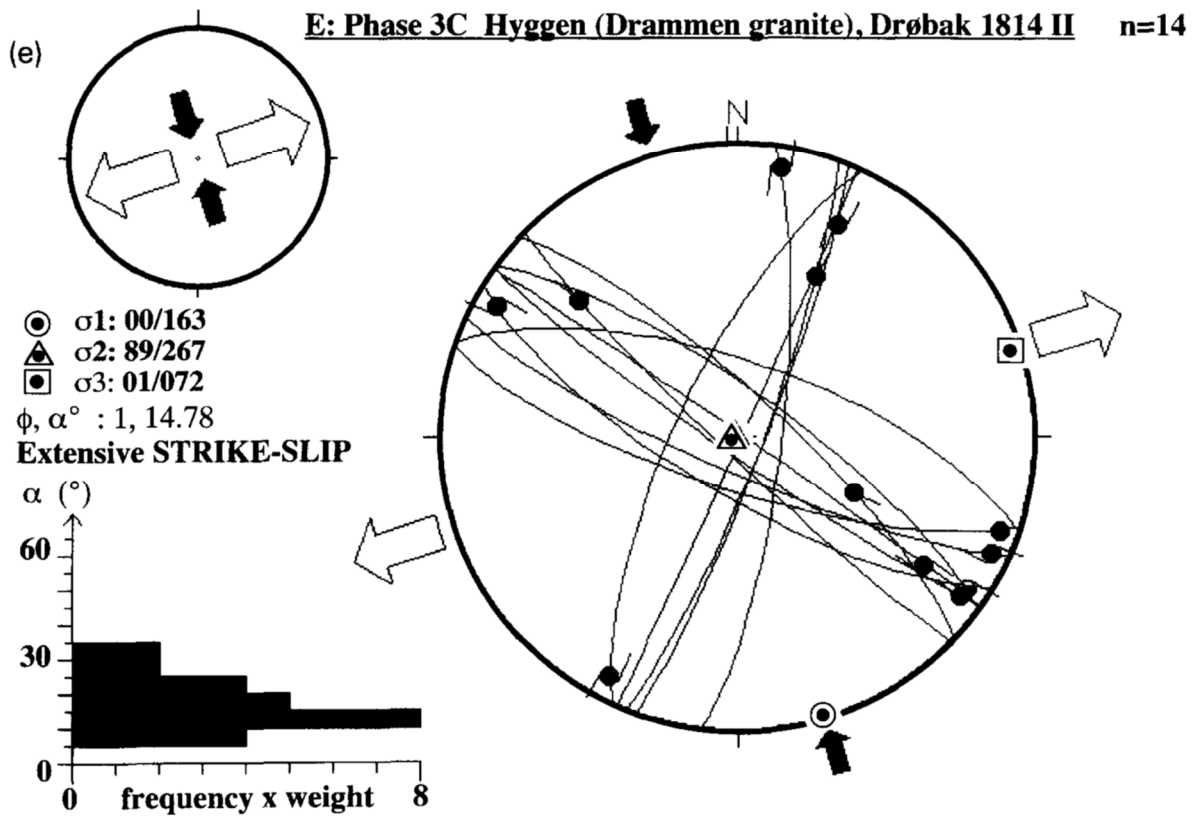
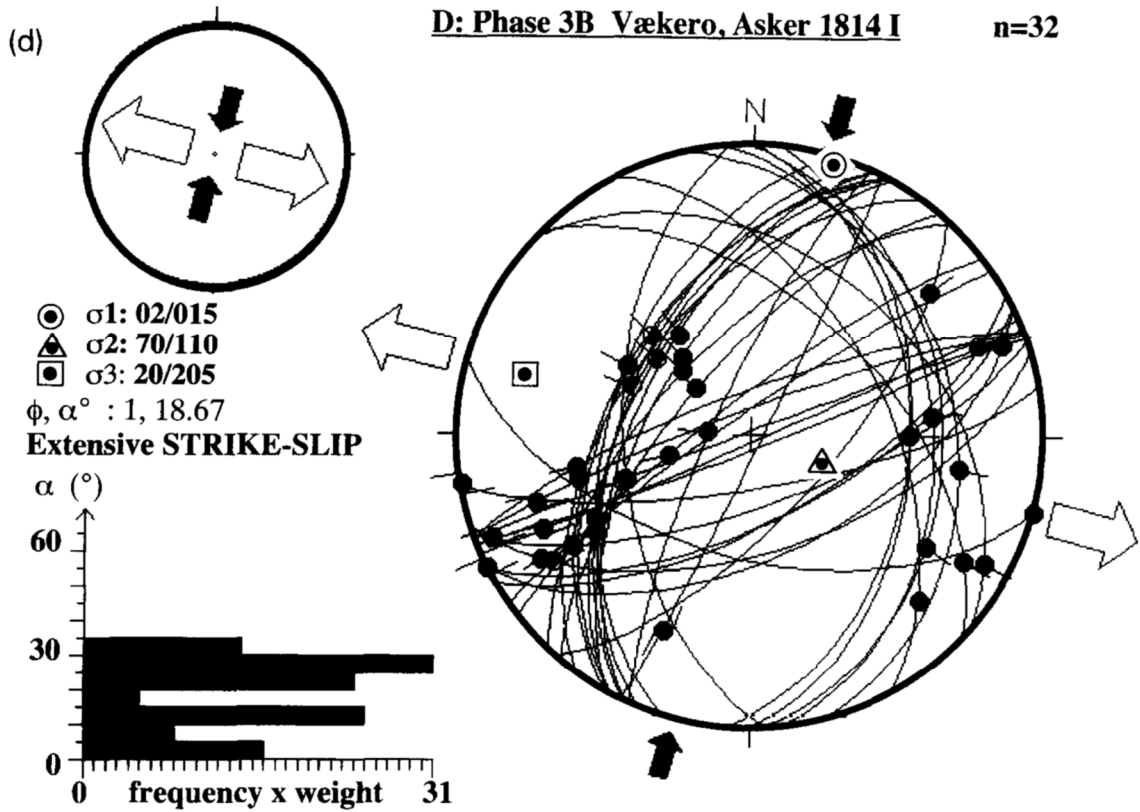


Figure 6.6.1: Figure text on next page

Figure 6.6.1. “Lower-hemisphere equal-area projections for the five different stress phases,  $\alpha$  is the mean deviation angle between the observed and computed slip directions,  $\beta$  is the shape ratio of the stress tensor  $(\sigma_2 - \sigma_3)/(\sigma_1 - \sigma_3)$ .  $n$  is number of measurements used in the computation of the given reduced stress tensor. [...] Phase 3A: compressive strike-slip with  $\sigma_1$  is WNW-ESE; Holtbråten (map sheet 1814 II). (d) Phase 3B: extensive strike-slip with  $\sigma_1$  is NNE-SSW; Vækerø (map sheet 1814 I). (e) Phase 3C: strike-slip with  $\sigma_1$  is N-S; Hyggen (map sheet 1814 II) [...]”. Figures and figure text from Heeremans et al. (1996) pp. 70, 71, and 72.

Heeremans et al. (1996) consider phase 3A to be caused by the stress regime created by the reactivation of the Sorgenfrei-Tornquist Zone. They suggest that dextral slip along the fault zone led to a shift from compression to strike-slip in the Oslo Region, which resulted in a stress regime characterised by compressional strike-slip. They assume all NW-SE to NNW-SSE faults with strike-slip fault movements have formed as a result of this transition, regardless of the age of the strata they deform. However, the Oslo Region lies in the Caledonian fold-and-thrust belt, and data for phase 3A match Caledonian stress tensors and were collected from outcrops consisting exclusively of Precambrian or Cambro-Silurian rocks (Heeremans et al. 1996), so the Caledonian effect should have been investigated before invoking effects of displacement on distant deformation zones such as the Sorgenfrei-Tornquist Zone. As pointed out by Heeremans et al. (1996): “*Note that the age of a rock in which a paleostress tensor is obtained only gives a lower age limit for the time during which the tensor was active*” (Heeremans et al. 1996, pp. 62). Importantly, this does *not* mean that the tensor is bound to have been active in the area at a later point. Heeremans et al. (1996) even say “*Phase 3A shows an orientation of  $\sigma_1$  perpendicular to the trend of the rift, which probably represents a pre-rift phase. The direction of  $\sigma_1$  and the age of the rocks in which this phase was analyzed correspond to a Caledonian stress tensor [...]*” (Heeremans et al., 1996, pp. 67). There is thus no evidence that the palaeostress tensors of 3A were active after the Caledonian Orogeny, other than the speculative association with a reactivation of the Sorgenfrei-Tornquist Zone based on its coinciding strike with the orientation of the calculated stress tensors. Heeremans et al. (1996) also states “*No conclusive overprinting relations in outcrops were found, and there is no independent evidence for the relative age of the pre-rift phases*” (Heeremans et al. 1996, pp. 62). Thus, the age of the faults is based entirely on insufficient evidence such as orientation and fault movement, and not by thorough mapping of the faults and their adjacent structures to exclude a Caledonian age. This means that phase 3A might very well reflect palaeostress tensors related to the Caledonian Orogeny rather than the

initial rifting stage of the Oslo Graben. Or at the very least, palaeostress tensors related to the Caledonian Orogeny *as well as* palaeostress tensors related to the stage of initial rifting.

According to the stereonet corresponding to one of the 3A stations (Fig. 6.6.1) it seems that the strike-slip tensors of 3A correspond to strike-slip faults of the Andersonian theory of faulting. A conjugate set of strike-slip faults are created  $30^\circ$  to either side of a horizontal maximum principal stress ( $\sigma_1$ , Fig. 6.6.2).

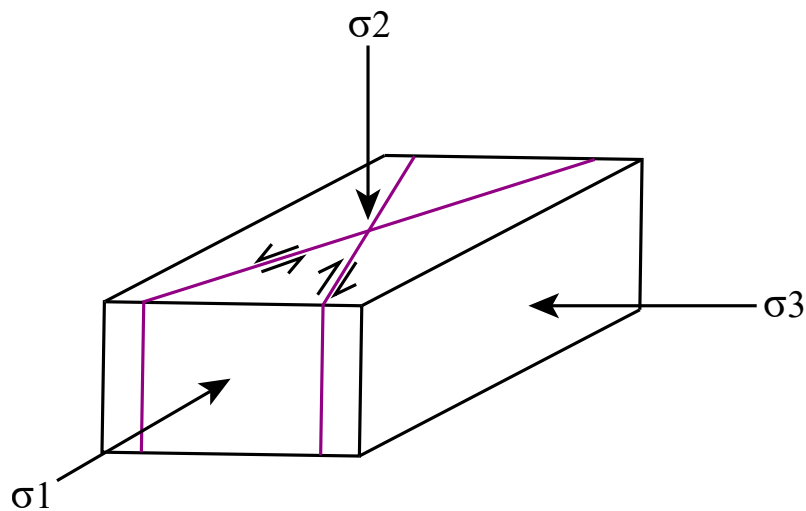


Figure 6.6.2: Strike-slip faulting according to the Anderson fault theory. A set of conjugate strike-slip faults form in the shape of an X, with approximately  $30^\circ$  between the faults and the maximum principal stress axis ( $\sigma_1$ ).

It appears that most faults sampled at this station belong to one of the two orientations of the conjugate set, with perhaps one sample representing the other orientation of the fault set. Another explanation for how strike-slip faults form is maximum principal stress ( $\sigma_1$ ) oriented parallel to the resulting strike-slip fault. This might occur in a compressional regime when adjacent parts of a thrust sheet propagate forwards at different speeds. In this scenario, the two areas of the thrust sheet will become separated by a tear fault with horizontal or horizontal to oblique lineation on the fault plane. Whether the tear fault would be sinistral or dextral would be determined by the relative velocity of the two adjacent parts of the thrust. It is possible that local trends can be detected in the case of tear faults. For example, identified tear faults at Slemmestad show sinistral movement (Fig. 5.3.1, Table 5.4.2), whilst tear faults on Bygdøy show predominantly dextral movement (Fig. 5.2.1, Table 5.4.2).



Heeremans et al. (1996) have illustrated the fault data of kinematic phase 3A by stereographic projection in Figure 6.6.1. The data presented in Figure 6.6.1 were collected from a station of Precambrian rock, and it is therefore not likely that the faults are Caledonian tear faults. Due to the thin-skinned style of Caledonian deformation in the Oslo Region, it is unlikely that faults of Caledonian age will be present in the autochthonous Precambrian basement. Faults in outcrops consisting of Precambrian rock are therefore not considered as candidates for Caledonian tear faults in this study. However, that does not necessarily mean they are post-Caledonian structures. Deformation observed in outcrops of Precambrian rock may belong to a deformation stage preceding the Caledonian deformation. Authors such as Ramberg and Larsen (1978), Ramberg and Spjeldnæs (1978) and Køber (2019) suggest that the Precambrian deformation of the crystalline basement has influenced the orientation of the Permian structures as the pre-existing Precambrian structures provided weaknesses in the rock. Faults that displace autochthonous Precambrian basement should therefore not automatically be assigned a Permo-Carboniferous age solely based on their orientation.

That being said, as the kinematic phases are comprised of faults sorted into groups based on orientation, the stereographic projection of Figure 6.6.1 should represent the kinematic phase as a whole. When comparing the fault data for kinematic phase 3A (Fig. 6.6.1) to the data on the identified tear faults presented in this study (Fig. 5.4.1) it becomes apparent that the orientations of the two fault sets are almost perfectly corresponding. This begs the question if the faults of kinematic phase 3A were mapped in detail and tested against the criteria in Table 5.4.1, would they still be classified as post-Caledonian strike-slip faults?

When reviewing the data of Heeremans et al. (1996) regarding kinematic phase 3A and 3B, it appears that only one of the locations includes an outcrop of upper Carboniferous rocks (sills; assigned to 3B). All other locations of both kinematic phase 3A and 3B include exclusively data collected from rocks of Precambrian to Silurian age. The structures that make up kinematic phase 3B were divided into groups based solely on the orientation of the maximum principal stress ( $\sigma_1$ ), and the suggested maximum age of all of the stress tensors was determined by the outcrop with the youngest rock. Faults grouped in 3B found in outcrops of Ordovician-Silurian age were automatically assigned a Post-Carboniferous age. In principal, however, they (and the faults grouped together in 3A) may equally well represent Caledonian tear faults. Similarly, the age of the faults observed in outcrops of Precambrian age remains to be proven. Fault characteristics beyond orientation should be considered when determining the age.

When comparing the data of phase 3C presented in stereonet by Heeremans et al. (1996; Fig. 6.6.1) to the tear fault data presented in Figure 5.4.1, there is a similarity in fault orientation. However, kinematic phase 3C comprises stations with rocks of Precambrian and Permian age only. As previously explained, Caledonian tear faults are not likely to appear in the Precambrian basement of the Oslo Region, but the faults are not necessarily post-Caledonian either. Further mapping of faults that are present in the Precambrian basement, with a focus on their interaction with Permian strata and structures should be performed to determine whether latest activity is Precambrian or Permian.

Heeremans et al. (1996) state that as kinematic phase 3B and C were not present in any syn-rift rocks younger than 280 Ma, the phases might represent the initial rifting stage of the Oslo Graben. And they go on to say that the strike-slip phases in their model support the theory that the creation of the Oslo Rift was preceded by dextral strike-slip movement along the Fennoscandian Border Zone, as previously put forth by Ziegler (1990 *in* Heeremans et al. 1996), Sundvoll and Larsen (1993), Olaussen et al. (1994) and Veevers et al. (1994). Heeremans et al. (1996) also mention that the N-S oriented syenite and dolerite dykes that show an *en echelon* pattern indicate a strike-slip stress regime, as suggested by Sundvoll and Larsen (1993).

Detailed geological mapping of Huk strongly suggests that at least one of these N-S trending syenite dykes has been emplaced in a former Caledonian tear fault. The syenite porphyry dyke separates two domains of different contractional deformation on land at Huk, which is indicative of a tear fault (Fig. 5.2.1, and Fig. 5.2.5.1, vs Fig. 5.2.7.4, Table 5.2.8.1.1). Due to the vegetation and manmade structures at Huk, it is difficult to say how far north the tear fault continues, and therefore, whether or not the dyke continues to be guided by tear fault through Bygdøy further north of Huk. As Caledonian tear faults and Permian dykes share a similar orientation, and dykes tend to follow pre-existing weaknesses in the rock, it is not unlikely that more cases of dykes emplaced in Caledonian tear faults may be discovered through further mapping of the Oslo Region. If the dykes are inclined to be emplaced in Caledonian tear faults, the pattern of emplacement observed in Ordovician and Silurian strata may not necessarily be a good indicator of stress regime during emplacement.

## 6.7 Late-Permian to post-Permian strike-slip and palaeostress reconstruction

Sippel et al. (2010) state that strike-slip stress tensors are present in rocks of “*all exposed ages*” (Sippel et al., 2010 pp. 695) with 28 out of 37 of the stress tensors having maximal principal stress ( $\sigma_1$ ) oriented NNW-SSE. They conclude from kinematic indicators and cross-cutting relations observed in the field that a phase of strike-slip deformation was present in the Oslo Region after the Permo-Carboniferous extensional regime responsible for the rifting. Sippel et al. (2010) go on to say that even though this stress field might postdate the rifting, the presence of strike-slip stress tensors in rocks of Permian age does not disprove the occurrence of earlier strike-slip fault events in the Oslo Region. They refer to the late Variscan strike-slip described by Heeremans et al. (1996). However, as presented in this study, a case can be made that such earlier strike-slip faulting may also wholly or partly represent Caledonian tear faults.

## 6.8 Implications for hypothesis of passive rifting in the Oslo Region

### 6.8.1 Late-Variscan far-field stresses

This study suggests that kinematic phase 2 and 3 as presented by Heeremans et al. (1996) are highly uncertain, and should not be considered valid unless further research is performed to provide more evidence. The hypothesis that the strike-slip faults in the Oslo Region have formed due to late-Variscan far-field stresses is not supported by the current, detailed mapping of such faults. As shown by this study, tear faults are an integral part of the Caledonian structural style, and the criteria in Table 5.4.1 should be considered when encountering NNW-SSE to NNE-SSW oriented sub-vertical faults during mapping. I did not observe any Permo-Carboniferous strike-slip faults either from direct observation or by interpretation of field data during the detailed mapping of Huk and Slemmestad. This begs the question of how prevalent this fault generation is in the Oslo Region. Furthermore, many of the strike-slip data presented by Heeremans et al. (1996), the data pertaining to kinematic phase 3A in particular, may be misidentified Caledonian tear faults rather than Permo-Carboniferous strike-slip faults. Kinematic phase 2 and 3 presented by Heeremans et al. (1996) rely on the existence of a late-Carboniferous compressional stress regime. This study shows that that may not be the case since the sills seem to have been emplaced due to factors other than a compressive stress regime. This would remove both kinematic phase 2 in its

entirety and the basis of age determination between stress tensor groups in phase 3; thus weakening the coherency of that phase considerably.

Without kinematic phase 2 to back up kinematic phase 3, and with the possibility that Caledonian tear faults were confused with strike-slip faults of kinematic phase 3, this study suggests the far-field stress from the shear movement along the Tornquist-Sorgenfrei Zone has had less of an impact on the initiation of the Oslo Graben than previously assumed. This view is not new; many others have suggested that active rifting due to a mantle plume has been the driving force behind, or at least an important factor of, the creation of the Oslo Graben (Heeremans et al., 2004; Larsen et al., 2008; Torsvik et al., 2008; Sippel et al., 2010; Neumann, 2019). Neumann (2019) concludes that the alkaline character of the early basaltic magmatism is a primary feature derived from the melting of sub-continental plume material, which points to the early existence of a mantle plume. This is supported by Sippel et al. (2010) who found only one conclusive extensional stress tensor group, i.e. radial extension at the rifting climax, which fits with a plume causing active rifting. Doming due to plume activity would cause vertical maximum principal stress ( $\sigma_1$ ) and horizontal, dilational intermediate principal stress ( $\sigma_2$ ) and minimum principal stress ( $\sigma_3$ ) of equal magnitude.

## 7. Conclusion

Detailed mapping of selected areas in the Oslo Region as presented in this thesis has given added insight into the tectonic evolution of the Oslo Region. This includes demonstrating the presence of Caledonian compressional tear faults as well as a further understanding of the Caledonian structural style, and a re-evaluation of previously proposed Permo-Carboniferous tectonic phases. The new findings and their implications are summarised below.

- 15 tear faults have been identified through detailed mapping of the two study areas (Fig. 5.2.1, Fig. 5.3.1, Fig. 5.4.1, Table 5.4.2, and Table 5.2.8.1.1) and by applying the criteria presented in Table 5.4.1. (Table 5.4.3).
- Three balanced cross-sections have been constructed (Fig. 5.2.5.1, Fig. 5.2.7.4, and Fig. 5.2.7.5). Cross-sections EF (Fig. 5.2.5.1) and GH (Fig. 5.2.7.4) illustrate how the Caledonian compressional structures have formed independently on each side of the tear fault identified at Hukodden bay (Sub-area 7; Fig. 5.2.1, Table 5.2.8.1.1). The western side of the Hukodden bay (Sub-area 1) contains an imbricate fan consisting of two fault-propagation folds. The eastern side of the Hukodden bay (Sub-area 6), however, contains an imbricate fan consisting of three fault-propagation folds where one has been deformed by two second order and one third order thrust. The difference in shortening of the Huk Fm. on either side of the bay has been calculated and is presented in Table 5.2.8.1.1. Cross-sections GH (Fig. 5.2.7.4) and IJ (Fig. 5.2.7.5) and accompanying figures Figure 5.2.7.9, and Figure 5.2.7.10 illustrate how a tear fault has caused displacement of an imbricate unit within an imbricate structure, the Hukodden imbricate structure (Fig. 5.2.7.1, Fig. 5.2.7.7)
- Due to their prevalence and impact on the surrounding geology at the study areas (Fig. 5.2.1 and Fig. 5.3.1), compressional tear faults have been interpreted as an integral part of the Caledonian structural style. Consequently, in order to differentiate between Caledonian tear faults and Permo-Carboniferous strike-slip faults in the Oslo Region, age determination should be performed through detailed mapping of the fault and by applying the criteria in Table 5.4.1.
- The detailed mapping of the study areas revealed no faults fulfilling the criteria for Permo-Carboniferous strike-slip faults. The absence of such faults at Huk and Slemmestad may support the suggestion put forth by Køber (2019) that the transfer

zone linking the Vestfold and Akershus graben segments is located north of the currently proposed KKTF transfer zone.

- The kinematic phases presented by Heeremans et al. 1996 are based on fault data that were collected without considering tear faults an integral part of the Caledonian structural style. Faults were sorted into kinematic groups on the basis of fault orientation and movement, and the maximum age of each fault group was determined by the outcrop with the youngest rock included in the data set. However, this study suggests age determination should be performed by detailed mapping of individual faults, and by referencing criteria for different generations of sub-vertical faults equivalent to those presented in this thesis (Table 5.4.1). Kinematic phase 3, which is suggested to represent a late-Variscan strike-slip regime (Heeremans et al., 1996), comprises fault orientations that are almost perfectly corresponding to the fault orientations of the Caledonian tear faults identified in this study (Fig. 5.4.1 and Fig. 6.6.1). I therefore suggest kinematic phase 3 should be considered highly uncertain until the faults of that tectonic phase have been individually mapped and checked against the criteria in Table 5.4.1.
- Kinematic phase 2 (Heeremans et al., 1996) is suggested to reflect a late-Carboniferous compressional regime. The existence of the compressional stress regime is based in large on the late Carboniferous emplacement of sills in the Oslo Region. As the strata-concordant sills at Huk were emplaced after the Caledonian deformation, their inclined position does not imply a compressional regime according to the Andersonian theory of faulting. Additionally, the horizontal sill at Slemmestad was observed to be emplaced between layers with high contrast in rigidity, which does not necessarily indicate a vertical minimal principal stress ( $\sigma_3$ ). The absence of evidence for a late Carboniferous to Early Permian compressional regime further weakens the late-Variscan strike-slip kinematic phase presented by Heeremans et al. (1996).
- Sippel et al. (2010) present a stress regime characterised by radial extension at the height of rifting in the Oslo Region, which they suggest may be indicative of active rifting at that stage. Neumann (2019) suggests the mineralogy of early basaltic magmatism point to the existence of a mantle plume at the early stages of rifting. The model of passive rifting has suggested rift initiation due to far-field stresses from the

reactivated Tornquist-Sorgenfrei Zone. However, this study calls into question the validity of the late-Variscan strike-slip regime suggested to represent the early stage of rifting. Consequently, it suggests that the far-field stresses from the reactivated Sorgenfrei-Tornquist Zone has had less of an influence on the structural/tectonic evolution of the Oslo Region than previously assumed, and that the dextral shear zone may not have been a driving force behind the initiation of the Oslo Rift.

## 7.1 Recommended further research

The results presented in this thesis have implications for the structural style of the Caledonian deformation and for the tectonic phases related to the Oslo Rift. Suggestions for further studies of these implications are listed below.

- Detailed mapping at a greater scale with a focus on Caledonian tear faults is recommended to further investigate their presence, extent, and implications at a regional scale. Caledonian tear faults may explain lateral breaks in Caledonian compressional structures that have earlier been attributed to Permian faulting.
- Further research to establish the relationship between Carboniferous sill emplacement and the early tectonic evolution of the Oslo Rift, if any, is recommended.
- Further research is also recommended to establish the validity of the late-Variscan strike-slip regime that has been suggested to precede or initiate the rifting in the Oslo Region. Detailed mapping of strike-slip faults that are contained to Lower Palaeozoic strata with Caledonian deformation should be performed by using the criteria in Table 4.5.1 to ensure Caledonian tear faults are excluded from the collected data. Only then should the data be used to calculate Permian stress tensors.
- Investigation of to what extent Caledonian tear faults have influenced the emplacement of Permian dykes in the Oslo Region.
- Detailed mapping of late Carboniferous to early Permian extensional faults can be performed in order to investigate whether faults formed during early rifting stages correspond to radial extension. If this is the case, they may support the model of active rifting initiated by a mantle plume beneath the Oslo Region.

## 8. References

- Allmendinger, R. W., Siron, C.R., & Scott, C. P. (2017). Structural data collection with mobile devices: Accuracy, redundancy, and best practices. *Journal of Structural Geology*, 102, pp. 98-112
- Allmendinger, R. W. (2020). *Stereonet 11*.  
<http://www.geo.cornell.edu/geology/faculty/RWA/programs/stereonet.html>
- Andersen, T. B. (1998). Extensional tectonics in the Caledonides of southern Norway, an overview. *Tectonophysics*, 285, 333–351.
- Andersson, A., Dahlman, B., Gee, D. G., & Snäll, S. (1985). The Scandinavian Alum Shales. *Sveriges Geologiska Undersökning, ca 56*, 1-50.
- Ballo, E. G., Augland, L. E., Hammer, Ø., & Svensen, H. H. (2019). A new age model for the Ordovician (Sandbian) K-bentonites in Oslo, Norway. *Palaeogeography, Palaeoclimatology, Palaeoecology*, 520, 203-213.
- Benesh, N. P., Plesch, A. & Shaw, J. H. (2014). Geometry, kinematics, and displacement characteristics of tear-fault systems: An example from the deep-water Niger Delta. *AAPG Bulletin*, 98(3), pp. 465-482. DOI: 10.1306/06251311013
- Bjørlykke, K. (1965). The Middle Ordovician of the Oslo Region, Norway. 20. The geochemistry and mineralogy of some shales from the Oslo Region. *Norsk Geologisk Tidsskrift*, 45, 435-456.
- Bjørlykke, K. (1973). Origin of limestone nodules in the Lower Palaeozoic of the Oslo Region. *Norsk geologisk Tidsskrift*, 53, 419-431.
- Bjørlykke, K. (1974). Depositional history and geochemical composition of Lower Palaeozoic epicontinental sediments from the Oslo Region. *Norges geologiske undersøkelse*, 305(24). 1-81.
- Bjørlykke, K. (2004). “Oslo-området geologi. En kort oversikt som vedlegg til film (DVD) fra områdene rundt indre Oslofjord” Retrieved from <https://www.mn.uio.no/geo/tjenester/kunnskap/geologi-oslofeltet/geologi-slofeltet.k.b.pdf>
- Bockelie, J. F. & Bockelie, T. G. (1970-1976a). Geologisk kart over Slemmestad CM 042-5-3. Manuskart M 1:5000. Paleontologisk Museum.
- Bockelie, J. F. & Bockelie, T. G. (1970-1976b). Geologisk kart over Sjøstrand CM 042-5-1. Manuskart M 1:5000. Paleontologiske Museum.
- Bockelie, J. F. & Bockelie, T. G. (1970-1976c). Geologisk kart over Konglungen CM 043-5-



1. Manuskart M 1:5000. Paleontologiske Museum.
- Bockelie, J. F. & Bockelie, T. G. (1970-1976d). Geologisk kart over Blakstad CL 043-5-4. Manuskart M 1:5000. Paleontologiske Museum.
- Bockelie, J. F. & Nystuen, J. P. (1985). The southeastern part of the Scandinavian Caledonides. In D. G. Gee & B. A. Sturt (Eds.), *The Caledonian Orogen - Scandinavia and Related Areas; Part 1* (pp. 69-88). Chichester, United Kingdom: John Wiley & Sons
- Bogdanova, S. V., Gorbatshev, R., & Garetsky, R. G. (2005). Europe: East European Craton. In R. C. Selley, L. R. M. Cocks, & I. R. Plimer (Eds.), *Encyclopedia of geology* (pp. 34-49). Academic Press. DOI: <https://doi.org/10.1016/B978-0-12-409548-9.10020-X>
- Bruton, D., Gabrielsen, R. H. & Larsen, B. T. (2010). The Caledonides of the Oslo Region, Norway – stratigraphy and structural elements. *Norwegian Journal of Geology*, 90, 93-121.
- Brøgger, W. C. (1882). Die Silurischen Etagen 2 und 3 im Kristianiagebiet und auf Eker. *Kongelige Frederiks Universitet, Christiania. Universitæts program. 2 Serie 1882*, 1-376.
- Brøgger, W. C. (1887). Geologisk kart over øerne ved Kristiania. *Nyt Magazin for Naturvidenskaberne*. 31, 1-36.
- Cawood, A. J., & Bond, C. E. (2020). Broadhaven revisited: a new look at models of fault–fold interaction. *Geological Society, London, Special Publications*, 487(1), 105-126.
- Cocks, L. R. M. and Torsvik, T. H. (2002). Earth geography from 500 to 400 million years ago: a faunal and palaeomagnetic review. *Journal of the Geological Society* 159(6), 631–644.
- Cocks, L. R. M. and Torsvik, T. H. (2005). Baltica from the late Precambrian to mid-Palaeozoic times: the gain and loss of a terrane’s identity. *Earth-Science Reviews* 72(1), 39–66.
- Cohen, K. M., Finney, S. C., Gibbard, P. L. & Fan, J. X. (2013) The ICS International Chronostratigraphic Chart. Episodes 36. 199-204. DOI: 10.18814/epiiugs/2013/v36i3/002
- Cohen, K. M., Finney, S. C., & Gibbard, P. L. (2016). ICS International Chronostratigraphic Chart 2016/04.
- Corfu, F., Andersen, T.B., & Gasser, D. (2014). The Scandinavian Caledonides: main features, conceptual advances and critical questions. *Geological Society London Special Publications* 390 (1). 9-43. DOI: 10.1144/SP390.25

- Delvaux, D. (1993). The TENSOR program for paleostress reconstruction: examples from the east African and the Baikal rift zones. *Terra Nova (abstr. suppl.)*, 5, 216.
- Domeier, M. (2015). A plate tectonic scenario in the Iapetus and Rheic oceans. *Gondwana Research*, 36, 257-295. DOI:10.1016/j. gr.2015.08.003.
- Dons, J. A. (1978). Terminology and History of Investigations. In J.A Dons and B.T. Larsen (Eds.). *The Oslo Paleorift. A review and guide to excursions*. (pp. 9-16). Norway: Norges Geologiske Undersøkelse, 337.
- Elvebakk, H. (2011). *Geofysisk logging av borehull ved Arnestad skole, Asker*. Norges geologiske undersøkelse, report no. 2011.016.
- Elvebakk, H. (2012). *Sammenstilling av geofysiske data fra borehull*. Statens vegvesen, report no. 124.
- Elvebakk, H. (2013). *Geofysisk logging av borehull ved Geologisk Museum, Tøyen, Oslo*. Norges geologiske undersøkelse, report no. 2013.040.
- Elvebakk, H., & Lutro, O. (2008). *Geofysisk logging av borehull ved Hamar Flyplass*. Norges geologiske undersøkelse, report no. 2008.079.
- Fossen, H. (2010) Extensional tectonics in the North Atlantic Caledonides: a regional view. *Continental Tectonics and Mountain Building: The Legacy of Peach and Horne*, (335), 767-793.
- Fossen, H. (2014) Contractional regimes. *Structural Geology* (5th ed., pp. 311-329). New York: Cambridge University Press.
- Gabrielsen, R. H., Nystuen, J. P., Jarsve, E. M., & Lundmark, A. M. (2015). The Sub-Cambrian Peneplain in southern Norway: Its geological significance and its implications for post-Caledonian faulting, uplift and denudation. *Journal of the Geological Society*, 172(6). DOI: 10.1144/jgs2014-154
- Galland, O., Bertelsen, H. S., Eide, C. H., Guldstrand, F., Haug, Ø. T., Leanza, H. A., Mair, K., Palma, O., Planke, S., Rabbal, O., Rogers, B., Schmiedel, T., Souche, A., & Spacapan, J.B. (2018). Storage and Transport of Magma in the Layered Crust—Formation of Sills and Related Flat-Lying Intrusions. In S. Burchardt (Ed.), *Volcanic and Igneous Plumbing Systems* (pp. 113-138). Elsevier.
- Geiser, P. A. (1988). The role of kinematics in the construction and analysis of geological cross sections in deformed terranes. In G. Mitra and S. F. Mojtai (Eds.), *Geometries and mechanisms of thrusting: Geological Society of America Special Paper*, 222 (pp.47-76).
- Graversen, O. (2015). Caledonian Foreland Thrust Tectonics in the Slemmestad area, Oslo

- Region, South Norway: an excursion guide. In A.M. Husås (Ed.), *Geological guides 2015- 5*. (pp. 1-31). Trondheim: Norges Geologiske Forning. ISBN: 978-82-8347-001-7
- Graversen, O., Nordgulen, Ø., & Lutro, O. (2017). Berggrunnskart OSLO 1914 IV, M 1: 50.000. Norges geologiske undersøkelse.
- Gressier, J. B., Mourgues, R., Bodet, L., Matthieu, J. Y., Galland, O., & Cobbold, P. (2010). Control of pore fluid pressure on depth of emplacement of magmatic sills: An experimental approach. *Tectonophysics*, 489(1-4), 1-13. doi: 10.1016/j.tecto.2010.03.004
- Groshong, R. H. (2006). Cross section, Data Projection and Dip-Domain Mapping. In R. H. Groshong (Ed.), *3-D Structural Geology: A practical Guide to Quantitative Surface and Subsurface Map Interpretation*. (2<sup>nd</sup> ed., pp. 113-180). Berlin: Springer.
- Hansen, J. & Harper, D. A. T. (2006). “Brachiopod bio-and ecostratigraphy in the lower part of the Arnestad Formation (Upper Ordovician), Oslo Region, Norway”. *Norsk Geologisk Tidsskrift*, 86, 403-413.
- Henningsmoen, G. (1974). A Comment. Origin of Limestone Nodules in the Lower Paleozoic of the Oslo Region. *Norsk Geologisk Tidsskrift*, 54, 401-412.
- Henningsmoen, G. (1955). Tur-beskrivelser 3. Bygdøy. In O. Holtedahl & J. A. Dons (Eds.), *Geologisk fører for Oslo-trakten* (1<sup>st</sup> ed., pp. 71-74) Oslo: Det Norske Videnskaps-Akademi i Oslo
- Henningsmoen, G. (1977). Chapter 4. Bygdøy. In Dons, J. A. (Ed.), *Geologisk fører for Oslo-trakten* (2<sup>nd</sup> ed., pp 96-101) Oslo: Universitetsforlaget.
- Henningsmoen, G. (1978). Sedimentary rocks associated with the lava series. In J.A Dons & B. T. Larsen (Eds.), *The Oslo Paleorift. A review and guide to excursions*. (pp. 17-24). Norway: Norges Geologiske Undersøkelse, 337.
- Henningsmoen, G. (1982). The Ordovician of the Oslo Region. A short history of research. In O. L. Bruton & S. H. Williams (Eds.), *Field Excursion Guide IV International Symposium on the Ordovician System*. (pp. 92-98). Paleontological Contributions from the University of Oslo, 279.
- Heeremans, M. M. H. (1997). *Siliciclastic magmatism and continental lithosphere thinning. Inferences from field studies and numerical modeling of the Oslo Graben and the anorogenic crustal evolution of southern Finland*. Amsterdam: The Netherlands: Netherlands Research School of Sedimentary Geology (NSG). 1-197.
- Heeremans, M. (2005). *A Plume beneath the Oslo Graben?* Retrieved from:

<http://www.mantleplumes.org/Norway.html>

- Heeremans, M., Faleide, J. I. & Larsen, B. T. (2004). Late Carboniferous-Permian of NW Europe: an introduction to a new regional map. In M. Wilson, E. -R. Neumann, G. R. Davies, M. J. Timmerman, M. Heeremans & B. T. Larsen (Eds.), *Permo-Carboniferous Magmatism and Rifting in Europe*, (pp. 75-88). Geological Society London Special Publication, 223.
- Heeremans, M., Larsen, B. T. & Stel, H. (1996). Paleostress reconstructions from kinematic indicators in the Oslo Graben, southern Norway: new constraints on the mode of rifting. *Tectonophysics*, 266, 55-79.
- Heeremans, M., Larsen, B. T. & Stel, H. (1997). Erratum to "Paleostress reconstruction from kinematic indicators in the Oslo Graben, southern Norway: new constraints on the mode of rifting" [*Tectonophysics* 266 (1996) 55 79]. *Tectonophysics*, 277(4), 339-344.
- Hubbert, M. K., & Willis, D. G. (1957). Mechanics of hydraulic fracturing. *AIME Petroleum Transactions*, 210, 153-168
- Huff, W. D. (2016). K-bentonites: a review. *American Mineralogist*, 101, 43–70. doi: 10.2138/am-2016-5339.
- Jakob, J., Andersen, T. B., & Kjøll, H. J. (2019). A review and reinterpretation of the architecture of the South and South- Central Scandinavian Caledonides— A magma-poor to magma-rich transition and the significance of the reactivation of rift inherited structures. *Earth-Science Reviews*, 192, 513-528. doi: 10.1016/j.earscirev.2019.01.004
- Jamison, W. R. (1993). Mechanical stability of the triangle zone: the backthrust wedge. *Journal of Geophysical Research: Solid Earth*, 98(B11), 20015-20030. doi: 10.1029/93JB01233
- Kartverket. (n.d.a). *Kartverkets misvisningsprogram*.  
<http://misvisning.kartverket.no/js-misv.html>
- Kartverket. (n.d.b) *Kartverkets vannstands- og tidevannsinformasjon*.  
<https://www.kartverket.no/sehavniva/sehavniva-lokasjonside/?cityid=10990121&city=Huk>
- Kiær, J. (1897). Faunistische Übersicht der Etage 5 des Norwegischen Silursystems. *Skr. Norske Videnskabselskabets Akademiske Skrifter, Kristiania. I. Matematisk- Naturv. Klasse 1897*, 3, 1-76.
- Kiær, J. (1902). Etage 5 i Asker ved Kristiania. *Norges geologiske undersøkelse*, 34, 1-112.
- Kiær, J. (1908). Das Obersilur im Kristianiagebeite: Eine Stratigrafische-faunistische

- Untersuchung. *Skr. Videnskabselskabets Akademiske Skrifter, Kristiania, I. Matematisk-Naturv. Klasse 1906, 2, 1 -595.*
- Kjerulf, T. (1857). Über die Geologie des südlichen Norwegens. *Nyt Magazin for Naturvidenskaberne*, 9, 193-333.
- Kumpulainen, R. & Nystuen, J. P. (1985). Late Proterozoic basin evolution and sedimentation in the westernmost part of Baltoscandia. In D. G. Gee and B. A. Sturt (Eds.), *The Caledonian Orogen - Scandinavia and Related Areas; Part 1* (pp. 213-232). Chichester: United Kingdom: John Wiley & Sons.
- Køber, V. (2019). *Strukturgeologisk tolkning av Krokskogenlavaplata ved bruk av grunnundersøkelser – Ringeriksbanen* (ID: URN:NBN:no-73847) [Master thesis, University of Oslo]. DUO.
- Larsen, B. T. & Olausen, S. (2005). The Oslo region: a study in classical palaeozoic geology, Stabekk, Oslo: *Geological Society of Norway (NGF)*. 1-88.
- Larsen, B. T., Olausen, S., Sundvoll, B. & Heeremans, M. (2008). The Permo-Carboniferous Oslo Rift through six stages and 65 million years. *Episodes* 31(1), 52-58.
- Larsen, B. T. & Sundvoll, B. (1983). The Oslo rift, a high-volcanicity continental rift formed from a Hercynian continent - continent collision. *IUGG XVIII General Assembly, Hamburg. Programme and Abstracts*, 2, 594.
- Larsen, B. T. & Sundvoll, B. (1984). The Oslo Graben: A passive High volcanicity continental Rift. (Abstract) *EOS* 65(45), 1084.
- Lutro, O., Graversen, O., Larsen, B. T., Naterstad, J., Bockelie, J. F., & Bockelie, T. (2017). Berggrunnskart ASKER 1814 I, M 1: 50 000. Norges geologiske undersøkelse.
- McClay, K. R. (1992). Glossary of thrust tectonics terms. In K. R. McClay (Ed.), *Thrust tectonics* (419-433). Springer Science & Business Media.
- Michelsen, O., & Nielsen, L. H. (1993). Structural development of the Fennoscandian border zone, offshore Denmark. *Marine and petroleum geology*, 10(2), 124-134.
- Morley, C. K. (1986a). Vertical strain variations in the Osen-Røa Thrust Sheet, North Western Oslo Fjord, Norway. *Journal of Structural Geology*, 8, 621-632.
- Morley, C. K. (1986b). The Caledonian thrust front and palinspastic restorations in the Southern Norwegian Caledonides. *Journal of Structural Geology*, 8, 753-765.
- Morley, C. K. (1987). Lateral and vertical changes of deformation style in the Osen-Røa thrust sheet, Oslo Region. *Journal of Structural Geology*, 9(3), 331-343.
- Morley, C. K. (1994). Fold-generated imbricates: examples from the Caledonides of Southern Norway. *Journal of Structural Geology*, 16(5), 619-631.

- Mueller, K., & Talling, P. (1997). Geomorphic evidence for tear faults accommodating lateral propagation of an active fault-bend fold, Wheeler Ridge, California. *Journal of Structural Geology*, 19(3-4), 397-411. DOI: [https://doi.org/10.1016/S0191-8141\(96\)00089-2](https://doi.org/10.1016/S0191-8141(96)00089-2)
- Naterstad, J., Bockelie, J.F., Bockelie, T., Graversen, O., Hjelmeland, H., Larsen, B.T. & Nilsen, O. 1990: Asker 1814 I, Geological bedrock map Scale 1:50 000. *Norges geologiske undersøkelse*.
- Neumann, E. R. (2019). Origin and evolution of the early magmatism in the Oslo Rift (Southeast Norway): Evidence from multiple generations of clinopyroxene. *Lithos*, 340, 139-151.
- Neumann, E. -R., Olsen, K. H., Baldridge, W. S. & Sundvoll, B. (1992). The Oslo Rift: a review. In: P.A. Ziegler (Ed.), *Geodynamics of Rifting, Volume I. Case History Studies on Rifts: Europe and Asia. Tectonophysics*, 208 (pp. 1-18). Amsterdam: Elsevier Science Publishers, B.V.
- NGU. (2019). *API OG WMS-TJENESTE*. <https://www.ngu.no/emne/api-og-wms-tjenester>
- Nordgulen, Ø. (1999). Geologisk kart over Norge, Berggrunnskart HAMAR, M 1:250 000. *Norges geologiske undersøkelse*.
- Nordgulen, Ø & Dehls, J. (2003). Bruk av digitale høydedata i strukturgeologisk analyse: Eksempel fra Oslo kommune. *Norges Geologiske Undersøkelse*, report no. 2003.013
- Nordgulen, Ø., Lutro, O., Solli, A., Roberts, D., & Braathen, A. (1998). *Geologisk og strukturgeologisk kartlegging for Jernbaneverket Utbygning i Asker og Bærum*. *Norges Geologiske Undersøkelse*, report no. 98.124.
- Novakova, L., & Pavlis, T.L., (2017). Assessment of the precision of smart phones and tablets for measurement of planar orientations: a case study. *Journal of Structural Geology*, 97, 93-103.
- Nystuen, J. P. (1981). The Late Precambrian "Sparagmites" of Southern Norway: A Major Caledonian Allochthon - The Osen-Røa Nappe Complex. *American Journal of Science*, 281, 69-94.
- Nystuen J. P. (1983). Nappe and thrust structures in the Sparagmite Region, southern Norway. *Norges Geologiske Undersøkelse*, 380, 67-83.
- Oftedahl, C. (1943). Overskyvninger i den norske fjeldkjede. *Naturen*, 47, 143-150.
- Olaussen, S., Larsen, B.T. & Steel, R., (1994). The Upper Carboniferous-Permian Oslo Rift:

- basin fill in relation to tectonic development. In A.F. Embry, B. Beauchamp, D.J. Glass (Eds.), *Pangea: Global Environments and Resources* (pp. 175-197). Canadian Society Petroleum Geologists Memoir 17.
- Owen, A. W., Bruton, D. L., Bockelie, J. F., & Bockelie, T. G. (1990). The Ordovician successions of the Oslo Region, Norway. *Norges geologiske undersøkelse, Special Publication 4*, 1-54.
- Pascal, C., Aarseth, M., Ebbing, J., Lauritsen, T., Lutro, O., & Olesen, O. (2010). *Quantitative assessment of geothermal resources in the Oslo and Bergen Regions*. Norges Geologiske Undersøkelse, report no. 2010.054.
- Perry, W. J. Jr. (1978). Sequential deformation in the Central Appalachians. *American Journal of Science*, 278, 518-542.
- Petroleum Experts. (n.d.a) *FieldMove User Guide*. Downloaded from <https://www.scribd.com/document/324544431/FieldMove-User-Guide> 17/07/2018  
<https://www.petex.com/products/move-suite/digital-field-mapping/> 01/09/2020
- Petroleum Experts. (n.d.b) *FieldMove in App Store Preview*.  
<https://apps.apple.com/no/app/fieldmove/id968405777?l=nb>
- Poblet, J. and Lisle R. J. (2011). Kinematic evolution and structural styles of fold-and-thrust belts. Kinematic Evolution and Structural Styles of Fold-and-Thrust Belts. *Geological Society of America, Special Paper*, 349(2), 1-24. doi: 10.1144/SP349.1
- Ramberg, I. B. & Larsen, B. T. (1978). Tectonomagmatic evolution. In J.A Dons & B.T. Larsen (Eds.). *The Oslo Paleorift. A review and guide to excursions*. (pp. 55-73). Norway: Norges Geologiske Undersøkelse, 337.
- Ramberg, I. B. & Spjeldnæs, N. (1978). The Tectonic History of the Oslo Region. In I.B. Ramberg & E.-R. Neumann (Eds.). *Tectonics and Geophysics of Continental Rifts* (pp. 167-194). Holland: D. Reidel Publishing Company. DOI:10.1007/978-94-009-9806-3
- Ramsay, J. G., & Huber, M. I. (1987). *The techniques of modern structural geology. Volume 2: Folds and fractures*. Academic press.
- Roberts, D. and Gee, D. G. (1985). An introduction to the structure of the Scandinavian Caledonides. In D. G. Gee and B. A. Sturt (Eds.), *The Caledonian Orogen - Scandinavia and Related Areas; Part 1* (pp. 55-68). Chichester, United Kingdom: John Wiley & Sons.
- Ryen, S.H. (2017). *Duplex structure at Hukodden*. [Poster presentation]. Norges Geologiske Forenings Vinterkonferanse, Oslo, Norway
- Schovsbo, N. H. (2002). Uranium enrichment shorewards in black shales: A case study from

- the Scandinavian Alum Shale. *GFF*, 124(2), 107-115.
- Scotese, C. R. & McKerrow, W. S. (1990). Revised world maps and introduction. In C.R. Scotese and W.S. McKerrow (Ed.) *Palaeozoic Palaeogeography and Biogeography* (pp. 1-21) London: Geological Society Memoir No. 12.  
doi:10.1144/GSL.MEM.1990.012.01.01
- Sippel, J., Saintot, A., Heeremans, M., & Scheck-Wenderoth, M. (2010). Paleostress field reconstruction in the Oslo region. *Marine and petroleum geology*, 27(3), 682-708.
- Spacapan, J. B., Galland, O., Leanza, H. A., & Planke, S. (2017). Igneous sill and finger emplacement mechanism in shale-dominated formations: a field study at Cuesta del Chihuido, Neuquén Basin, Argentina. *Journal of the Geological Society*, 174(3), 422-433. doi: 10.1144/jgs2016-056
- Stamm, N. R. (2014). Changes to the Ordovician, ca 1925 – 2014. United States Geological Survey. [https://ngmdb.usgs.gov/Geolex/resources/docs/Ordovician\\_1925-2014.pdf](https://ngmdb.usgs.gov/Geolex/resources/docs/Ordovician_1925-2014.pdf) visited 20.12.2016
- Størmer, L. (1953). The Middle Ordovician of the Oslo Region, Norway 1. Introduction to stratigraphy. *Norsk geologisk Tidsskrift*, 31, 37-141.
- Sundvoll, B., & Larsen, B. T. (1993). Rb-Sr and Sm-Nd relationships in dyke and sill intrusions in the Oslo Rift and related areas. *Norges Geologiske Undersøkelse*, 425, 31-42.
- Sundvoll, B. & Larsen, B. T. (1994). Architecture and early evolution of the Oslo Rift. *Tectonophysics*, 240(1-4), 173-189.
- Sundvoll, B., Larsen, B. T. & Wandaas, B. (1992). Early magmatic phase in the Oslo Rift and its related stress regime. *Tectonophysics*, 208, 37-54.
- Sundvoll, B., Neumann, E.-R., Larsen, B. T. & Tuen, E. (1990). Age relations among Oslo rift magmatic rocks: implications for tectonic and magmatic modelling. *Tectonophysics*, 178, 67-87.
- Timmerman, M. J. (2004). Timing, geodynamic setting and character of Permo-Carboniferous magmatism in the foreland of the Variscan Orogen, NW Europe. *Geological Society, London, Special Publications*, 223(1), 41-74.
- Torsvik, T. H. & Cocks, L. R. M. (2016). *Earth History and Palaeogeography*. Cambridge University Press. DOI: <https://doi.org/10.1017/9781316225523>
- Torsvik, T. H., Smethurst, M. A., Meert, J. G., Van der Voo, R., McKerrow, W. S., Brasier,



- M. D., Sturt, B.A. & Walderhaug, H. J. (1996). Continental break-up and collision in the Neoproterozoic and Palaeozoic—a tale of Baltica and Laurentia. *Earth-Science Reviews*, 40(3-4), 229-258.
- Torsvik, T. H., Smethurst, M. A., Burke, K., & Steinberger, B. (2008). Long term stability in deep mantle structure: Evidence from the ~300 Ma Skagerrak-Centered Large Igneous Province (the SCLIP). *Earth and Planetary Science Letters*, 267, 444-452.
- Twiss, R. J. & Moores, E. M. (1992). *Structural Geology* (1<sup>st</sup> ed.). United States of America: W. H. Freeman and Company.
- Twiss, R. J. & Moores, E. M. (2006). *Structural Geology* (2<sup>nd</sup> ed.). United States of America: W. H. Freeman and Company.
- Veevers, J. J., Clare, A., & Wopfner, H. (2007). Neocratonic magmatic-sedimentary basins of post-Variscan Europe and post-Kanimblan eastern Australia generated by right-lateral transtension of Permo-Carboniferous Pangaea. *Basin Research*, 6(2-3), 141-157.
- Wilson, M., Neumann, E. -R., Davies, G. R., Timmerman, M. J., Heeremans, M., & Larsen, B. T. (2004). Permo-Carboniferous magmatism and rifting in Europe: introduction. *Geological Society, London, Special Publications*, 223(1), 1-10.
- Woodward, N. B., Boyer, S. E., & Suppe, J. (1989). *Balanced Geological Cross Sections: An Estimate Technique in Geological Research and Exploration*. U.S.A.: American Geophysical Union.
- Worsley, D., Aarhus, N., Bassett, M. G., Howe, M. P. A., Mørk, A. & Olausson, S. (1983). The Silurian succession of the Oslo region. *Norsk Geologiske Undersøkelse*, 384, 1–57.
- Ziegler, P. A. (1990). *Geological Atlas of Western and Central Europe* (2<sup>nd</sup> ed.). Shell International and Geological Society of London.

## Appendix 1: Comprehensive descriptions of lithostratigraphic units

### Alum Shale Formation

The Alum Shale Fm. is part of the Røyken Group. It has no members (Owen et al., 1990).

The Alum Shale Fm. is of middle Cambrian to Lower Ordovician in age, and even though the unit has an estimated stratigraphic thickness of about 80-100 metres in the Oslo Region (Andersson et al., 1985; Schovsbo, 2002; Bruton et al., 2010), it varies greatly throughout the area, mainly due to tectonic activity from the Caledonian orogeny. The formation contains black shales that are rich in organic material, as well as discontinuous beds and concretions of stinkstone, or bituminous limestone (Owen et al., 1990). The concretions, or nodules, are ellipsoidal to plate-like in shape, and can reach sizes of up to 3 metres in diameter (Henningsmoen, 1974). In the Oslo Region, both the black shales and the stinkstone nodules of the Alum Shale Fm. contain trilobite and graptolite fossils (Andersson et al., 1985). However, the trilobite fossils are much more common and better preserved in the limestone nodules than they are in the shales (Bjørlykke, 1974). The black shale facies contains both carbon and sulphur, as well as trace elements such as uranium and vanadium (Bjørlykke, 1974).

The Alum Shale Fm. can be distinguished from other black shales in the area, such as the Galgeberg Mb. of the Tøyen Fm. and the Sjøstrand and Engervik members of the Elnes Fm., by its black streak colour (Owen et al., 1990) and large stinkstone nodules. The Tøyen and Elnes shales also contain limestone nodules, but they are considerably smaller.

Observed at multiple locations in the south of the Slemmestad area and at two locations at Bygdøy, north of Bygdøy Sjøbad, and at Killingen island.

### Bjørkåsholmen Formation

The Bjørkåsholmen Fm. has no members, and is part of the Røyken Group. It is formerly known as 3aα, Ceratopyge Limestone (Owen et al., 1990).

The formation consists of a continuous bed of pale grey limestone, which in some places is interbedded with dark grey shale. The limestone bed is micritic, except for a brown bed of

calcarenite in the uppermost part (Bjørlykke, 1974). The formation has a thickness of about 1 m. There is a sharp boundary between the light grey limestone nodules of the Bjørkåsholmen Fm. and the underlying dark grey shales of the Alum Shale Fm. (Owen et al., 1990).

The Bjørkåsholmen Fm. can resemble the Huk Fm. when observed in the field, as both formations consist of massive limestones, which weather to a pale grey colour. The Bjørkåsholmen limestone and the upper limestone of the Huk Fm. (The Hukodden Mb.) both have bands of orange colour due to oxidation of pyrite concretions within the limestone. However, it is usually an easy task to tell the two formations apart. The Huk Fm. contains two members of massive limestone beds, which are separated by a layer of dark shale and nodular limestone (see below). The Bjørkåsholmen Fm., on the other hand, unless it has been displaced and repeated by thrusting, will appear as a lone bed of massive limestone, interbedded with dark shales. The Bjørkåsholmen Fm. is considerably thinner than both the upper and lower limestone beds of the Huk Fm. It can further be distinguished from the upper layer of the Huk Fm. by the complete absence of *Cycloendoceras commune* fossils.

Observed at multiple locations in the Slemmestad area, and at Killingen island and north of Bygdøy Sjøbad at Bygdøy.

## Tøyen Formation

Formerly known as 3b, Lower Didymograptus Shale, the Tøyen Fm. is part of the Røyken Group and includes two members, the Hagastrand Mb. and the Galgeberg Mb. (Owen et al., 1990).

## Hagastrand Member

The Hagastrand Mb., formerly known as 3b $\alpha$  (pars), is composed of layers of light grey to grey, and sometimes black, shale with discontinuous to continuous beds of dolomitic limestone (Bjørlykke, 1974; Owen et al., 1990). Due to embedded pyrite nodules, both the grey shales and the limestone beds show rusty weathering in some places. The Hagastrand Mb. has a thickness of about 10 m. There is a clear boundary between the massive limestone of the Bjørkåsholmen Fm. and the grey shales of the Hagastrand Mb. (Owen et al., 1990).

## Galgeberg Member

The Galgeberg Mb. is formerly known as 3b $\beta$ - $\epsilon$ . It is composed almost entirely of black graptolitic shale with horizons of pyrite. The uppermost part of the member is marked by the appearance of a few limestone nodules, and lighter shales. The Galgeberg Mb. is approximately 12 metres thick. The boundary between the members of the Tøyen Fm. is clear, the limestones and grey shales of the Hagastrand Mb. meet the black shales of the Galgeberg Mb. with no transitional boundary (Owen et al., 1990).

The contact between the Galgeberg Mb. and the lower limestone of the Huk Fm. is marked by a band of pyrite nodules in the last 20 cm of the shales, and a grey layer of silty shale about 5 cm in thickness directly underlying the massive limestone.

The Galgeberg Mb. has been observed at both Slemmestad and on southern Bygdøy, whilst the older member, the Hagastrand Mb., has only been observed at Slemmestad.

## Huk Formation

The Huk Fm. is formerly known as 3c or 3c $\alpha$ - $\gamma$ , Orthoceras Limestone. It is part of the Røyken Group, and includes three members in the Oslo Region: the Hukodden Mb., the Lysaker Mb., and the Svartodden Mb.

The formation comprises two massive limestone units separated by a layer of marly shales interbedded with limestone nodules. The combined thickness of the Huk Fm.'s members is about 7 m. The base marks a sharp boundary to the black shales of the Tøyen Fm., and the top marks an equally sharp boundary to the black shales and limestone nodules of the lowermost member of the Elnes Fm. (Owen et al., 1990).

The formation in its entirety, as well as individual members of the formation, has been observed repeatedly throughout both southern Bygdøy and the Slemmestad area.

## Hukodden Member

The Hukodden Mb. is formerly known as 3 $\alpha$ , Megistaspis Limestone, and constitutes the bottom member of the Huk Fm. It consists of massive pale limestone with some shelly material. It has a thickness of approximately 1.6 m (Owen et al., 1990).

## Lysaker Member

The Lysaker Mb. is the middle member of the Huk Fm., and it is formerly known as 3cβ, Asaphus Shale. It contains light grey marly shales with limestone nodules and sometimes discontinuous beds of limestone (Bjørlykke, 1974). The limestone to shale ratio varies throughout the member, and fossils can often be found within the nodules.

The thickness of the member varies throughout the Oslo-Asker region, with a thickness of about 2,5-3 metres at Bygdøy and in the Slemmestad area. The variation may in part be due to tectonic activity (Owen et al., 1990). Because of this, it is difficult to ascertain the Lysaker Mb.'s true thickness.

## Svartodden Member

The Svartodden Mb. is formerly known as 3cγ, Endoceras Limestone. As the upper part of the Huk trinity, it comprises a pale grey massive limestone with an approximate thickness of 2,5-3 metres. It is easily recognisable by its large amount of *Cycloendoceras commune* fossils (Owens et al., 1990). The nautiloid cephalopod can be utilised as a way up indicator.

The Hukodden Mb. is very similar in appearance to the Svartodden Mb. limestone, but can usually be distinguished from the upper Huk Mb. by inspecting the limestone bed thoroughly to rule out the presence of *Cycloendoceras commune* fossils. One can also look for the pyrite-rich border between the Hukodden Mb. and the underlying black shales of the Tøyen Fm. The Hukodden Mb. has bands of rust that run parallel to the bedding due to pyrite nodules within the limestone. These bands are observed in the middle and at the top of the member as well, and not just at the bottom where it directly overlies the Tøyen shales. The border between the Svartodden Mb. and the Elnes Fm. is not characterised by an abundance of pyrite.

## Elnes Formation

The Elnes Fm. is formerly known as 4aα<sub>1-4</sub>, Upper Didymograptus Shale, and is a part of the Oslo Group. The formation comprises three members in the Oslo region: the Sjøstrand Mb., the Engervik Mb., and the Håkavik Mb.

The Elnes Fm. can sometimes be difficult to differentiate from the Tøyen Fm. The Galgeberg Mb. of the Tøyen Fm. and the Sjøstrand Mb. of the Elnes Fm. both consists of black shales with pyrite and lone limestone nodules. They are poor in fossil content, and are therefore very difficult to tell apart when observed in the field. Bjørlykke (1965) stated that the Elnes Fm. has a higher concentration of magnesium and chlorite than the Tøyen Fm. This was confirmed by Bjørlykke (1974) after further investigation showed that the chlorite content of the area increased upwards from the Tøyen Fm. throughout the Huk Fm. and into the Elnes Fm. This is not a helpful way to distinguish the two from each other in the field, but samples may be collected and analysed if there is doubt about the black shales in an outcrop.

### Sjøstrand Member

The Sjøstrand Mb. is formerly known as 4a $\alpha$ <sub>1-2</sub>, Upper Didymograptus Shale. It consist almost entirely of black shale, with some scattered limestone nodules. The base is marked as right above the uppermost continuous limestone bed of the Helskjær Mb. (Owen et al., 1990), however, this member of the Elnes Shale is not observed at Bygdøy or Slemmestad during the mapping for this thesis. Størmer (1953) observed the member's thickness to be about 49 m at Slemmestad and 32 m at Bygdøy. It is, however, uncertain if this is the true thickness of the layer, or if it is due to repetition by Caledonian folding and thrusting (Owen et al., 1990).

### Engervik Member

The Engervik Mb. is formerly known as 4a $\alpha$ <sub>3</sub>, Ogygiocaris Shale, and is made up of black shale with nodules and continuous beds of limestone. Some of the nodules and limestone beds contains the trace fossil *Chondrites*. The Engervik Mb. has an approximate thickness of 15-19 m, but due to tectonic activity, it is difficult to know whether this is the member's true thickness or not (Owen et al., 1990).

### Håkavik Member

The Håkavik Mb. is formerly known as 4a $\alpha$ <sub>4</sub>, The bronni beds or Trinucleus bronni. The member's lower boundary comprises a 10 cm thick bed of calcareous silt and sand which weathers to a brown colour. The *Chondrites* fossils of the Engervik Mb. is not found within

the Håkavik Mb. (Bjørlykke, 1974, Owen et al., 1990). The basal bed shows convolute lamination structures (Bjørlykke, 1974), which are helpful to determine whether or not the bed has been overturned. The overlying beds that make up the rest of the Håkavik Mb. are alternating grey shale and grey to brown calcareous silt with some grey limestone nodules. Cross- and planar lamination structures are not limited to the lowermost part of the Håkavik Mb., but it's not as common in the upper calcarenites beds. The Håkavik Mb. has a thickness of approximately 12-14 m.

## Vollen Formation

The Vollen Fm. is formerly known as 4a $\beta$ , Ampyx Limestone. It is part of the Oslo Group, and is a formation with no members (Owen et al., 1990). The base of the Vollen Fm. is set as the shale overlying the last of the calcarenite beds of the Håkavik Mb. of the Elnes Fm. The base of the Vollen Fm. also contains *Chondrites* fossils within the limestone beds and nodules (Bjørlykke, 1974; Owen et al., 1990). The beds of limestone and calcareous shale occur together in repeating units of 10 cm and 40 cm in thickness. This alternation is likely due to a rhythmic sedimentation rate controlled by Milankovitch cycles (Bjørlykke, 1974; Owen et al., 1990, Ballo et al., 2019).

It is difficult to determine the thickness of the Vollen Fm. as there are no outcrops that show the formation in its entirety in the Oslo Region. Additionally, most outcrops are either incomplete or show at least some degree of deformation by thrusting (Owen et al., 1990). Owen et al. (1990) state that 40-44 m of the Vollen Fm. is exposed in the Slemmestad area and on Bygdøy. Geological mapping for this project has interpreted about 70,27 metres of the Vollen Fm., including the lower and upper boundaries, to be exposed at Bygdøy, west of the restaurant (Fig. 5.2.1). The beds of the outcrop has an average dip of approximately 50°. Using trigonometry, the true thickness of the unit is calculated to be 53,83 metres. East of this, by Bekkebukta, approximately 81,1 m of the Vollen Fm., from lowest boundary to upper boundary, is exposed. Using the same trigonometrical calculation, this equals a vertical thickness of about 62,1 m.

The sedimentary succession both by the restaurant at Hukodden and to the east by Bekkebukta shows clusters of thrust faults, with up to five thrust faults being present within a 1 metre thick parcel of rock. At first glance it appears the multiple thrust faults within the formation has led to minimal offset. However, it is difficult to distinguish the lower part of the

formation from the upper part, and it is therefore difficult to say with certainty whether or not the thrust faults have led to noticeable offset and serious stratigraphic thickening of the strata. Due to this, the true thickness of the Vollen Fm. at Bygdøy is difficult to ascertain. Thrust faults at a higher stratigraphic level reveals repetitions of the Vollen Fm. inside the overlying shale-dominated Arnestad Fm.

The Vollen Fm. and the Engervik Mb. (Elnes Fm.) may appear very similar when observed in the field. One way to tell which is which is by looking at the unit above and/or below if the boundary is present and undeformed. For example, the Håkavik Mb. of the Elnes Fm. is a useful marker bed, as its brown, silty, beds make it easy to recognise and can provide way-up indicators. However, if this boundary is not present, it can be difficult to know whether one is looking at beds of the Vollen Fm. or the Engervik Mb. Personal communication with Hans Arne Nakrem and Øyvind Hammer provided invaluable in distinguishing the two units from one another in the field (er det en bedre måte å si dette på, virker som ei litt lang setning?). The most obvious difference is the visual appearance of the limestone beds. The limestone of the Engervik Mb. form straight layers, whereas the Vollen limestone has a dented and uneven appearance. Another way to tell them apart is by looking at the limestone to shale ratio. The Vollen Fm. is categorised as a limestone by Owen et al. (1990), whereas the Engervik Mb.'s main lithologies are described as "*grey shale with limestone horizons*" (Owen et al., 1990, p.18).

The Vollen Fm. has been observed both at Slemmestad and on Bygdøy.

## Arnestad Formation

The Arnestad Fm. is formerly known as 4b $\alpha$ , Lower Chasmops Shale, and is part of the Oslo Group. It has no members (Owen et al., 1990). The base of the Arnestad Fm. is defined by dark shales with horizons of limestone. The formation is shale-dominated, with alternating layers of thick shale and thinner limestone. The limestone appears as both continuous and nodular and is less than 10 cm thickness. In contrast, the shale usually has a thickness of about 30-40 cm, although beds reaching a thickness of 70 cm has been recorded as well. The alternation of limestone and shale in the Arnestad Fm. is, as with the Vollen Fm., thought to be controlled by Milankovitch cycles (Ballo et al., 2019). The true thickness of the Arnestad Fm. is unknown as there are no outcrops that reveal a complete and undeformed section. Hansen and Harper (2006) estimate the formation to be at least 60 m in thickness.



The shales are dark grey in the eastern part of the Oslo Region (in Oslo), which is different to the western part (Asker and Ringeriket) where they are green-grey in colour. The dark grey shales weather to a light grey colour.

The Arnestad Fm. contains beds of altered volcanic ash known as K-bentonites (Ballo et al., 2019). These beds are found from North America in the west, through Baltoscandia, all the way to western Russia (Bruton et al., 2010). The ash originated from volcanic island arcs in the Iapetus Ocean (Huff, 2016; Ballo et al., 2019)

This formation has been observed on southern Bygdøy. The boundary between the Vollen Fm. and the Arnestad Fm. is present, but the upper boundary of the Arnestad Fm. is not found at this location.

## Appendix 2: Suggestion for order of tectonic events at Hukodden

This is only one of many possible suggestions for the order of deformation events on either side of the identified tear fault at Hukodden. A lack of outcrops NE of the syenite porphyry dyke that cuts through Huk makes it difficult to identify differences in geology on either side of the syenite porphyry dyke NW of Hukodden (Sub-area 7; Fig. 5.2.1). Therefore, it is difficult to say for certain how far NW the identified tear fault continues.

Western side of the identified tear fault, illustrated in cross-section EF (Fig. 5.2.5.1)

- The fold at the naturist beach (Sub-area 4 and 5) forms and is torn by a tear fault resulting in an overturned anticline in the NE and an anticline with parasite folds in the SW.
  - o The fold most likely forms above a local detachment zone within the Alum Shale Fm. as the volume of the Alum Shale and Bjørkåsholmen formations are needed to achieve the shape and size of the fold recorded in outcrops at location 4 and 5.
  - o It is possible the splay from the local detachment zone pictured in map (Fig. 5.2.1) and cross-sections AB, CD, and EF (Fig. 5.2.5.1 and Fig. 5.2.6.2) forms at this stage and starts to cut through the fold, creating a fault-propagation fold. This splay may be the active thrust fault in the tear fault-thrust fault dynamic.
- A local detachment zone in the Galgeberg Mb. (Upper Tøyen) forms and a ramp-flat structure in the sub-surface forms SE of the fold. The ramp cuts from Galgeberg Mb. (Upper Tøyen) to within the Elnes Fm. The sole thrust continues to be active, making the ramp structure the first horse in what could become an in-sequence duplex structure.
- The splay from the local detachment zone beneath the fold at the naturist beach forms, or is still active, it cuts through both fold limbs of the fold and thrusts it over the ramp

structure, displacing the Vollen and Arnestad formations of the ramp structure in the process.

- The ramp-flat structure in the NW (the ramp beneath Sub-areas 4 and 5; Fig. 5.2.1 and Fig. 5.2.5.1) may be halted by the formation of the backthrust, or it may be halted by something else, which in turn leads to the creation of the backthrust. The backthrust accommodates the residual displacement along the ramp.
- The backthrust dies, resulting in faulting outside of the original triangle zone
- The local detachment zone of the ramp-flat structure in the sub-surface of Sub-areas 4 and 5 (Fig. 5.2.1 and Fig. 5.2.5.1) propagates forwards and a new ramp structure forms in the SE in the sub-surface of Sub-area 1 (Fig. 5.2.1 and Fig. 5.2.5.1).
- The sole thrust of the ramp structure cuts from Galgeberg Mb. (Upper Tøyen) to Engervik Mb. (Middle Elnes), and the hanging-wall is thrust up onto the ramp-flat structure.
- At some point the hanging-wall becomes stuck, possibly because the local detachment fault cuts up from the shaly Elnes Fm. and into the limestone-dominated Vollen Fm., which either terminates the detachment fault or seriously impedes its forward propagation.
- This leads to out-of-sequence deformation of the hanging-wall of the ramp structure in the form of fault-propagation folds. First, the fault-propagation fold, which today is visible in the Hukodden skerries in Sub-area 1, forms, then the fault-propagation fold, which today is visible at the southeastern headland in Sub-area 1, forms (Fig. 5.2.1 and Fig. 5.2.5.1).
- At this point, the syncline in Sub-area 2 has formed with the ramp structure in the NW comprising one fold limb, and the ramp structure in the SE comprising the other (Fig. 5.2.5.1).
- Continuous compression from NW may cause the backthrust to reactivate, if only a little, as a pop-up structure forms in the fold hinge of the syncline (Fig. 5.2.5.1). The pop-up structure forms due to accumulation of strain in one area as the thrust sheet is prevented from moving forward. The adjacent triangle structure might be subjected to internal deformation to stabilise the backthrust wedge, this might be done in the form of multiple smaller scale faults, similar to the smaller scale faults in the adjacent pop-

up structure. The order of events regarding the formation of the triangle zone and pop-up zone is uncertain and further research is needed.

Eastern side of the identified tear fault, illustrated in cross-section GH (Fig. 5.2.7.4) and in Figure 5.2.7.9.

- Due to lack of outcrops on this side of the identified tear fault, it is not possible to say whether the fold in Sub-areas 4 and 5 exists east of the tear fault (Fig. 5.2.1, Fig. 5.2.5.1, and Fig. 5.2.7.4). The first part of the suggested order of events is otherwise similar to events on the western side of the identified tear fault.
  - A local detachment zone in the Galgeberg Mb. (Upper Tøyen) forms and a ramp-flat structure in the sub-surface forms (to the NW of balanced cross-section GH; Fig. 5.2.7.4). A ramp cuts from the local detachment zone in the Galgeberg Mb. (Upper Tøyen) to within the Elnes Fm. The sole thrust continues to be active, making the ramp structure the first horse in what could become an in-sequence duplex structure.
- Due to poor outcrops east of the identified tear fault, it is uncertain whether the backthrust exists on this side. If the backthrust is not present here, it may indicate that the tear fault was active at this stage.
  - If the backthrust is not present NE of the syenite porphyry dyke/the identified tear fault in Sub-area 3 (Fig. 5.2.1), the detachment fault of the ramp structure may have continued to cut through the upper members of the Elnes Fm. This may have formed another ramp leading to the repetition of the Engervik Mb. (Middle Elnes) and Håkavik Mb. (Upper Elnes) in Sub-area 7 (Fig. 5.2.1 and Fig. 5.2.7.4).
  - If the backthrust exists NE of the syenite porphyry dyke/the identified tear fault in Sub-area 3 (Fig. 5.2.1), this repetition of the upper Elnes Fm. members may have formed post-backthrusting.
  - It is probable that the Elnes Fm. repetitions formed at an early stage as they are steeply dipping and were probably tilted by the ramp structure in the SE.

- Another suggested series of events are similar or the same to the western side of the tear fault:
  - The local detachment zone in the Galgeberg Mb (Upper Tøyen) propagates forwards and forms a new ramp-flat structure in the SE in the sub-surface of Sub-area 6 (Fig. 5.2.1 and Fig. 5.2.7.4).
  - The sole thrust of the ramp structure cuts from the Galgeberg Mb. (Upper Tøyen) to within the Elnes Fm., and the hanging-wall is thrust up onto the ramp-flat structure.
  - At some point the hanging-wall becomes stuck, possibly because the sole thrust cuts up from the shaly Elnes Fm. and into the limestone-dominated Vollen Fm., which either terminates the detachment fault or seriously impedes its forwards propagation.
  
- The deformation of the hanging-wall of the ramp-flat structure happens according to what is described in Section 5.2.7. Three fault-propagation folds form out-of-sequence and the northwesternmost, the Hukodden imbricate structure, is displaced and deformed by several splays.
  
- The shortening in Sub-area 6 (the three fault-propagation folds, including internal deformation of the Hukodden imbricate structure; Fig. 5.2.1 and Fig. 5.2.7.4) is greater than the shortening in Sub-area 1 (the two fault-propagation folds; Fig. 5.2.1 and Fig. 5.2.5.1). The hanging-wall of the ramp-flat structure to the west (Sub-area 1; Fig. 5.2.1) is therefore interpreted to have propagated forwards as the hanging-wall to the east (Sub-area 6; Fig. 5.2.1) had already become stuck and started the out-of-sequence deformation.

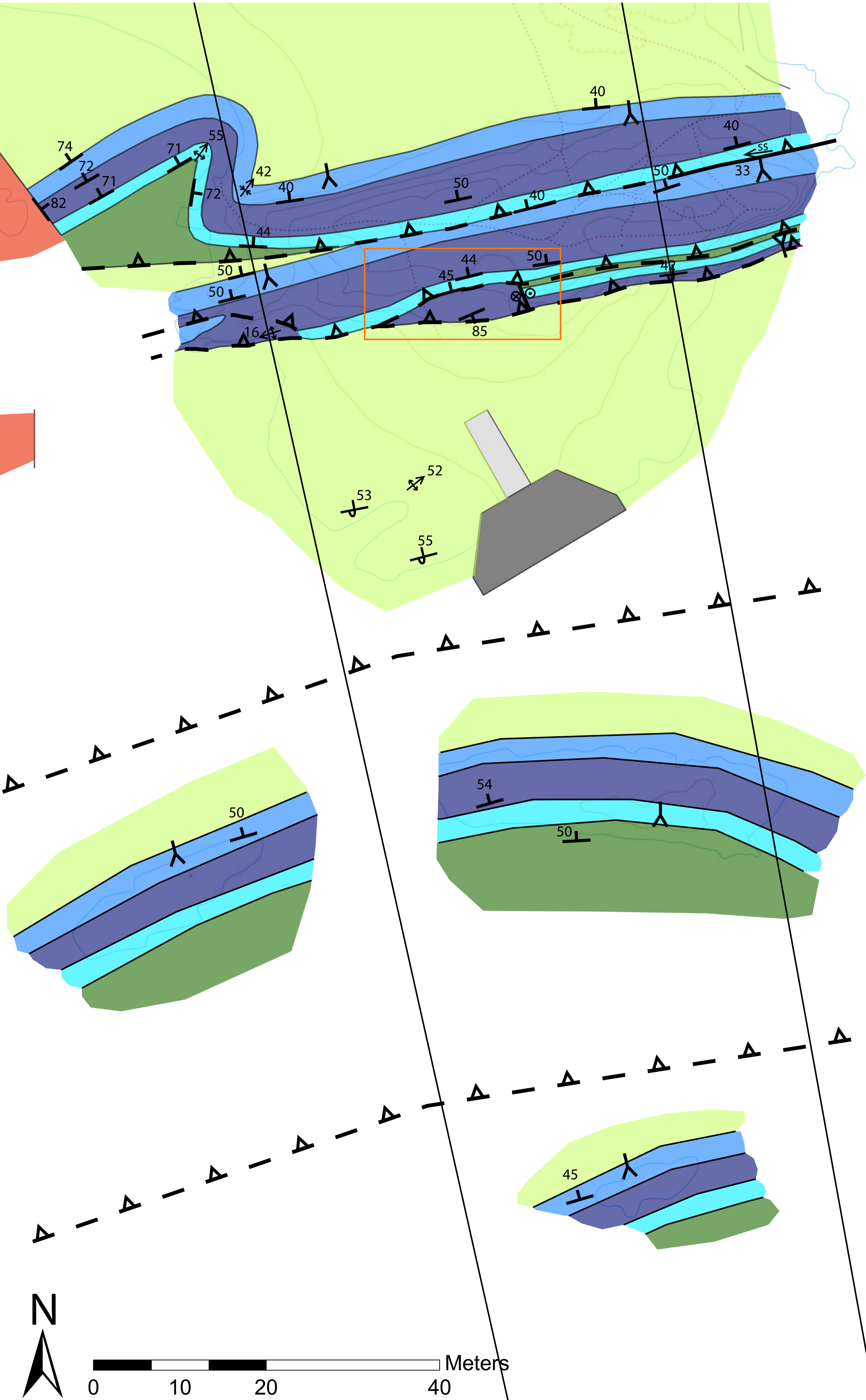
### Appendix 3: Geological maps, legend, balanced cross-sections, cross-sections, figures accompanying balanced cross-sections, and drone photo

- Plate 1: Geological map of Huk
- Plate 2: Detailed geological map of Huk, Sub-area 6 (detailed)
- Plate 3: Geological map of Slemmestad
- Plate 4: Legend for all geological maps and cross-sections
- Plate 5: Cross-sections AB and CD
- Plate 6: Balanced cross-section EF
- Plate 7: Balanced cross-section GH
- Plate 8: Cartoon accompanying balanced cross-section GH
- Plate 9: Balanced cross-section IJ
- Plate 10: Cartoon accompanying balanced cross-section IJ
- Plate 11: Cross-sections KL and MN
- Plate 12: Drone photo of Sub-area 6

# Appendix 3, Plate 1: Geological map of Huk

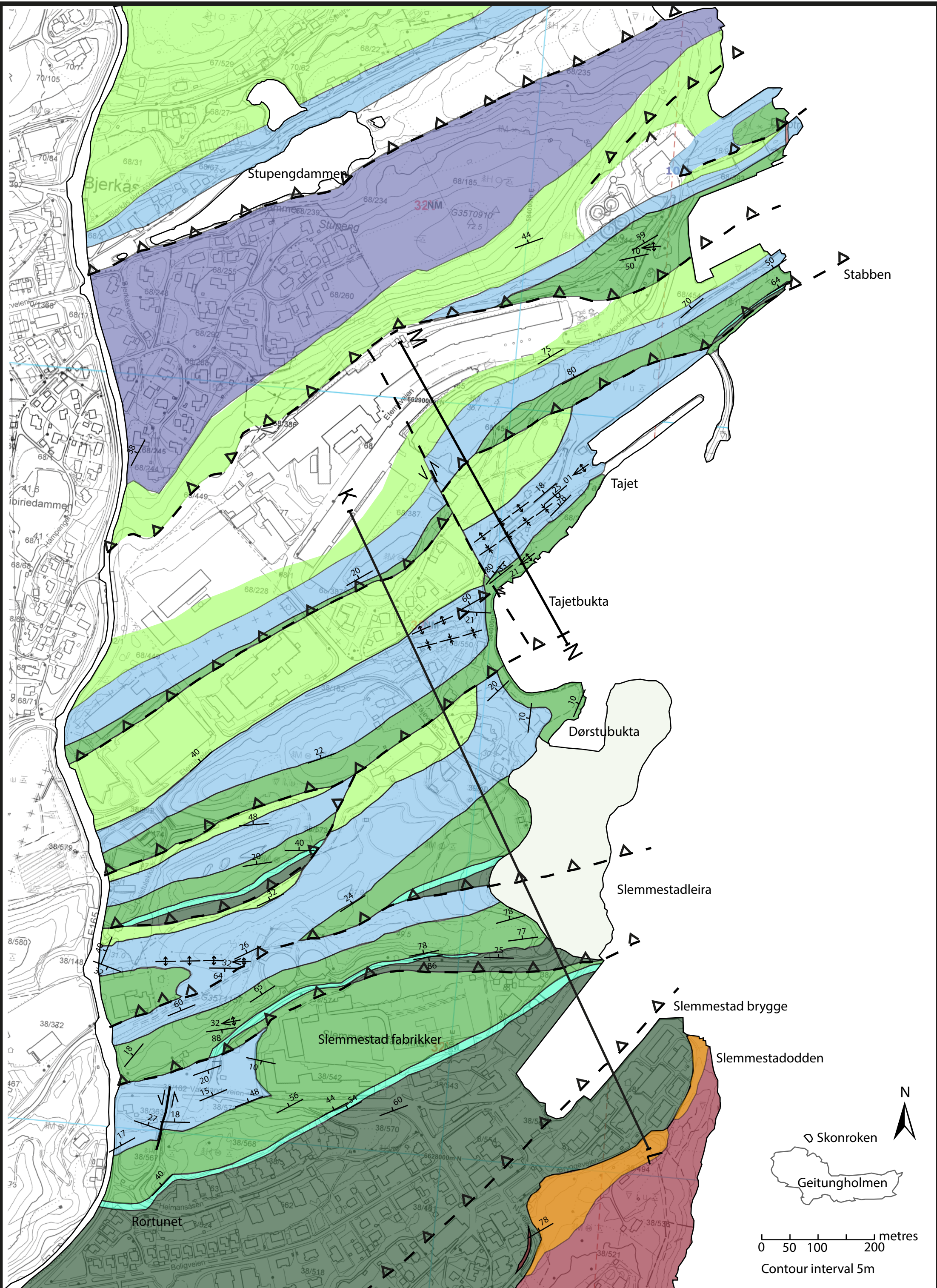


# Appendix 3, Plate 2: Detailed geological map of Sub-area 6: Hukodden East








# Appendix 3, Plate 3: Geological map of Slemmestad





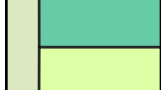
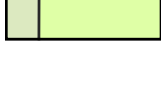


# Legend for maps and profiles








## Intrusive rocks of Carboniferous, Permian, and Triassic age



-  Syenite porphyry
-  'Mænaite' = microsyenite with albite
-  Mafic dyke

## Oslo Group, Mid and Late Ordovician

-  Arnestad Formation
-  Vollen Formation
-  Elnes Formation
-  Håkavik Member
-  Engervik Member
-  Sjøstrand Member

## Røyken Group, Mid Cambrian to Mid Ordovician

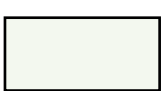
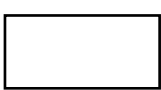
-  Huk Formation
-  Svartodden Member
-  Lysaker Member
-  Hukodden Member
-  Tøyen Formation
-  Galgeberg Member
-  Hagastrand Member

-  Bjørkåsholmen Formation
-  Alum Shale Formation

## Bedrock









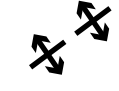




-  Bedrock

## Other

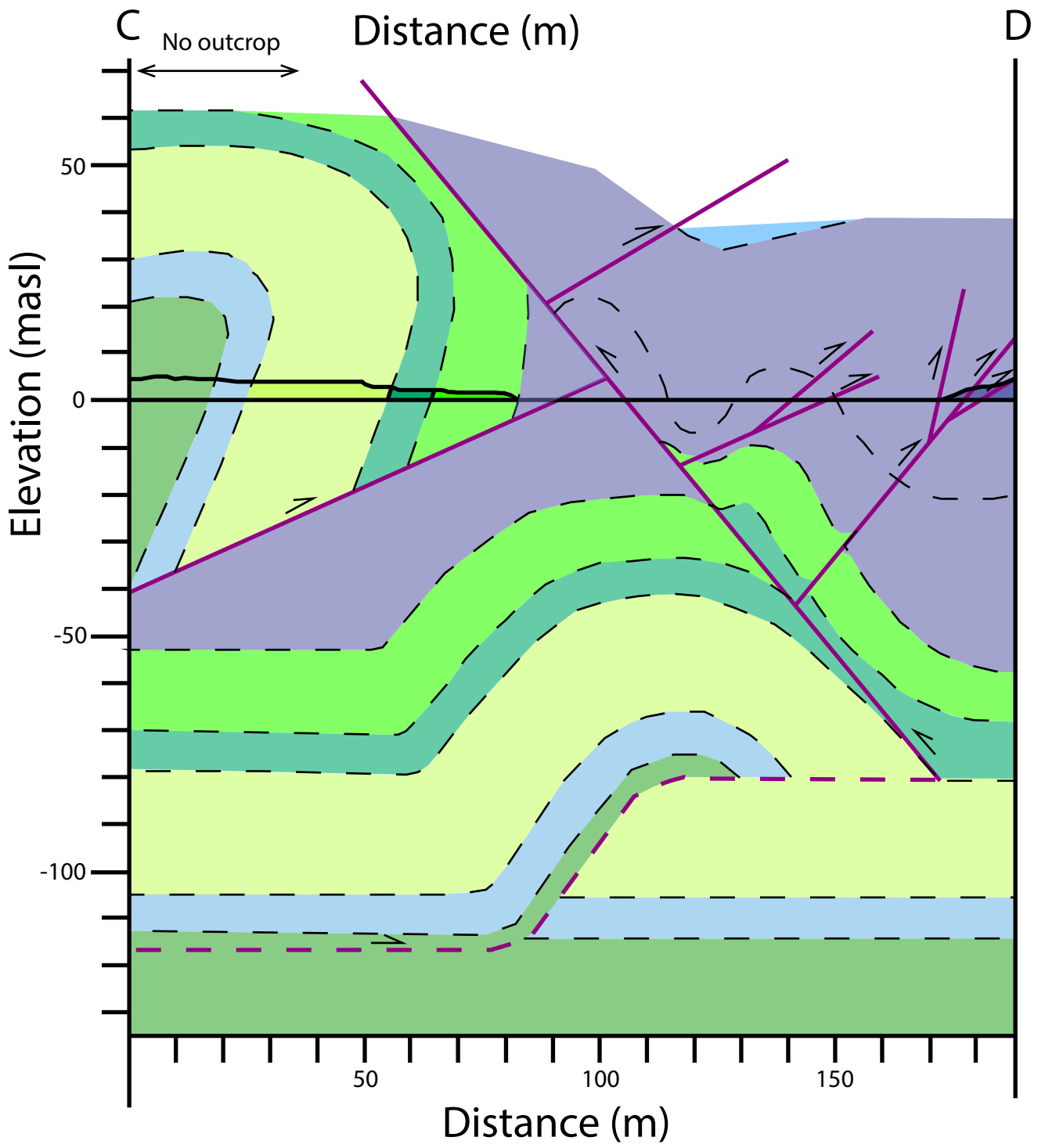
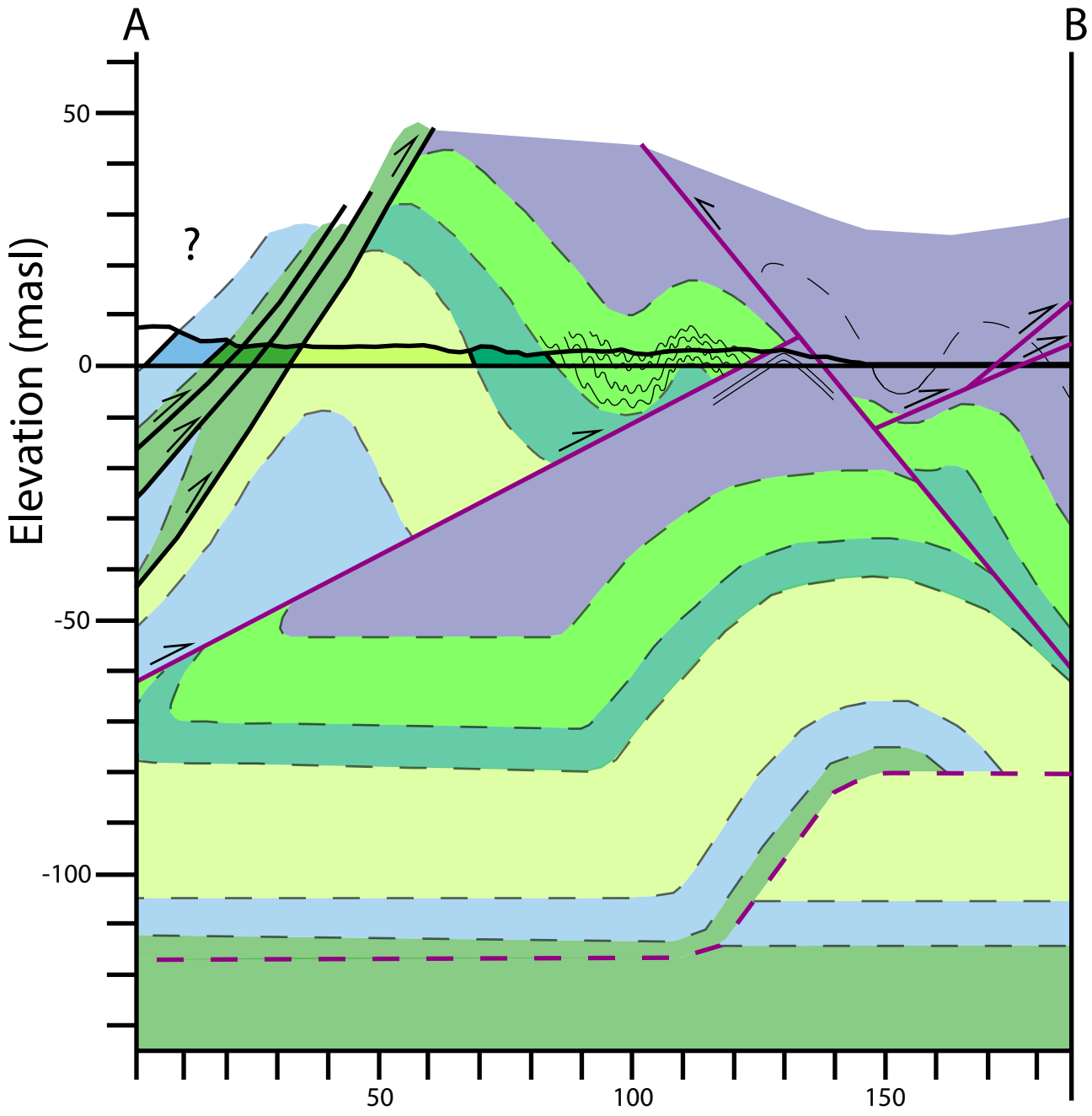
-  Anthropogenic cover
-  No outcrops

Where lithologies are inferred in areas of no outcrops, colours are lighter in shade

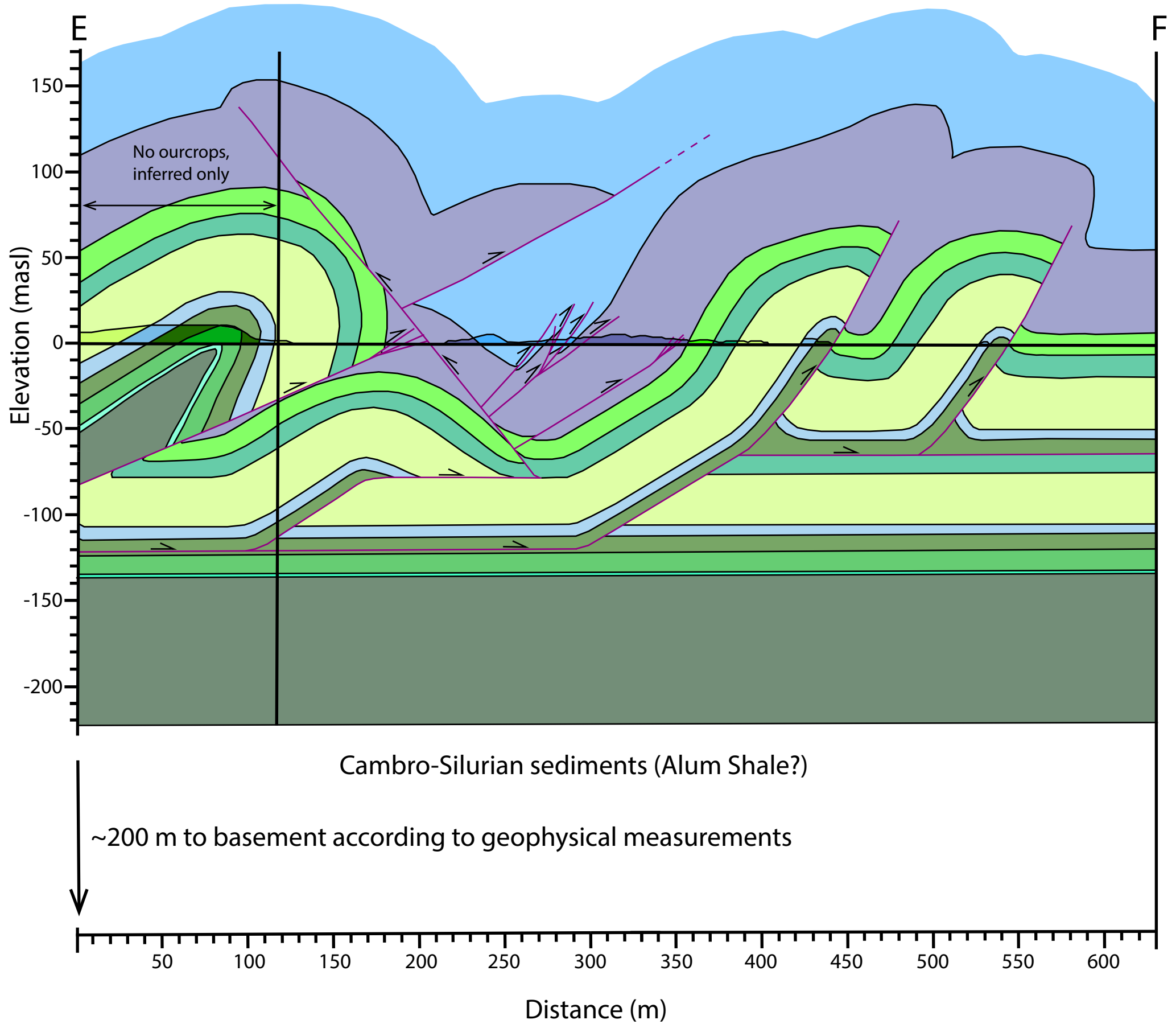
## Geological lines and symbols

-  Lithological boundary, definite
-  Lithological boundary, inferred
-  Thrust fault, definite
-  Thrust fault, inferred
-  Tear fault, definite
-  Tear fault, inferred
-  Fold axis with plunge indicated, synform
-  Fold axis with plunge indicated, antiform
-  Axial plane trace, antiform
-  Axial plane trace, synform
-  Strike and dip, dip indicated
-  Strike and dip, overturned, dip indicated
-  Line of cross section

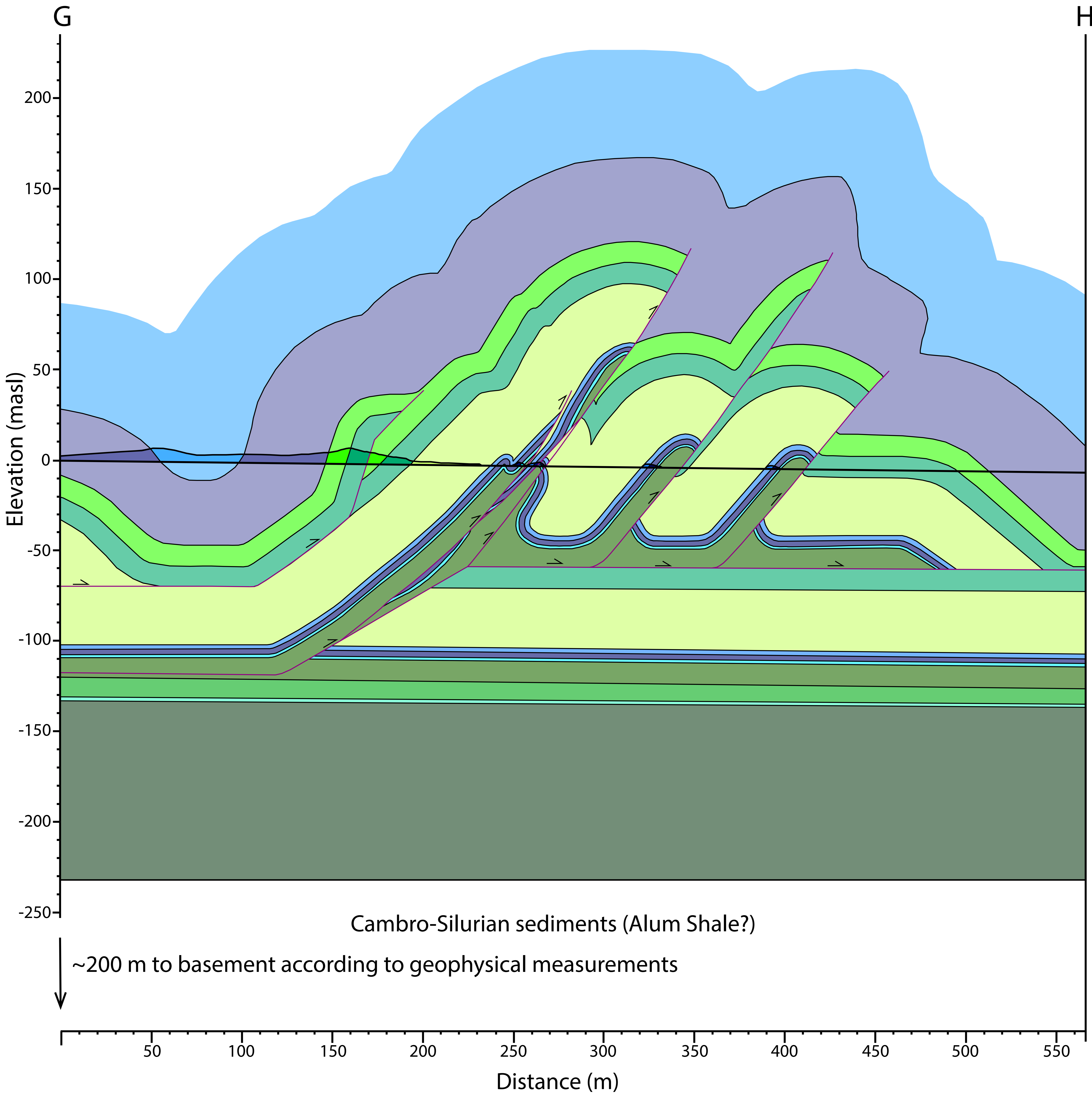
Appendix 3, Plate 5: Cross-section AB and CD



# Appendix 3, Plate 6: Balanced cross-section EF

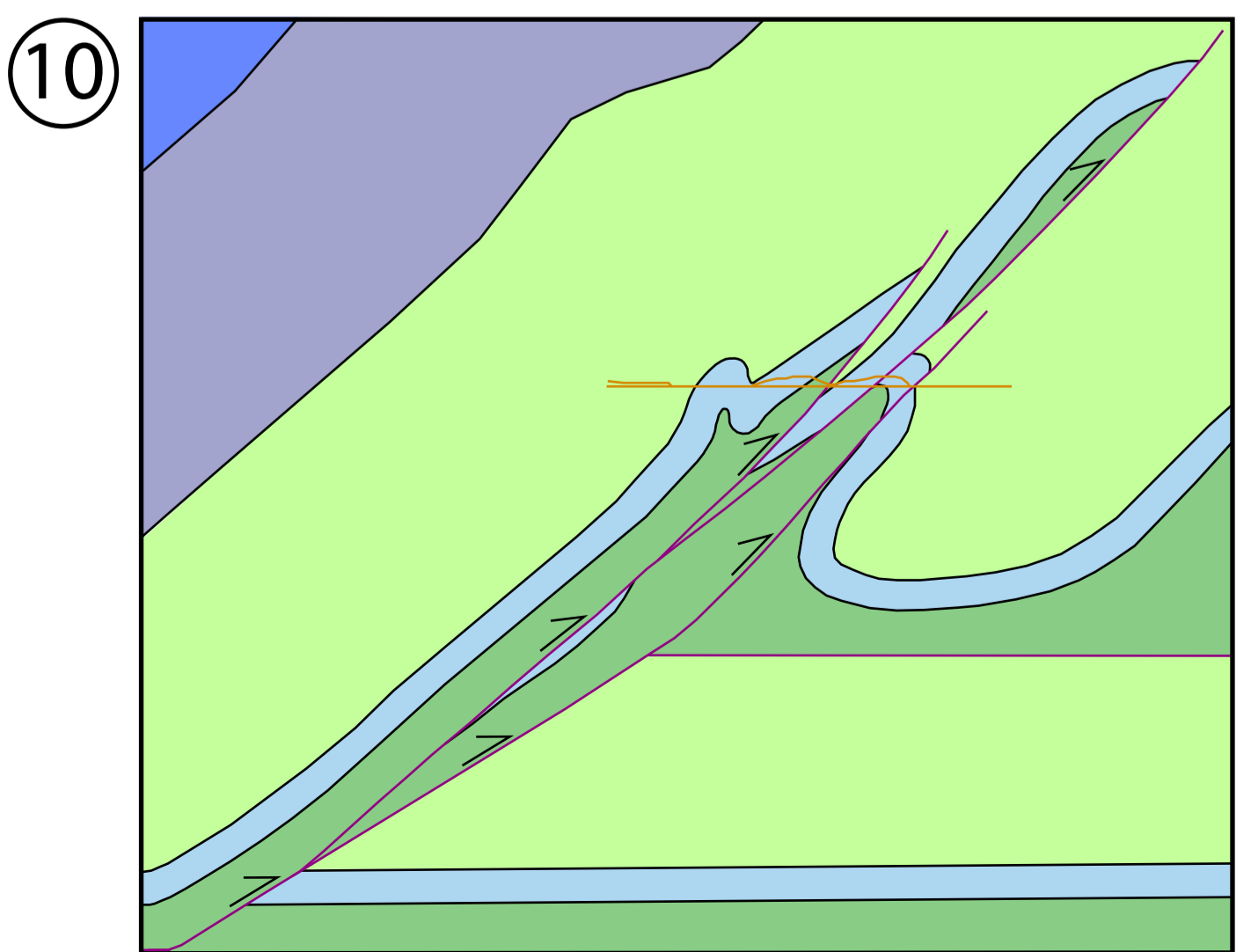
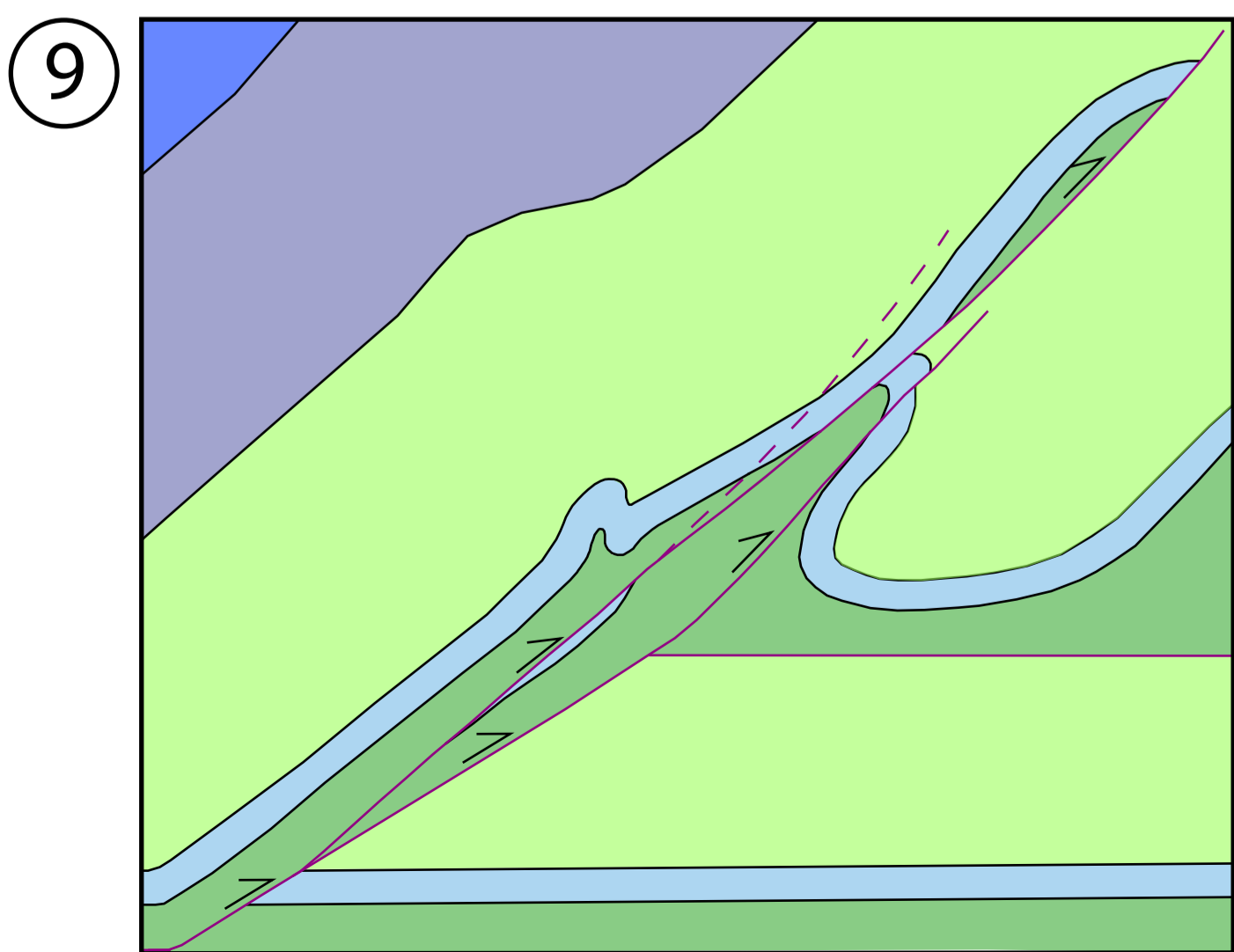
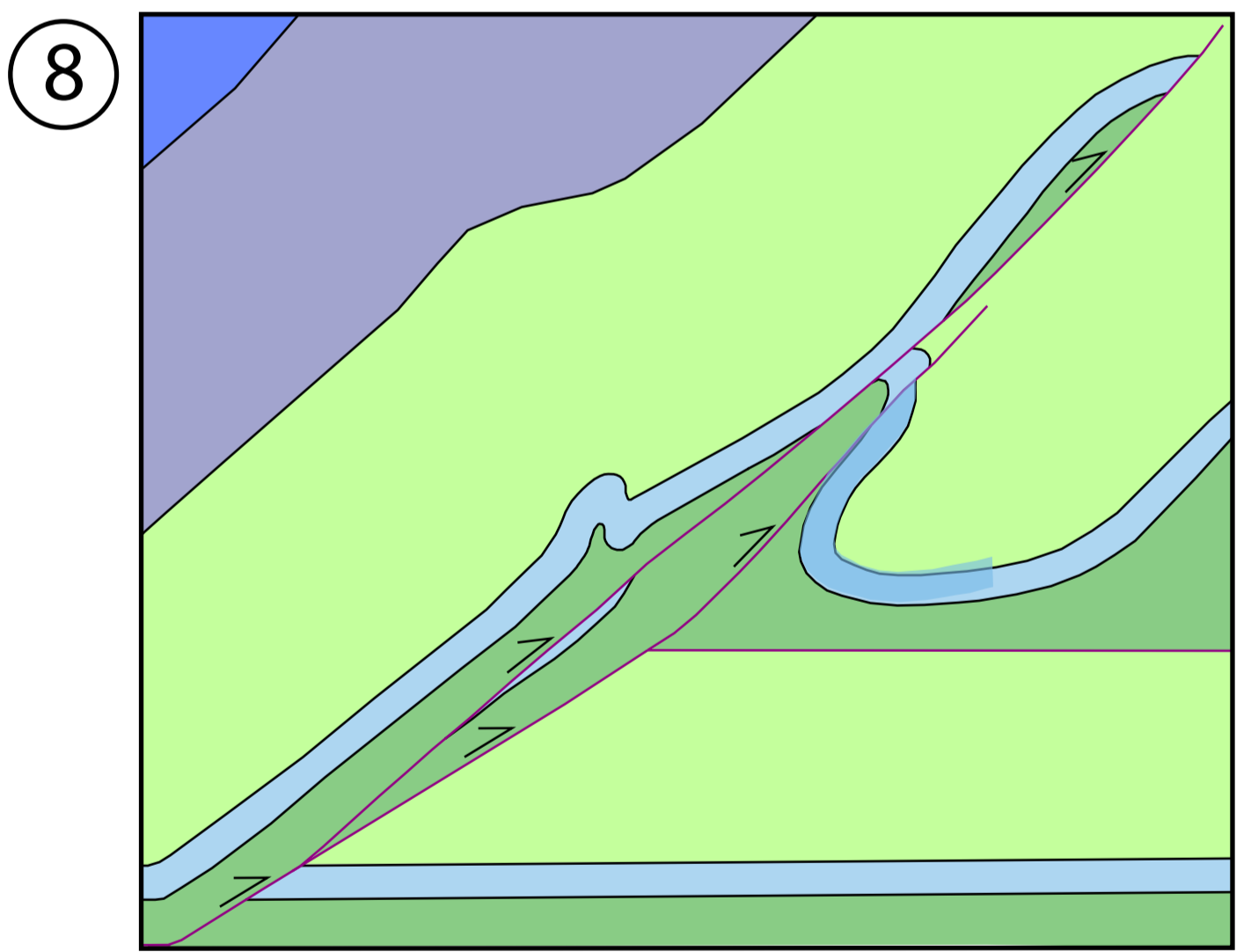
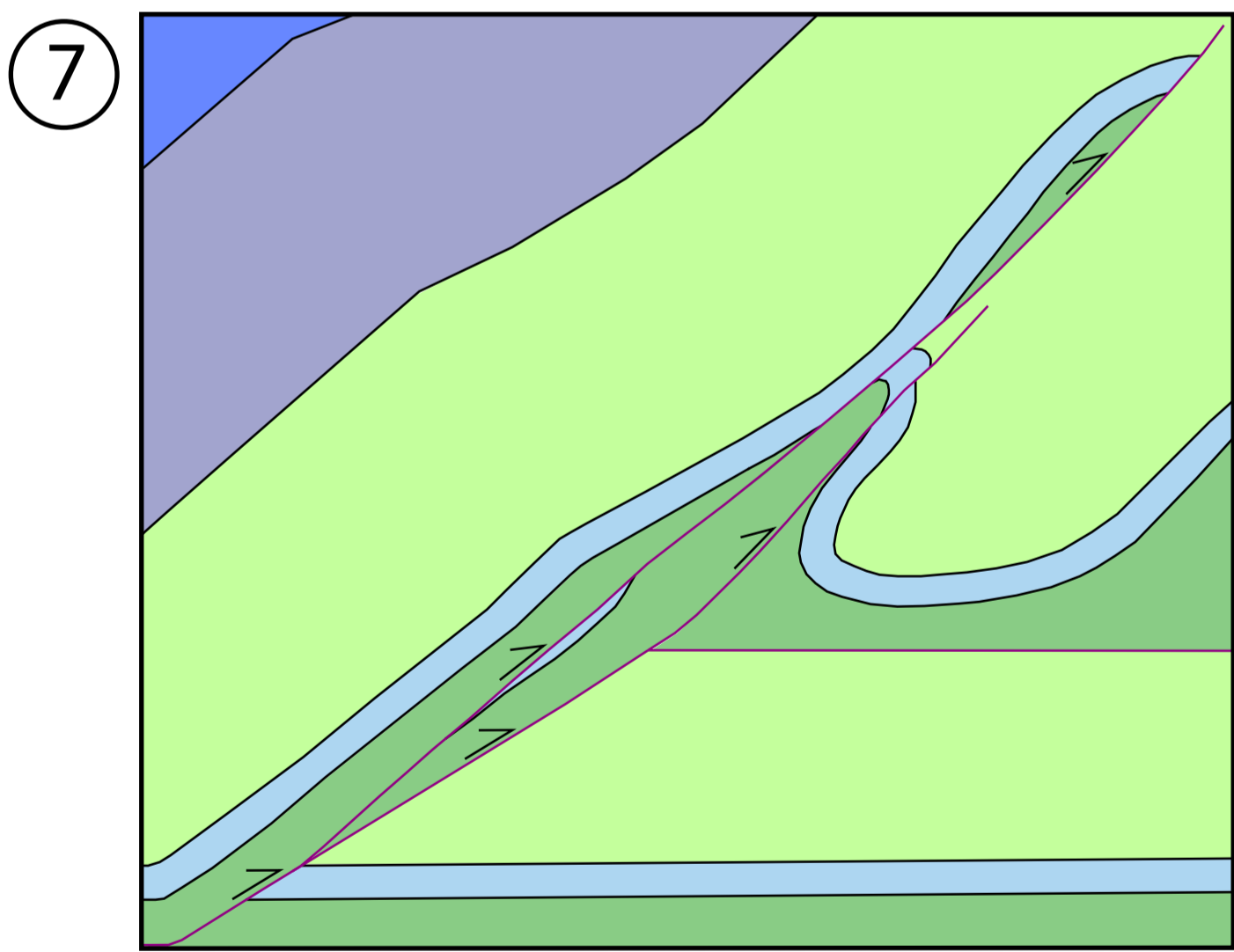
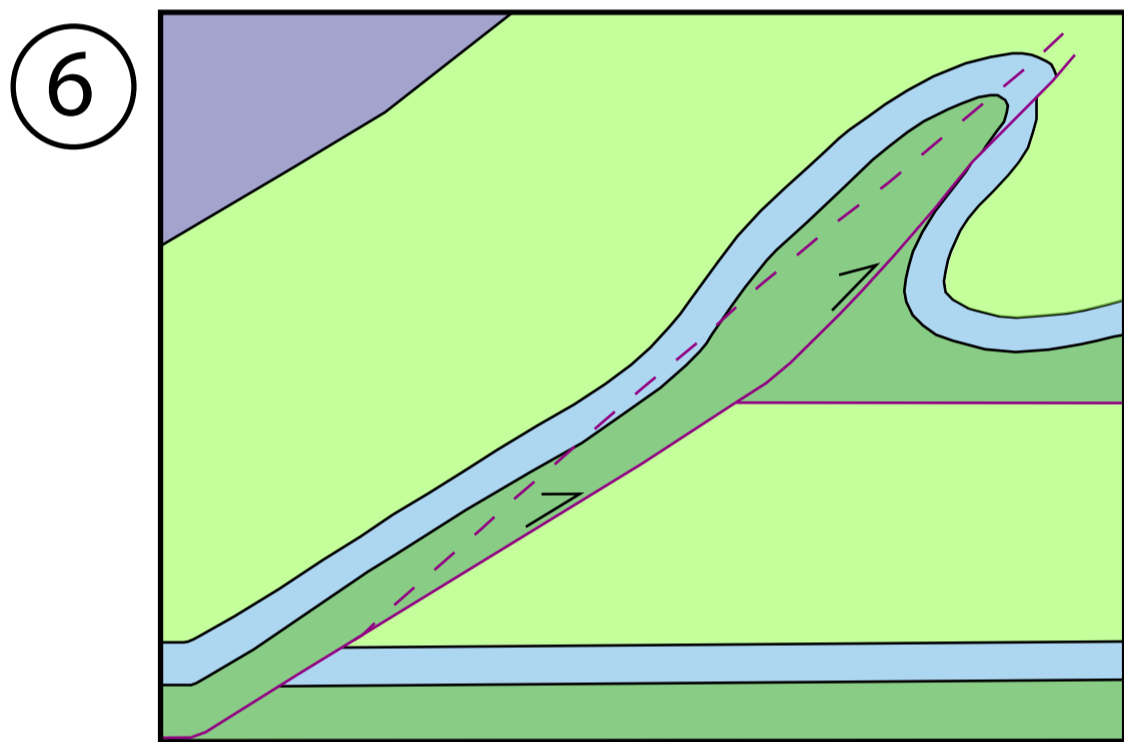
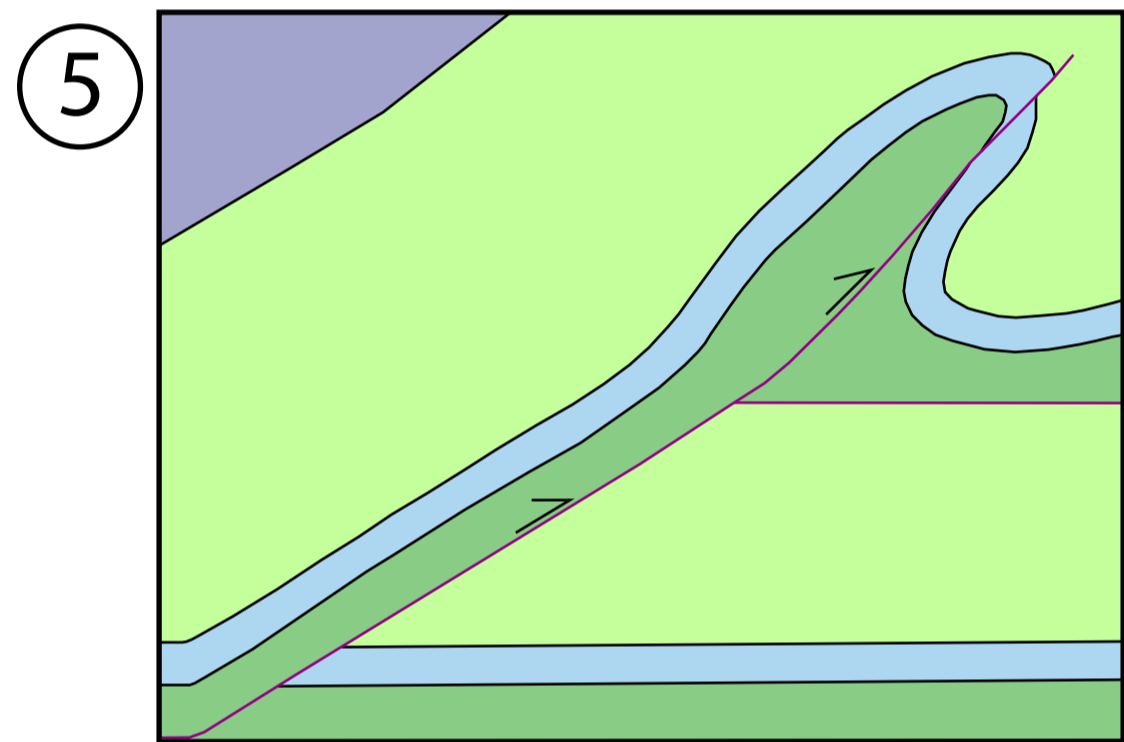
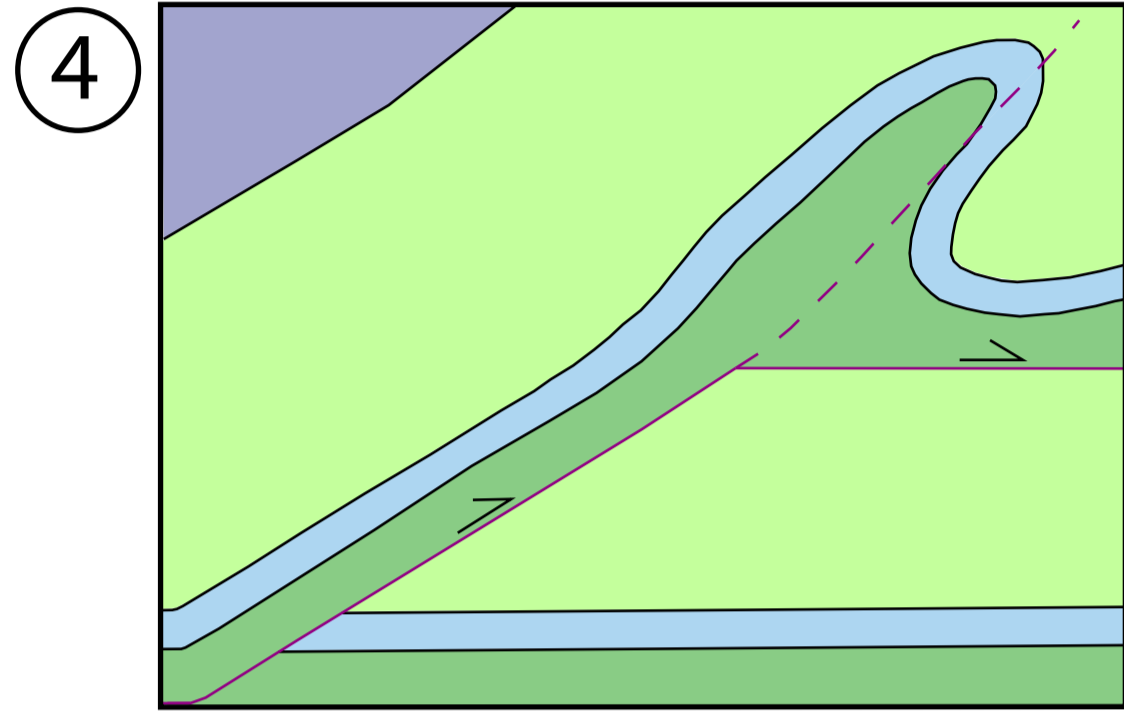
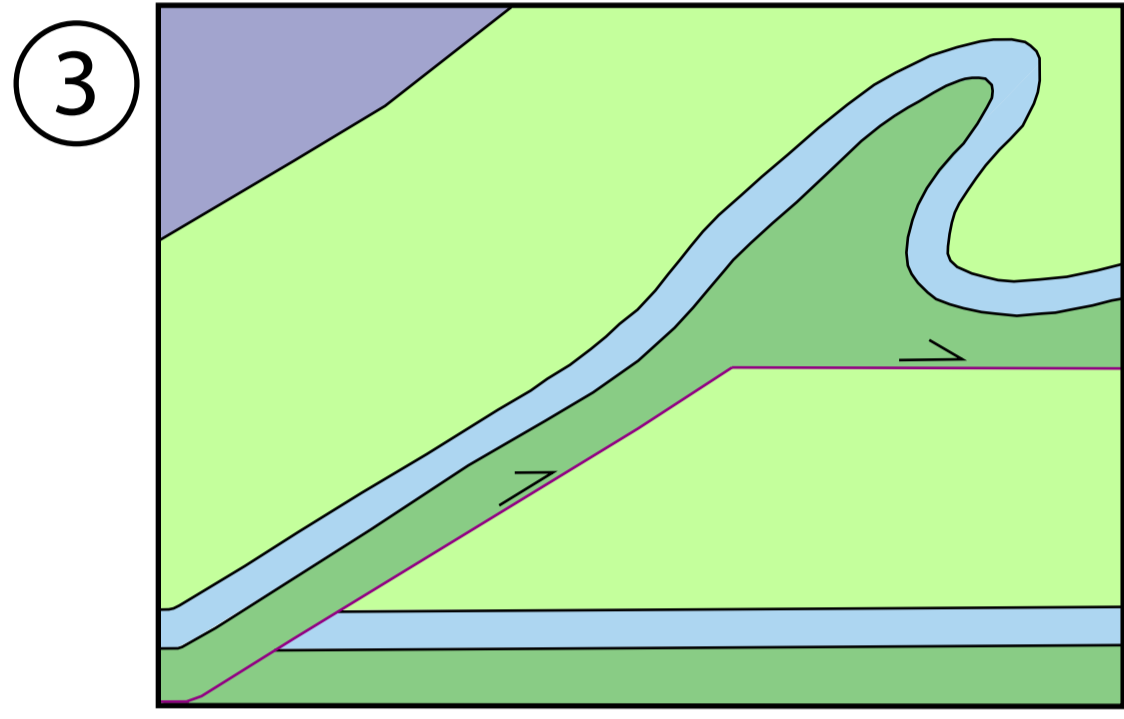
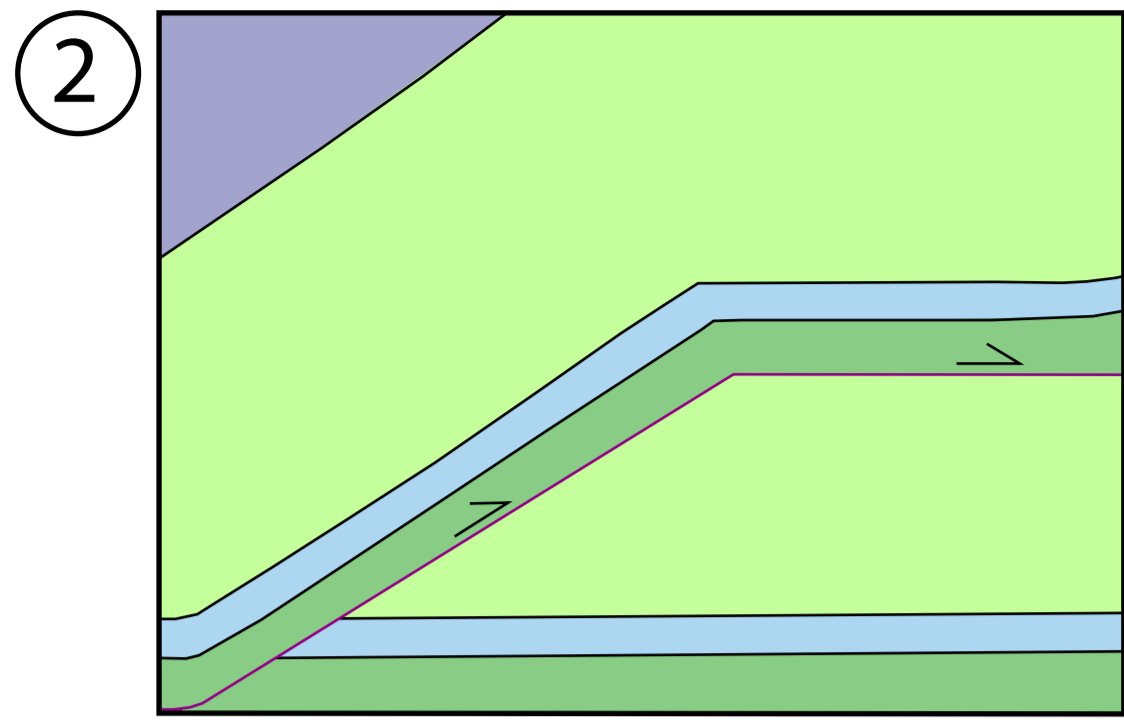
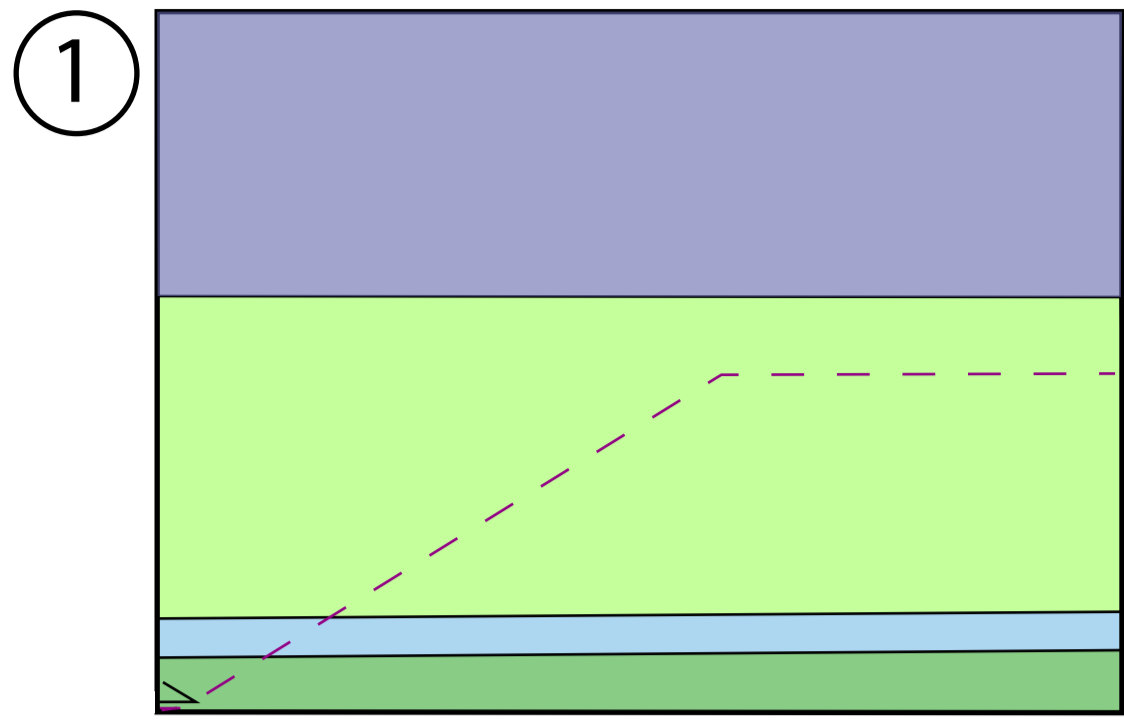


# Appendix 3, Plate 7 : Balanced cross-section GH

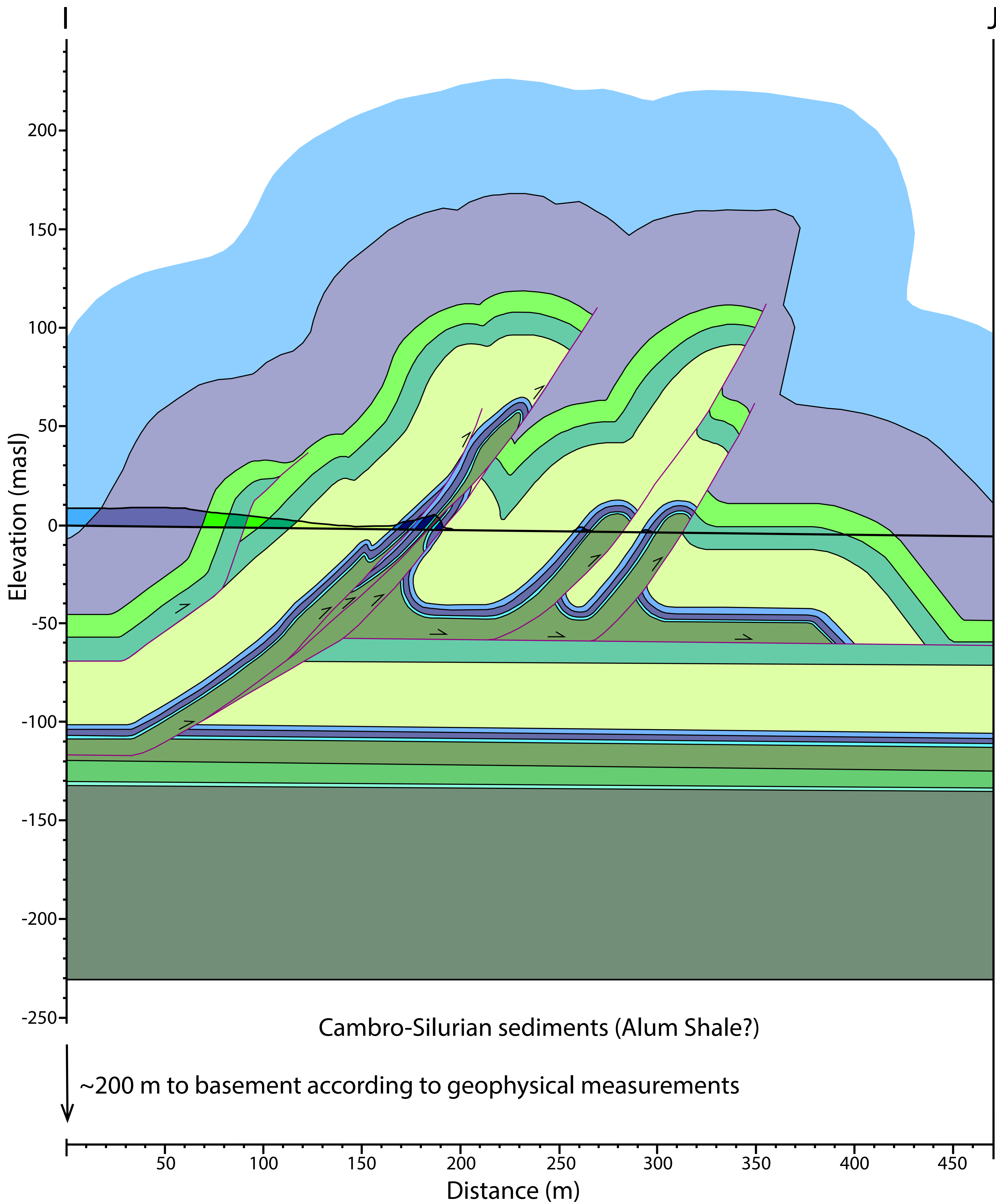


Appendix 3, Plate 8:

Illustration of the steps in the palinspastic restoration of the Hukodden imbricate structure in balanced cross-section GH

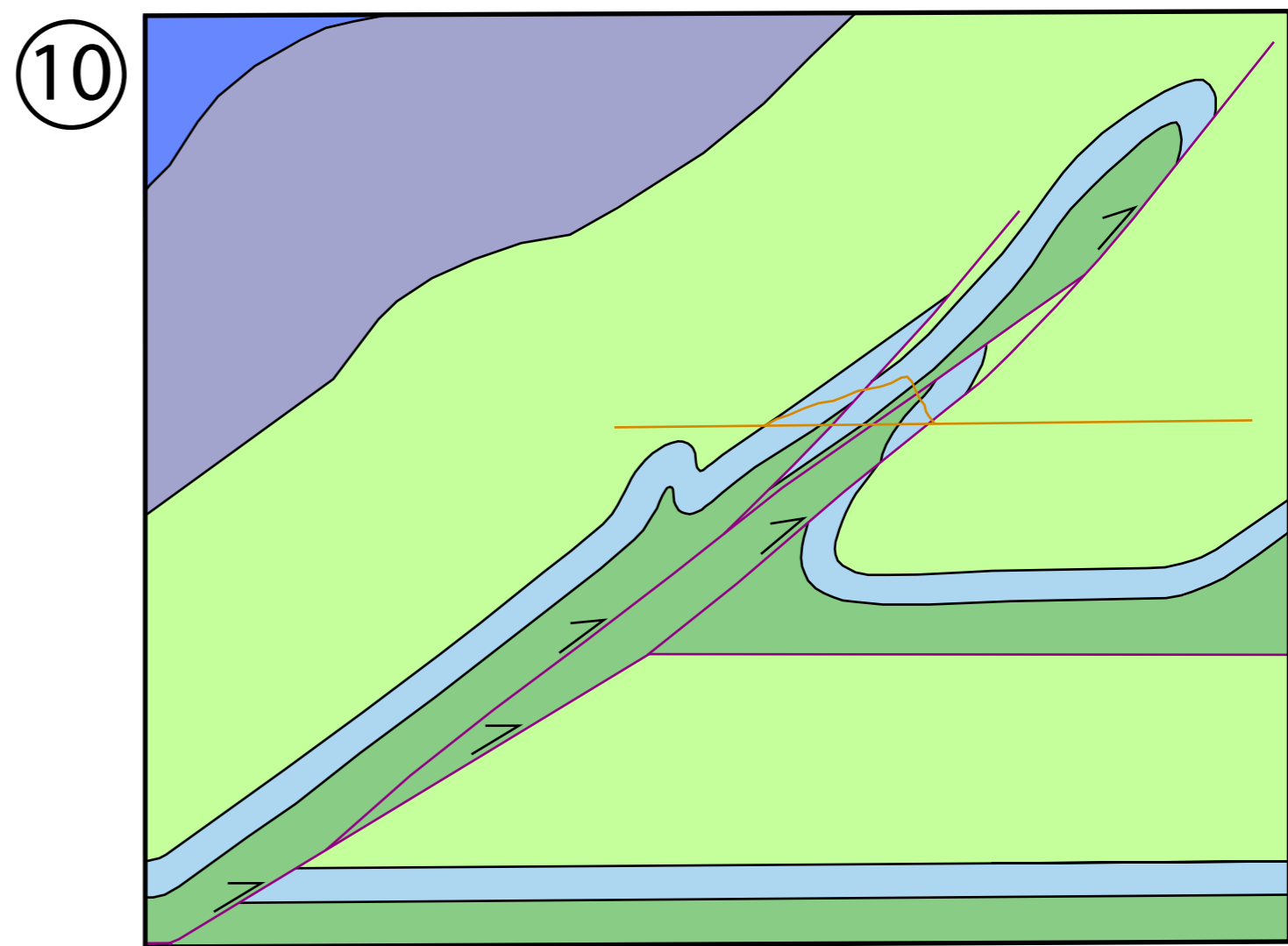
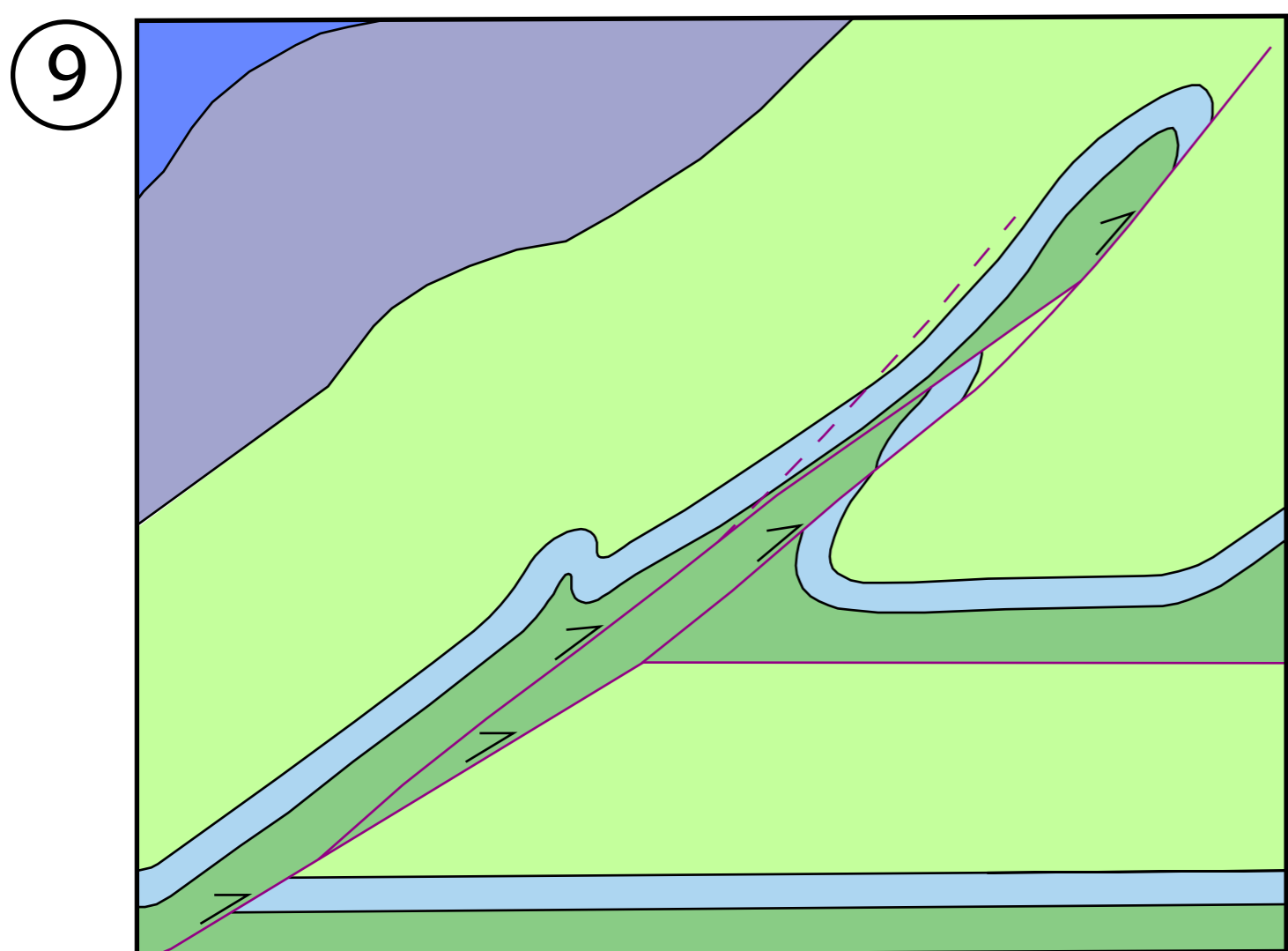
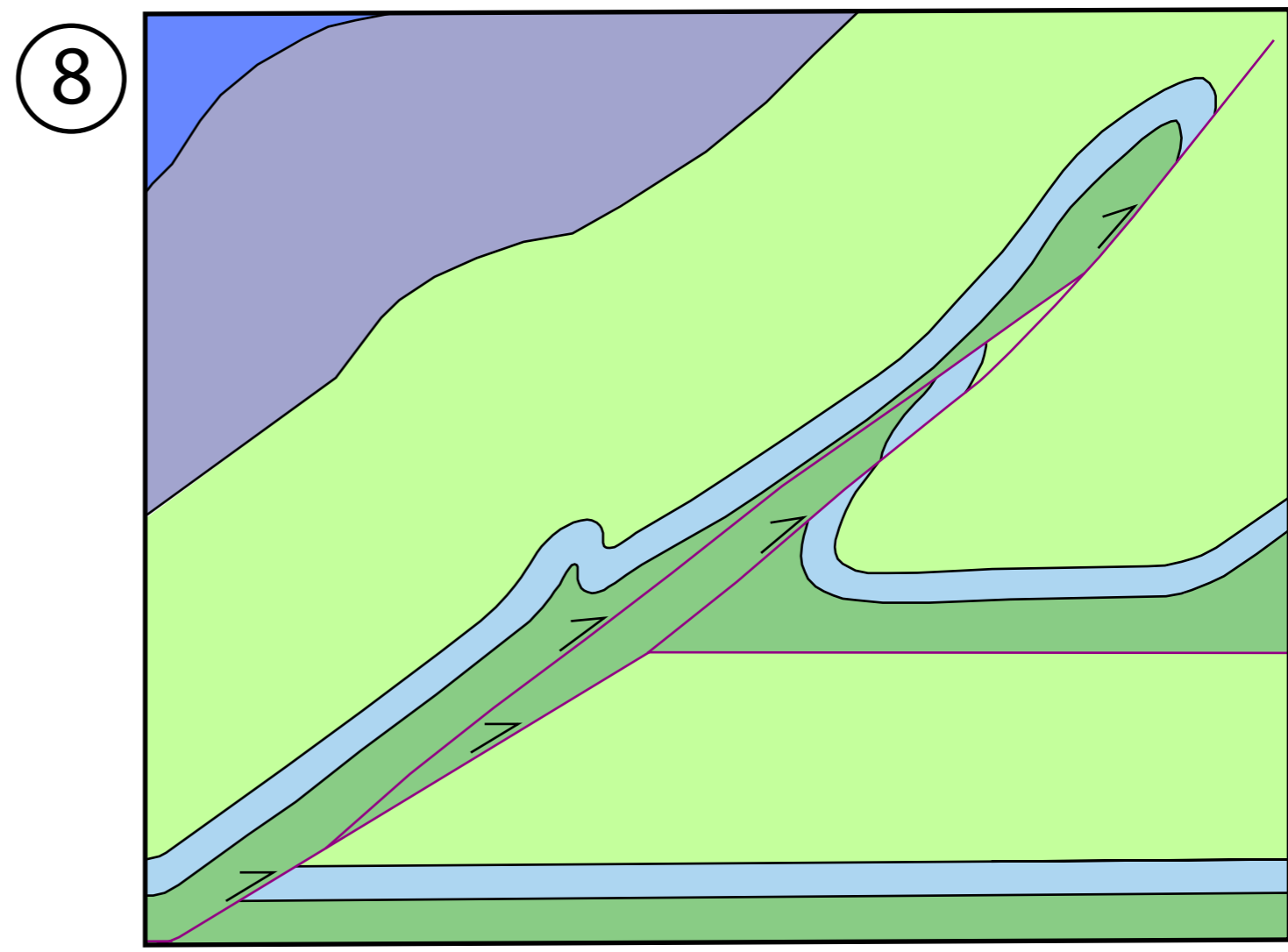
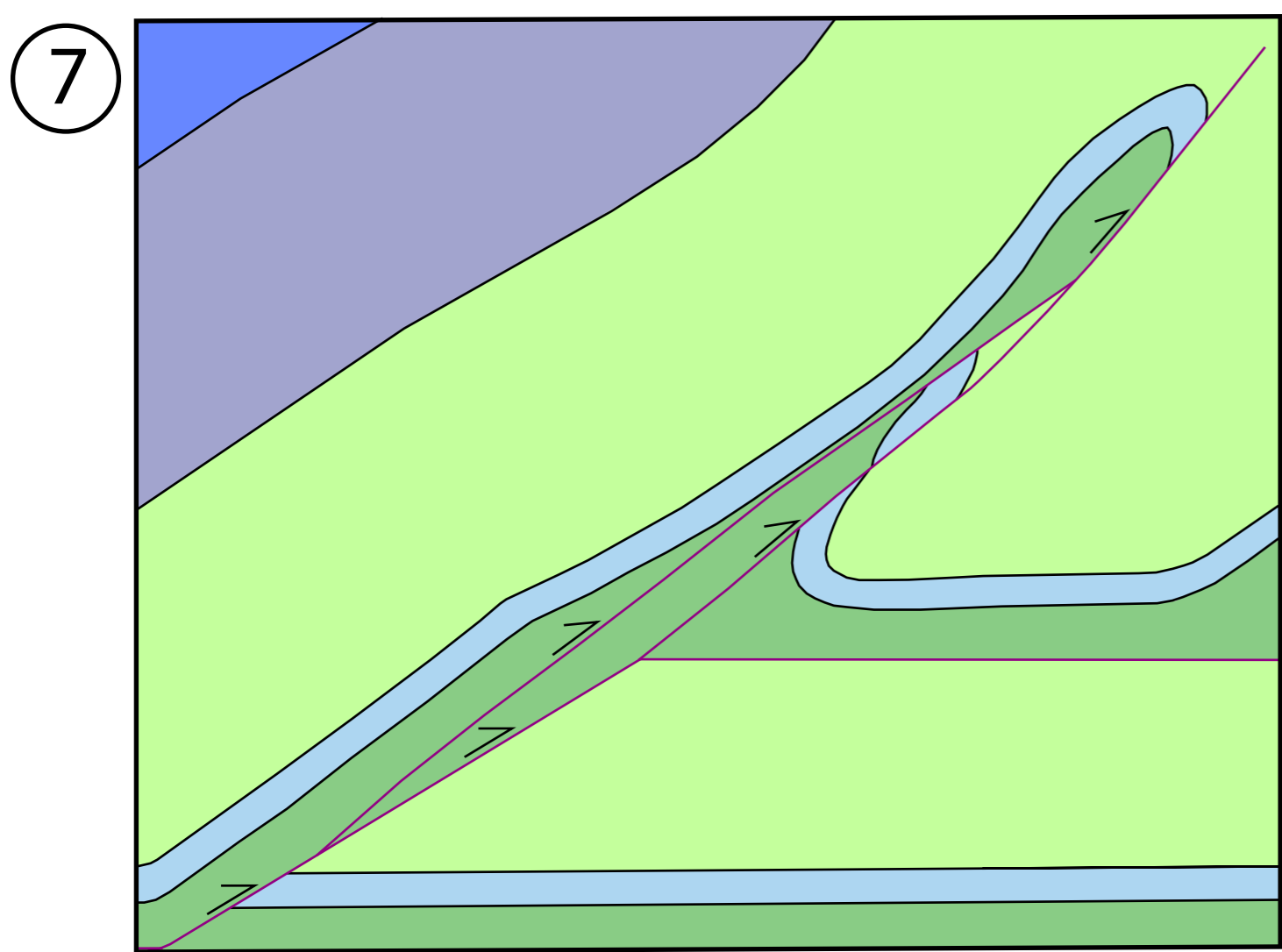
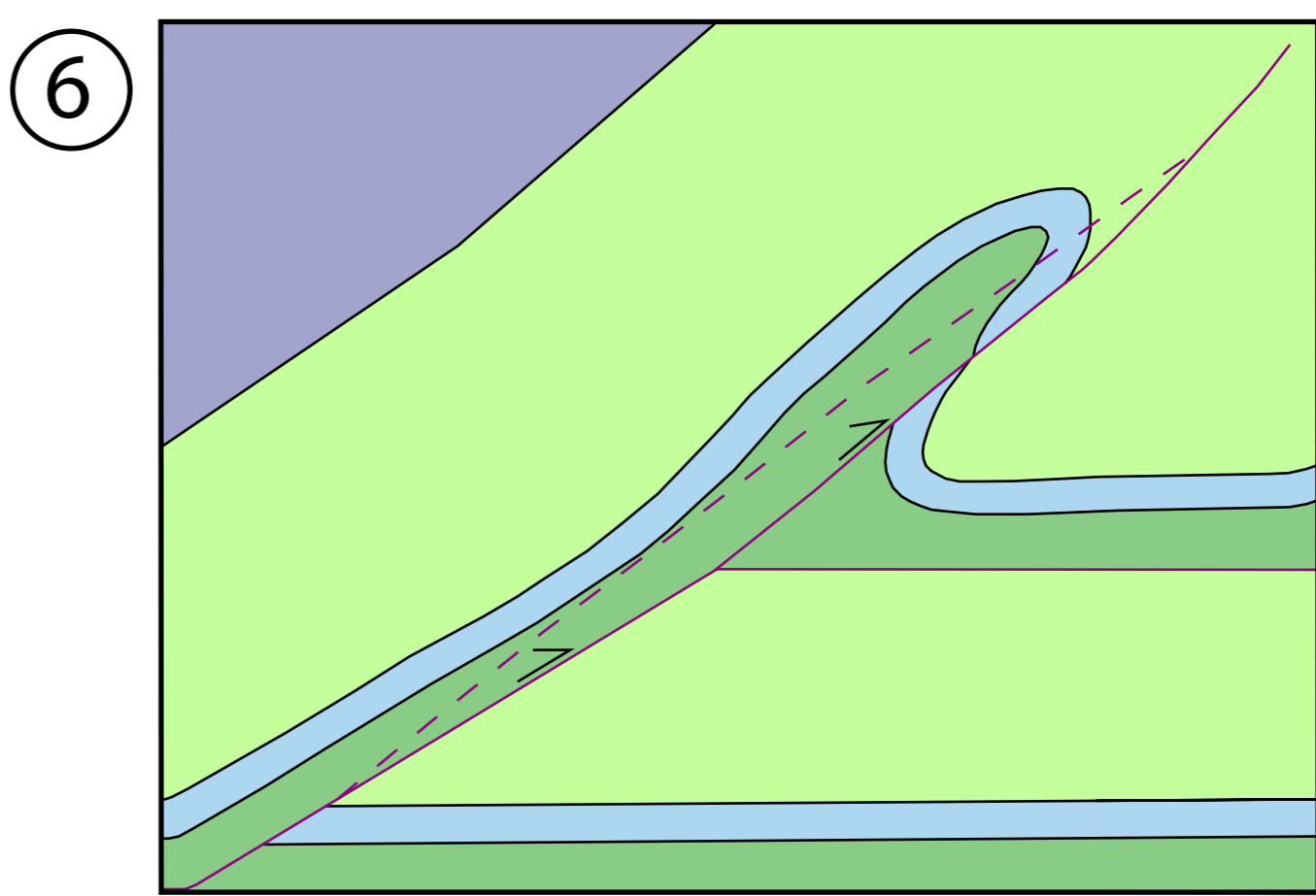
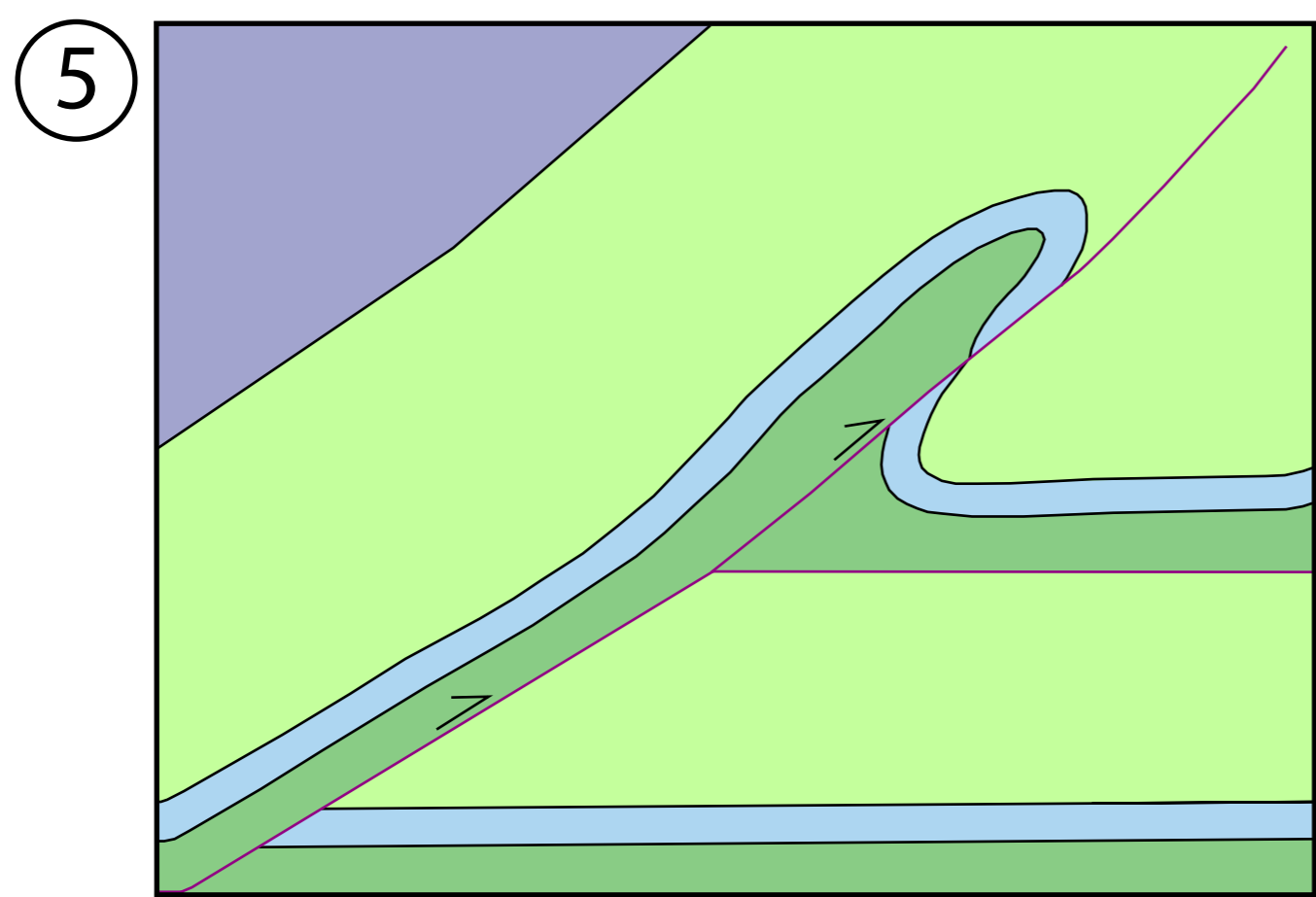
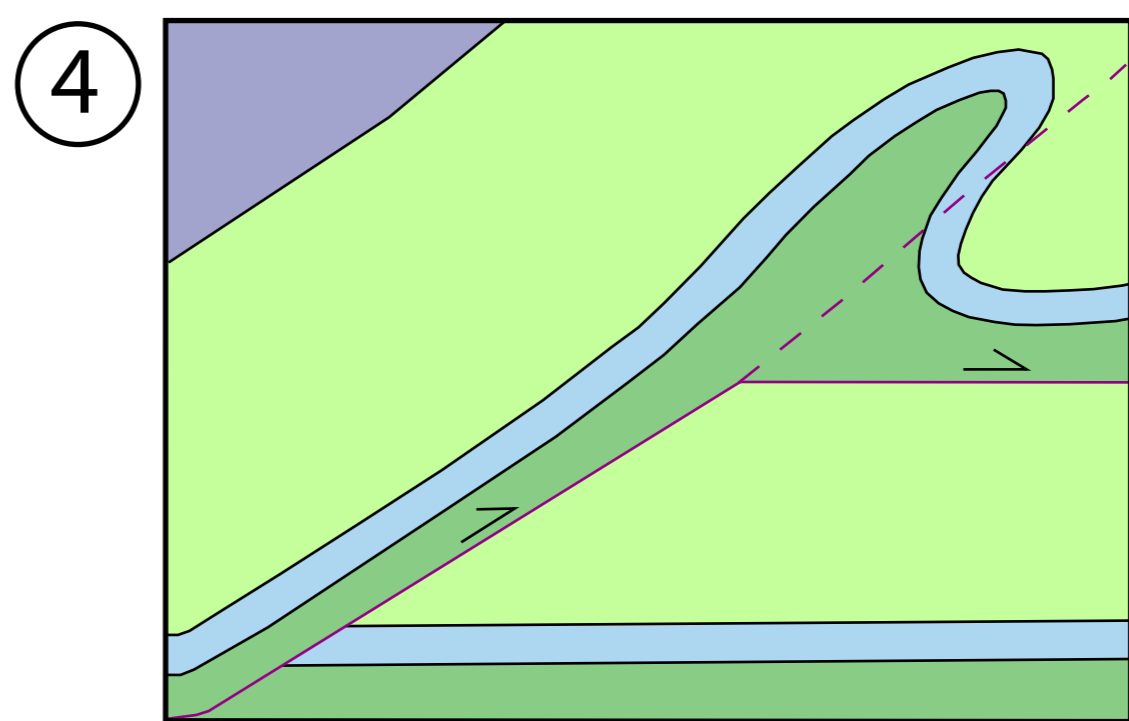
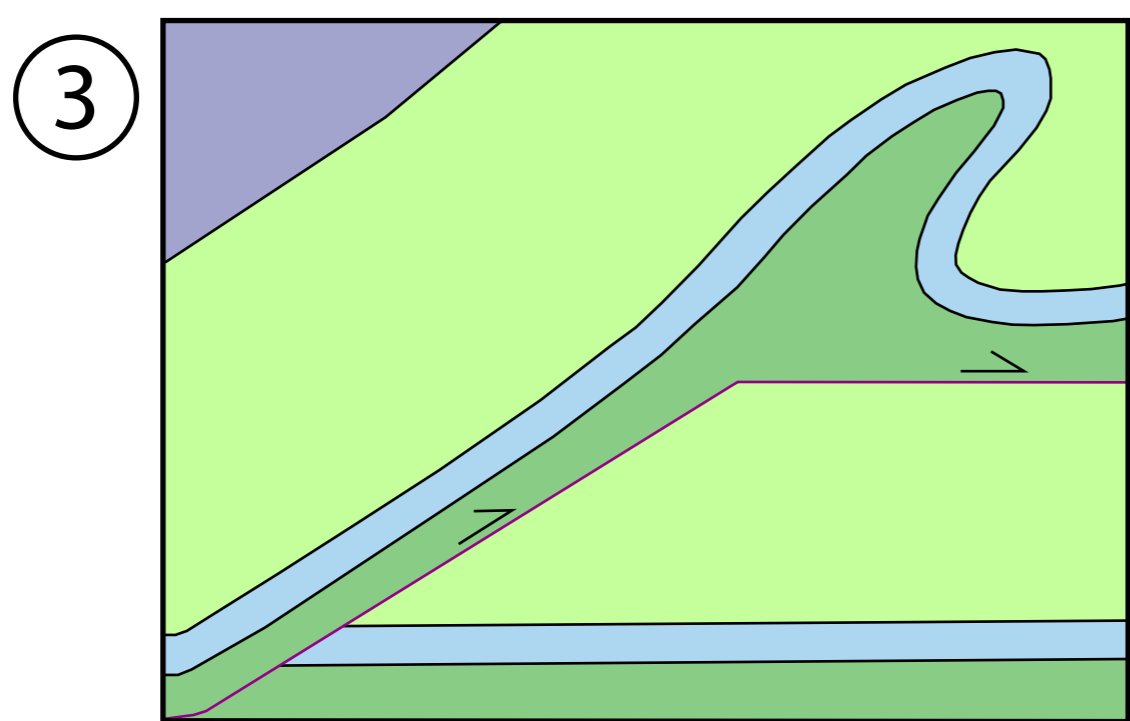
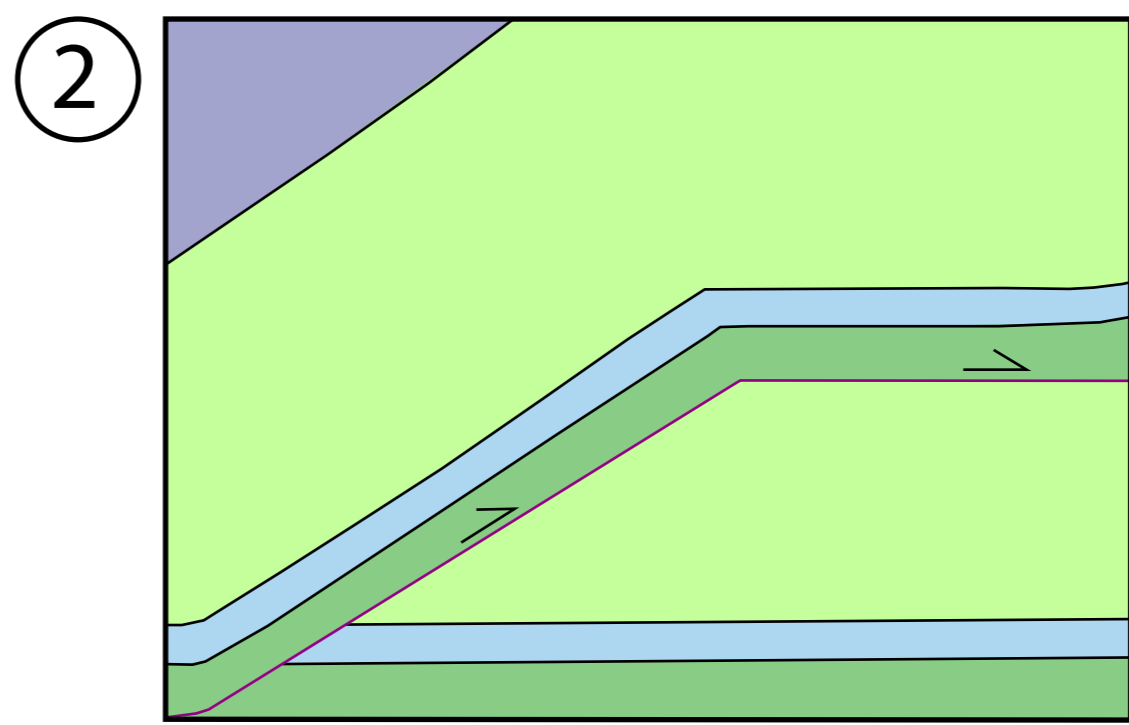
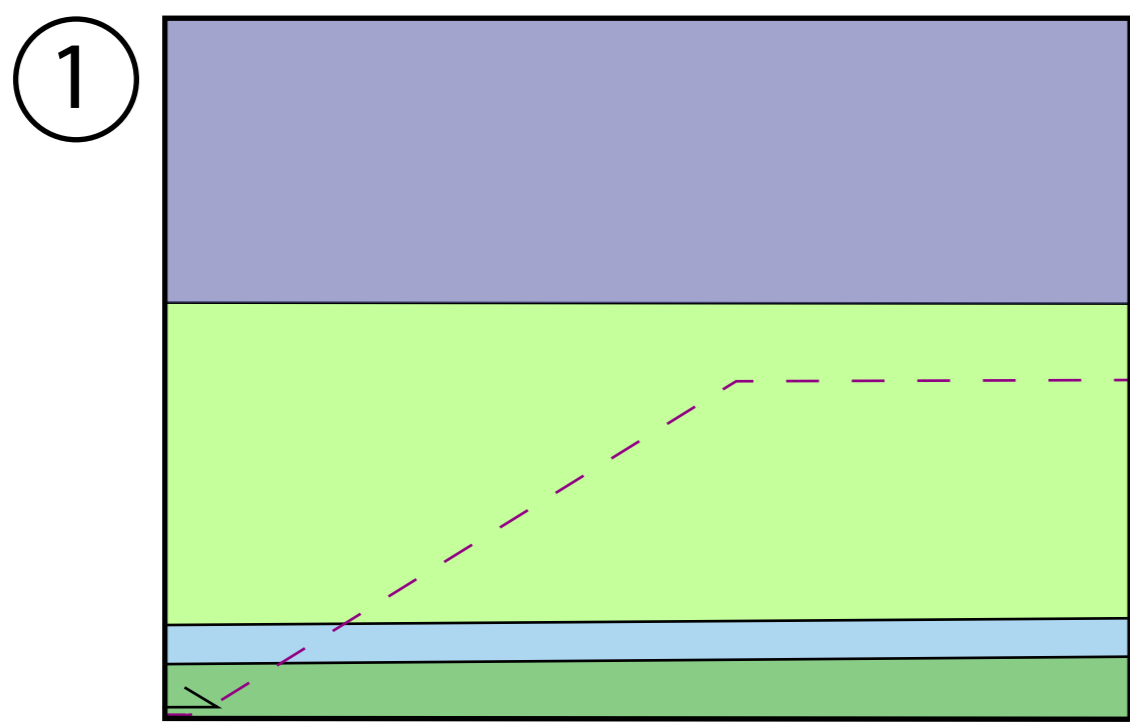


# Appendix 3, Plate 9: Balanced cross-section IJ



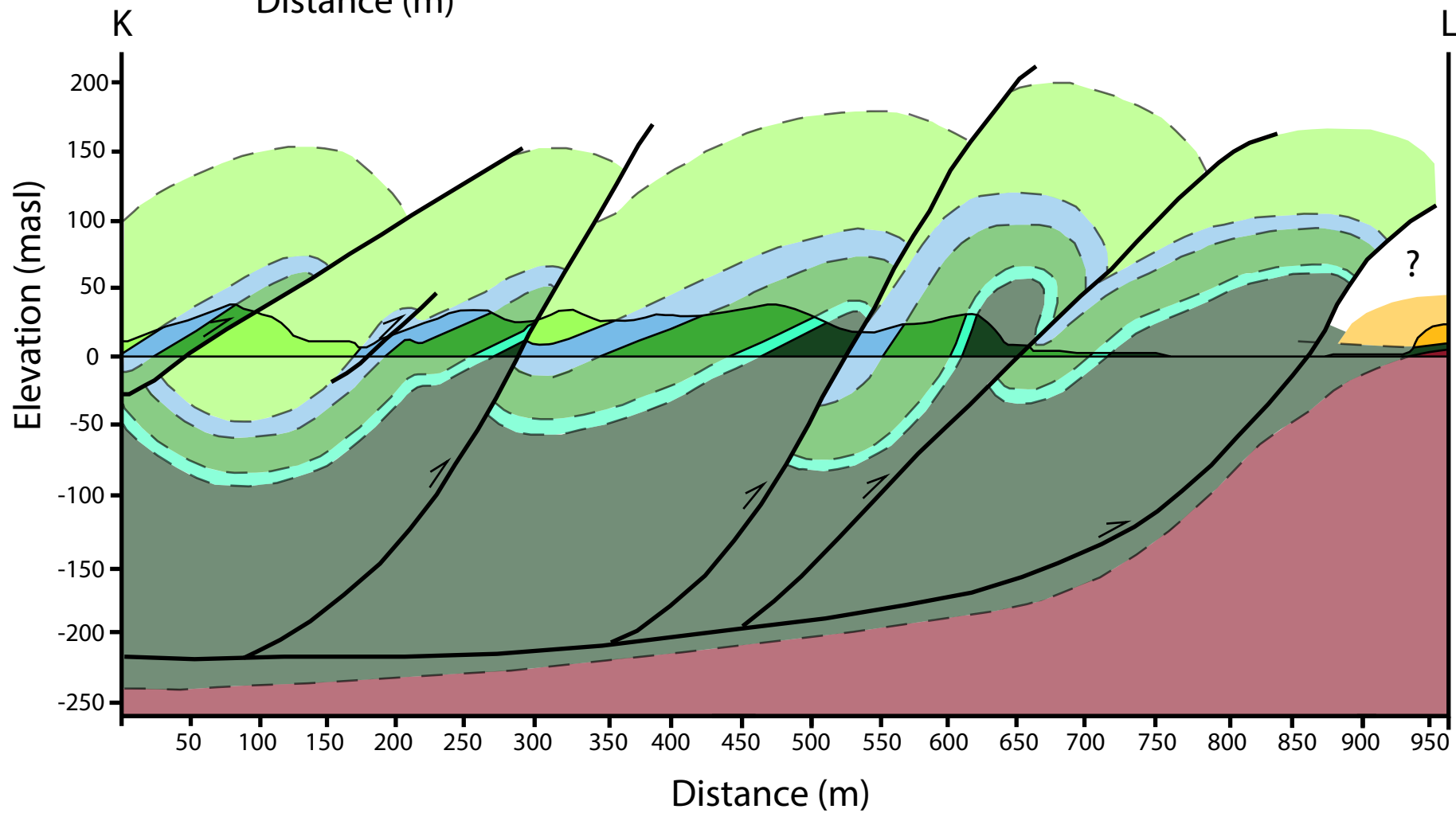
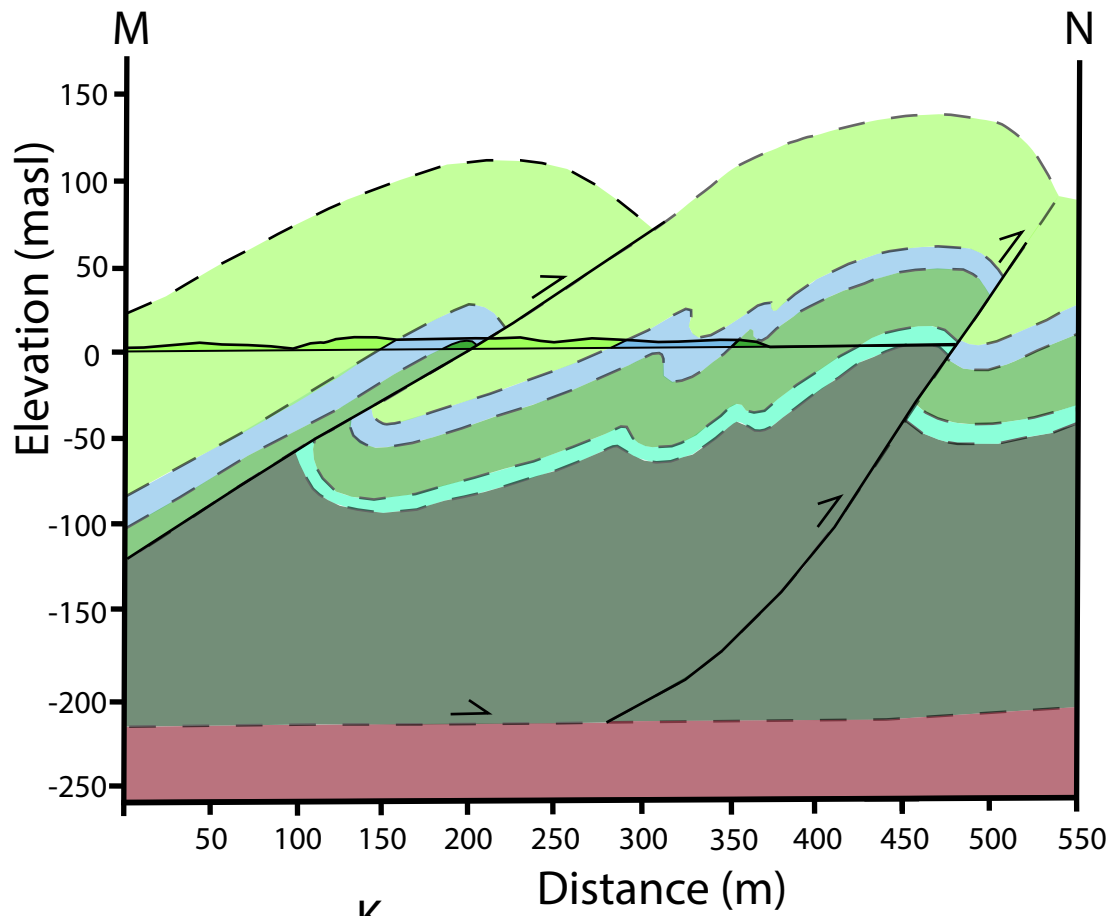
Appendix 3, Plate 10:

Illustration of the steps in the palinspastic restoration of the Hukodden imbricate structure in balanced cross-section IJ





# Appendix 3, Plate 11: Cross-section KL and MN



# Appendix 3, Plate 12: Drone photo of Sub-area 6: Hukodden East

